

อุทกพลศาสตร์และการถ่ายเทมวลในถึงสัมผัสแบบอากาศยก
ชนิดไหลวนภายในด้วยตัวกระจายอากาศรูปวงแหวนในน้ำเค็ม



นางสาวดวงกมล เรือนงาม

วิทยานิพนธ์นี้เป็นส่วนหนึ่งของการศึกษาตามหลักสูตรปริญญาวิศวกรรมศาสตรมหาบัณฑิต


สาขาวิชาวิศวกรรมเคมี ภาควิชาวิศวกรรมเคมี

คณะวิศวกรรมศาสตร์ จุฬาลงกรณ์มหาวิทยาลัย

ปีการศึกษา 2549

ลิขสิทธิ์ของจุฬาลงกรณ์มหาวิทยาลัย

HYDRODYNAMICS AND MASS TRANSFER IN INTERNAL LOOP
AIRLIFT CONTACTOR WITH ANNULUS SPARGER IN SALINE WATER



Miss Duangkamol Ruen-ngam

A Thesis Submitted in Partial Fulfillment of the Requirements
for the Degree of Master of Engineering Program in Chemical Engineering

Department of Chemical Engineering

Faculty of Engineering

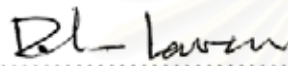
Chulalongkorn University

Academic Year 2006

Copyright of Chulalongkorn University

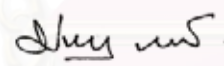
Thesis Title HYDRODYNAMICS AND MASS TRANSFER IN INTERNAL
 LOOP AIRLIFT CONTACTOR WITH ANNULUS SPARGER IN
 SALINE WATER
By Miss Duangkamol Ruen-ngam
Field of study Chemical Engineering
Thesis Advisor Associate Professor Prasert Pavasant, Ph.D.

Accepted by the Faculty of Engineering, Chulalongkorn University in
Partial Fulfillment of the Requirements for the Master's Degree

.....Dean of the Faculty of Engineering
(Professor Direk Lavansiri, Ph.D.)

THESIS COMMITTEE

.....Chairman
(Assistant Professor Muenduen Phisalaphong, Ph.D.)

.....Thesis Advisor
(Associate Professor Prasert Pavasant, Ph.D.)

.....Member
(Associate Professor Seeroong Prichanont, Ph.D.)

.....Member
(Assistant Professor Worapon Kiatkittipong, D.Eng.)

ดวงกมล เรืองงาม : อุทกพลศาสตร์และการถ่ายเทมวลในถังสัสมัสดแบบอากาศยกชนิดไหลวนภายในด้วยตัวกระจายอากาศรูวงแหวนในน้ำเค็ม. (HYDRODYNAMICS AND MASS TRANSFER IN INTERNAL LOOP AIRLIFT CONTACTOR WITH ANNULUS SPARGER IN SALINE WATER) อาจารย์ที่ปรึกษา: รองศาสตราจารย์ ดร.ประเสริฐ ภาวนันต์, 132 หน้า.

การศึกษาผลของความเค็มต่อลักษณะทางอุทกพลศาสตร์และการถ่ายเทมวลสารระหว่างวัฏภาคก๊าซและของเหลว ดำเนินการโดยใช้ถังปฏิกรณ์แบบอากาศยกปริมาตร 17 ลิตร สูง 1.2 เมตร ขนาดเส้นผ่านศูนย์กลาง 0.137 เมตร ท่อในยาว 1 เมตร โดยเปลี่ยนขนาดเส้นผ่านศูนย์กลางท่อใน 4 ค่า ได้ค่าอัตราส่วนของพื้นที่ไม่ให้ก๊าซต่อพื้นที่ให้ก๊าซ (A_g/A_l) เปลี่ยนแปลงในช่วง 0.061-1.01 แปรค่าความเร็วลม (u_{sg}) ในช่วง 0.01-0.07 เมตรต่อวินาที และความเค็มที่ใช้ คือ 0 15 30 และ 45 ส่วนในพันส่วน ขนาดของฟองแสดงในรูปของ Sauter mean diameter พบว่าขนาดฟองในน้ำเค็มมีขนาดเล็กกว่าน้ำเปล่า เนื่องจากผลต่างซึ่งแสดงในรูป ΔP ระหว่างแรงผลักระหว่างฟองซึ่งจะป้องกันการรวมตัวของฟองเกิดจากประจุไอออนในสารละลายสร้างพันธะกับน้ำ (hydrophilic repulsive force) และแรงตึงผิว (Laplace pressure) ซึ่งสนับสนุนการรวมตัวซึ่งค่านี้มากจะเกิดการแตกของฟอง จากการคำนวณพบว่าช่วงฟองเกิดการรวมตัวอยู่ในช่วง 15-20 นิวตันต่อตารางเมตร จากการทดลองพบว่าเมื่อเพิ่มความเร็วก๊าซในช่วง 0.01-0.07 เมตรต่อวินาที ขนาดฟองเล็กลงจาก 6 เป็น 1 มิลลิเมตร เนื่องมาจากปริมาณก๊าซที่เพิ่มขึ้นในระบบทำให้เกิดการชนกันง่ายขึ้นของฟอง และมีค่า ΔP มากกว่า 20 นิวตันต่อตารางเมตร ซึ่งเกิดการแตกตัวของฟอง ผลของระยะทางตามแนวแกนพบว่าในช่วงความเร็วต่ำ ($u_{sg} < 0.04$ เมตรต่อวินาที) ฟองขนาดใหญ่พบที่บริเวณส่วนล่าง และพบฟองขนาดเล็กในบริเวณส่วนกลางและบนของถังปฏิกรณ์ เนื่องมาจากส่วนบนและส่วนกลางมีความปั่นป่วนมาก พบค่า ΔP ประมาณ 27-65 นิวตันต่อตารางเมตร ซึ่งเกิดการแตกตัวของฟอง ฟองจึงมีขนาดเล็ก ผลของ A_g/A_l พบว่าพื้นที่ส่วนให้ก๊าซขนาดใหญ่ทำให้ฟองแตกตัวเกิดฟองขนาดเล็ก ได้ค่า ΔP ประมาณ 50-97 นิวตันต่อตารางเมตร ค่าอัตราการถ่ายโอนมวลสารระหว่างวัฏภาคก๊าซและของเหลว ($k_L a$) ในน้ำเค็มมีค่าน้อยกว่าในน้ำเปล่าเรียงตามลำดับคือ 0 ppt > 30 ppt > 15 ppt > 45 ppt และค่าพื้นที่ผิวต่อปริมาตรจำเพาะของฟอง (a) พบว่ามีค่ามากในน้ำเค็ม อย่างไรก็ตามค่าสัมประสิทธิ์การถ่ายโอนมวลจากก๊าซไปสู่ของเหลว (k_L) พบว่าในน้ำเปล่ามีค่ามากกว่าน้ำเกลือ ในน้ำเกลือมีลักษณะการแพร่แบบธรรมชาติ ขึ้นกับขนาดฟอง และการแพร่แบบบังคับขึ้นกับทั้งขนาดฟองและความแตกต่างของความเร็วสัมพัทธ์ระหว่างก๊าซและของเหลว

ภาควิชาวิศวกรรมเคมี

สาขาวิศวกรรมเคมี

ปีการศึกษา 2549

ลายมือชื่อนิสิต..... ทพทศ เรืองงาม

ลายมือชื่ออาจารย์ที่ปรึกษา..... ชัย นว.....

4770294421 : MAJOR CHEMICAL ENGINEERING

KEY WORD: PRESSURE DIFFERENCE / BUBBLE BEHAVIOUR / MASS

TRANSFER / HYDRODYNAMICS

DUANGKAMOL RUEN-NGAM: HYDRODYNAMICS AND MASS
TRANSFER IN INTERNAL LOOP AIRLIFT CONTACTOR WITH ANNULUS
SPARGER IN SALINE WATER. THESIS ADVISOR: ASSOC. PROF.
PRASERT PAVASANT, Ph.D., 132 pp.

The investigation of the effect of salinity on the performance of airlift contactor was achieved using the 17L internal loop airlift system with a column height of 1.2 m, and 0.137m diameter, and a draft tube height of 1 m. The diameters of the draft tubes were altered to vary the ratio between downcomer and riser cross sectional areas (A_d/A_r) from 0.061-1.01. The aeration was supplied in the superficial gas velocity (u_{sg}) from 0.01- 0.07 m/s and the salinity levels were altered from 0, 15, 30, and 45ppt. The Sauter mean diameter of the bubble appeared to be smaller in saline water than in fresh water due to two main reasons. The first one was the presence of hydrophilic repulsive force which inhibited bubble coalescence, and the second was the high Laplace pressure which promoted the breakup of the bubbles. The range of pressure difference, ΔP , acting on the bubble which was found to promote bubble coalescence was between 15-20 N/m². In saline water, the bubble size decreased with superficial gas velocity, u_{sg} , where a reduction from 6 to 1 mm was observed with an increase in u_{sg} from 0.02-0.07 m/s. This was caused by the collision of bubbles at high gas hold-up in the system at higher gas flow rate which occurred at ΔP greater than 20 N/m² and consequently supported bubble break-up. Axial variation in bubble size was only observed at low u_{sg} (less than 0.04m/s) where bubbles in the bottom section of the airlift was larger than those in the middle and top sections. This was because the conditions in the middle and top sections were turbulent and with high ΔP (27-65 N/m²), bubble break-up occurred. The effect of downcomer to riser area ratio was quite important and the highest range of ΔP (approx. 50-97 N/m²) was found at the smallest downcomer area configuration which led to bubble break-up conditions. The overall volumetric mass transfer coefficient appeared lower in the saline water than in the fresh water where the levels of $k_L a$ could be ordered from high to low as 0 ppt > 30 ppt > 15 ppt > 45 ppt. The specific area was found to be high in the saline water systems, however, the mass transfer coefficient was much higher in the fresh water system than in the saline water. The mass transfer coefficient was controlled by both natural and forced convections which were related significantly to the diameter and slip velocity of the gas bubbles.

Department Chemical Engineering

Field of study Chemical Engineering

Academic year 2006

Student's signature Duangkamol Ruengnam

Advisor's signature Prasert Pavasant

ACKNOWLEDGEMENTS

This thesis will never have been completed without the help and support of many people and organizers who are gratefully acknowledged here. Firstly, I would like to express my sincere gratitude to Associate Professor Prasert Pavasant, my advisor, for his suggestions, guidance, warm encouragement and generous supervision throughout my master program. I am also grateful to Assistant Professor Dr. Muenduen Phisalaphong, Associate Professor Dr. Seeroong Prichanont and Assistant Professor Dr. Worapon Kiatkittipong for their helpful and many valuable comments.

Special gratitude to Graduated School Research Fund. for supporting financial. Special thank should also be directed towards Dr. Porntip Wongsuchoto (P'Puud) for many available helps, supported the informations and comments. I would like to gratefully thank for department of chemical engineering that give a chance for studying in field of engineer. I cannot forget to express my thankfulness to my lovely friends, Tang Jubb Oo Nui Rin and Supersearch's group research, P'Boom (Missist Khanidtha Meewasna, Marungrueng) N'phong (Miss Duangmanee Reungsuk) N'Tik (Miss Apipreeya Kongsuwan) N'X (Viriya Madacha) M (Mr. Pimol Panchonghan) and other are P'poot P' Ron Nui Mag N'Kaey N'Note N'Toey N'Big N'Mhoo N'Mauy N'Jim N'Bass.

Finally, I would like to express me sincere my sincere indebtedness to my family for their worth supports throughout my Master courses.

สถาบันวิทยบริการ
จุฬาลงกรณ์มหาวิทยาลัย

Contents

	Page
ABSTRACT IN THAI	iv
ABSTRACT IN ENGLISH	v
ACKNOWLEDGEMENTS	vi
TABLE OF CONTENTS	vii
LIST OF TABLES	x
LIST OF FIGURES	xi
LIST OF ABBREVIATIONS & NOTATIONS	xiii
CHAPTER I INTRODUCTION	1
1.1 Motivations.....	1
1.2 Objectives.....	2
1.3 Scopes of this work.....	3
CHAPTER II BACKGROUNDS & LITERATURE REVIEW	7
2.1 Airlift contactors	7
2.1.1 Type and configuration of airlift contactors	7
2.1.2 Three main regions of airlift contactors.....	7
2.2 Gas-liquid hydrodynamics and mass transfer.....	8
2.2.1 Hydrodynamics behavior	8
2.2.1.1 Gas holdup.....	8
2.2.1.2 Liquid velocity.....	9
2.2.2 Gas-liquid mass transfer	10
2.3 Flow regimes.....	12
2.4 Bubble size distribution.....	12
2.4.1 Determination of bubble size distribution.....	12
2.4.2 Bubble size and gas-liquid mass transfer.....	14
2.5 Effects of geometry and liquid properties on airlift contactor performance.....	15

	Page
CHAPTER III MATERIAL AND METHODS	37
3.1 Experimental setup.....	37
3.2 Experimental procedures	38
3.2.1 Bubble characteristics measurement	38
3.2.2 Gas holdup measurement.....	38
3.2.3 Liquid velocity.....	39
3.2.4 Mass transfer coefficient measurement.....	39
3.3 Experimental Analysis.....	40
3.3.1 Bubble size calculation.....	40
3.3.2 Gas holdup calculations.....	41
3.3.2.1. Overall gas holdup.....	41
3.3.2.2. Riser gas holdup.....	42
3.3.2.3. Downcomer gas holdup.....	42
3.3.3 Liquid velocity.....	43
3.3.4 Volumetric mass transfer coefficient calculation.....	43
 CHAPTER IV RESULTS & DISCUSSION	 48
4.1 Error compensation in photographic technique.....	48
4.2 Effect of salinity on average bubble size.....	48
4.3 Effect of superficial velocity.....	51
4.4 Local bubble size distribution in airlift systems.....	51
4.5 Axial bubble size distribution in airlift contactors.....	52
4.6 Effect of the ratio between downcomer and riser cross-sectional areas on bubble size.....	52
4.7 Overall volumetric mass transfer coefficient (k_La) in the airlift systems operating with sea water.....	53
4.6 Estimate of k_La	55

	Page
CHAPTER V CONCLUSIONS & RECOMMENDATIONS	72
5.1 Achievements & Contributions.....	72
5.2 Limitations & Recommendations.....	73
REFERENCES	74
APPENDICES	80
BIOGRAPHY	132



สถาบันวิทยบริการ
จุฬาลงกรณ์มหาวิทยาลัย

List of Tables

Table	Page
Table 1.1 Comparison of gas-liquid contacting devices.....	4
Table 2.1 Review on the investigations of liquid properties on the performance of pneumatic contactors.....	18
Table 2.2 Review on various liquid properties on hydrodynamic performance in pneumatic contactors.....	29
Table 3.1 Dimensions of draft tubes.....	45
Table 3.2 Locations of digital video camera for bubble size measurement.....	45
Table 4.1 Estimation values of disjoining pressures (Π) in different salinity levels.....	59
Table 4.2 Estimation value of pressure driving forces for bubble coalescence in various conditions.....	59
Table 4.3 Parameter values from the initial establishment of k_L correlation Equation (4.9).....	60
Table 5.1 Summation of characteristics in airlift contactor with different salinity levels.....	73

List of Figures

Figure	Page
Figure 1.1 The type of gas-liquid contactors: (a) stirrer tank reactor, (b) bubble column, (c) airlift contactor.....	6
Figure 2.1 Two configurations of ALCs: (split cylinder internal loop ALC (b) and (c) concentric internal loop ALCs (d) external loop ALC...	32
Figure 2.2 Schematic flow directions in airlift system.....	33
Figure 2.3 Interrelationship between bioreactor performance characteristics (Chisti, 1989).....	33
Figure 2.4 Oxygen transport path from the bubble to the bulk liquid and various regions where transport resistance encountered (Seader and Henley, 1998).....	34
Figure 2.5 Flow regimes in vertical flow (Teitel and Bornea, 1980 and Azbel and Nicholas, 1983).....	34
Figure 2.6 Effect of NaCl solution on gas holdup in various types of reactor.....	35
Figure 3.1 Schematic diagram of the concentric internal loop airlift contactor employed in this work.....	46
Figure 3.2 Configuration of airlift contactor and annulus sparger in this work.....	47
Figure 3.3 Major and minor axes of bubble images.....	48
Figure 4.1 Bubble sizes in ALC running at different salinity level ($A_d/A_r = 0.067$).....	61
Figure 4.2 Bubble sizes in ALC running at different salinity levels ($A_d/A_r = 0.661$).....	62
Figure 4.3 Pressure different in ALC running at different draft tube sizes ($A_d/A_r = 0.067-0.661$) and superficial gas velocity in blanket.....	63
Figure 4.4 Frequency distribution of bubble sizes at various superficial gas velocities in ALC with $A_d/A_r = 0.661$ (salinity = 30).....	64
Figure 4.5 Bubble size at different locations in ALC with $A_d/A_r = 0.661$ (salinity = 30 ppt).....	65
Figure 4.6 Bubble sizes at different draft tube sizes ($A_d/A_r = 0.067-1.01$) in	

Figure	Page
ALCs (salinity = 30 ppt).....	66
Figure 4.7 Overall volumetric mass transfer coefficient at different salinity levels (salinity =0, 15, 30 and 45 ppt) in ALC ($A_d/A_r = 0.661$).....	67
Figure 4.8 Effects of superficial gas velocity, u_{sg} on (a) overall gas holdup and (b) riser gas holdup with different draft tube sizes.....	68
Figure 4.9 Specific interfacial area at different salinity levels (salinity = 0, 15, 30 and 45 ppt) in ALC ($A_d/A_r = 0.661$).....	69
Figure 4.10 Effects of superficial gas velocity, u_{sg} on overall specific mass transfer coefficient, k_L	70
Figure 4.11 Comparison of $(k_L a)$ from experiment and $(k_L a)$ estimated by Equation (4.9) at different salinity levels (salinity = 0, 15, 30 and 45 ppt).....	71

List of Abbreviations & Notations

Abbreviations

ALCs	Airlift contactors
Gr	Grashof Number $\left(\frac{d_{Bs}^3 \rho_L \Delta \rho g}{\mu_L^2} \right)$
Re	Reynolds Number $\left(\frac{d_{Bs} v_s \rho_L}{\mu_L} \right)$
Sc	Schmidt Number $\left(\frac{\mu_L}{\rho_L D_L} \right)$
Sh	Sherwood Number $\left(\frac{k_L d_{Bs}}{D_L} \right)$

Notations

a	Specific interfacial area (m^2/m^3)
A_d	Downcomer cross sectional area (m^2)
A_r	Riser cross sectional area (m^2)
c	Dissolved oxygen concentration (mg/l)
c^*	Saturated oxygen concentration of solute (mg/l)
c_o	Initial dissolved oxygen concentration (mg/l)
d_B	An equivalent sphere diameter of bubble (mm)
d_{Bs}	Sauter mean diameter (mm)
d_o	Orifice diameter (cm)
D	Gas diffusivity (m^2/s)
D_L	Liquid diffusivity (m^2/s)
D_{ALC}	Airlift diameter (cm)
D_{dt}	Draft tube diameter (cm)
D_i	Inside draft tube diameter (cm)
D_{io}	Outer draft tube diameter (cm)
h	Video level (cm)
H	Height (cm)

Notations

g	Gravitational acceleration (cm/s^2)
k_L	Overall mass transfer coefficient (m/s)
k_{La}	Overall volumetric mass transfer coefficient (1/s)
n_i	Bubble number with an equivalent sphere diameter (-)
N	Gas-liquid mass flux (mg/s.m^2)
p	Major axes of bubble (mm)
p_A	Partial pressure of molecule A (atm)
P	Pressure difference (N/m^2)
q	Minor axes of bubble (mm)
Q	Volumetric flow rate (m^3/s)
t	Time (s)
u_{sg}	Superficial gas velocity (m/s)
u_α	Bubble rise velocity (m/s)
v	Liquid velocity (cm/s)
V	Volume (cm^3)
Z	Height of liquid level in manometer (cm)

Greek symbols

ε	Gas holdup (-)
μ	Viscosity (Pa.s)
π	Pi (-)
ρ	Density (kg/m^3)
σ	Surface tension (N/m)

Subscripts

d	Downcomer
r	Riser
o	Overall gas holdup
t	Gas-liquid separator

CHAPTER I

INTRODUCTION

1.1 Motivations

Current commercial manufactures of products such as pharmaceuticals (e.g. penicillins, streptomycins), enzymes, bulk chemicals (e.g. citric acid, ethanol), foods (e.g. vinegar, yoghurt, soy sauce, cheese, beer) and feeds (e.g. single cell protein) including treatment of several types of wastewaters rely significantly on the success in the cultivation of microbial populations. This, in several circumstances, is then dependent upon the availability of oxygen for microbial respiration in order for them to grow or to produce required products at proper rates as oxygen is often the least soluble and frequently the limiting nutrient. Hence, an enormous number of research works focused on the development of appropriate gas-liquid devices to obtain high oxygen transfer rate without necessitating high operating/installing costs.

Common gas-liquid contactors generally used in several biochemical processes are based on agitating type as these stirred reactors have been intensively examined and therefore commonly known among chemical engineers. However, there are several limitations on the use of such reactors; examples include high shear stress and high heat production which can easily be harmful to the cultivation of several shear sensitive microorganisms. Milder, pneumatic reactors such as bubble columns and airlift contactors were often proposed as alternative designs of gas-liquid contacting devices due to several reasons, e.g. adequate mixing and mass transfer, ease of design and maintenance. Table 1.1 provides a summary of the advantages and disadvantages of different types of reactors whereas Figure 1.1 is the simplified drawing of the reactors mentioned in this section.

Previous researches on airlift contactors with air-water systems have been extensively conducted which focused mainly on the effect of geometrical airlift contactors and liquid properties such as Limpanuphap's investigation in 2003. She concentrated on the effect of hydrodynamics and gas-liquid mass transfer in internal loop airlift contactor running with sea water however the important parameter such as

bubble size distribution had not been investigated. Later, Tanthikul (2004) investigated the hydrodynamic and mass transfer of the large scale multiple draft tube airlift contactor with large cross sectional area operated with both fresh and sea water. Again, the bubble size had not been visited in this work due to the unavailability of the reliable measurement technique. Moreover, recent applications of airlift systems at the Biochemical Engineering Research Laboratory, Department of Chemical Engineering, Faculty of Engineering, Chulalongkorn University, involved the cultivation of saline water microorganisms as they are significant as a feed supplement in most aqua-culture larvae i.e. shrimp and fish such as the cultivation of *Chaetoceros calcitrans* (Loataweesup, 2002) and the culture of *H. pluvialis* for the production of astaxanthin (Kaewpintong, 2004) etc. All reported successful operation which emphasized the significance of airlift systems.

In spite of all above advantages, there are still limited numbers of research works on the behavior of airlift contactor operated with saline water. Thus this work concentrates on characterizing the performance of airlift contactors where important parameters such as bubble size distribution, hydrodynamics, and mass transfer behavior of such system under various operating and geometric designing conditions will be examined.

1.2 Objectives

- 1.2.1 To investigate the effect of salinity on bubble size characteristics, hydrodynamics in internal loop contactors
- 1.2.2 To investigate the effect of superficial velocity and the ratio of downcomer to riser cross sectional areas on the behavior of internal loop airlift reactors running with sea water at different salinity levels
- 1.2.3 To investigate the effect of bubble size on gas-liquid mass transfer characteristics operated with sea water in the internal loop airlift reactors.

1.3 Scopes of this work

- 1.3.1 The investigations are restricted to bench-scale internal loop airlift contactors (ALCs) with annulus sparger and dimensions as shown in Table 3.1.
- 1.3.2 The systems are operated in an air-water and air-saline water systems with salinity of 15, 30 and 45 ppt.
- 1.3.3 In all investigations, the ALC systems are subjected to the following assumptions:
- Power consumption and gas composition are constant.
 - The system is isothermal which operates at 25°C, and the effect of the dynamics of the dissolved oxygen at electrode is negligible.
 - The system is operated at atmospheric pressure.
- 1.3.4 Only those bubbles within the focal region of the camera will be measured for their sizes.
- 1.3.5 The investigations of mass transfer characteristics are restricted to oxygen transfer only.
- 1.3.6 In the investigations of superficial velocity and hydrodynamic behavior, gas density is considered negligible compared to the density of the liquid.

Table 1.1 Comparison of gas-liquid contacting devices
(Chisti, 1989; Wongsuchoto, 2002 and Limpanuphap, 2003)

Type of gas-liquid contacting device	Advantages	Limitations
1. Stirred tank reactor (STR)	<ol style="list-style-type: none"> 1) Well defined performance and scale up 2) High mass transfer 3) Easy control of the gas dispersion and medium mixing by stirrer speed 4) Efficient gas dispersions by stirrers 5) Suitable for highly viscous media 	<ol style="list-style-type: none"> 1) High power consumption per unit volume of liquid 2) Difficulty in avoiding contamination due to seal of shaft 3) High shear stress and lack of uniformity in the fields of shear 4) Low oxygen transfer efficiency with respect to power input 5) Production of high degree of heat
2. Bubble column (BC)	<ol style="list-style-type: none"> 1) Simplicity of design and construction: no moving mechanical part needed for agitation 2) Ease of maintenance 3) Eliminating the danger of contamination through seals 4) Low power consumption 	<ol style="list-style-type: none"> 1) Low mass transfer efficiency in gas-liquid system 2) Lack of uniformity of liquid flow path

Type of gas-liquid contacting devices	Advantages	Limitations
3. Airlift contactor (ALC)	<ol style="list-style-type: none">1) Simplicity of design and construction: no moving mechanical part needed for agitation2) Ease of maintenance3) Eliminating the danger of contamination through seals4) Low power consumption5) Low capital cost6) Low and homogeneous shear stress region and uniform turbulence7) Better defined flow pattern8) Controllable liquid circulation rate	<ol style="list-style-type: none">1) Low mass transfer efficiency in gas-liquid system

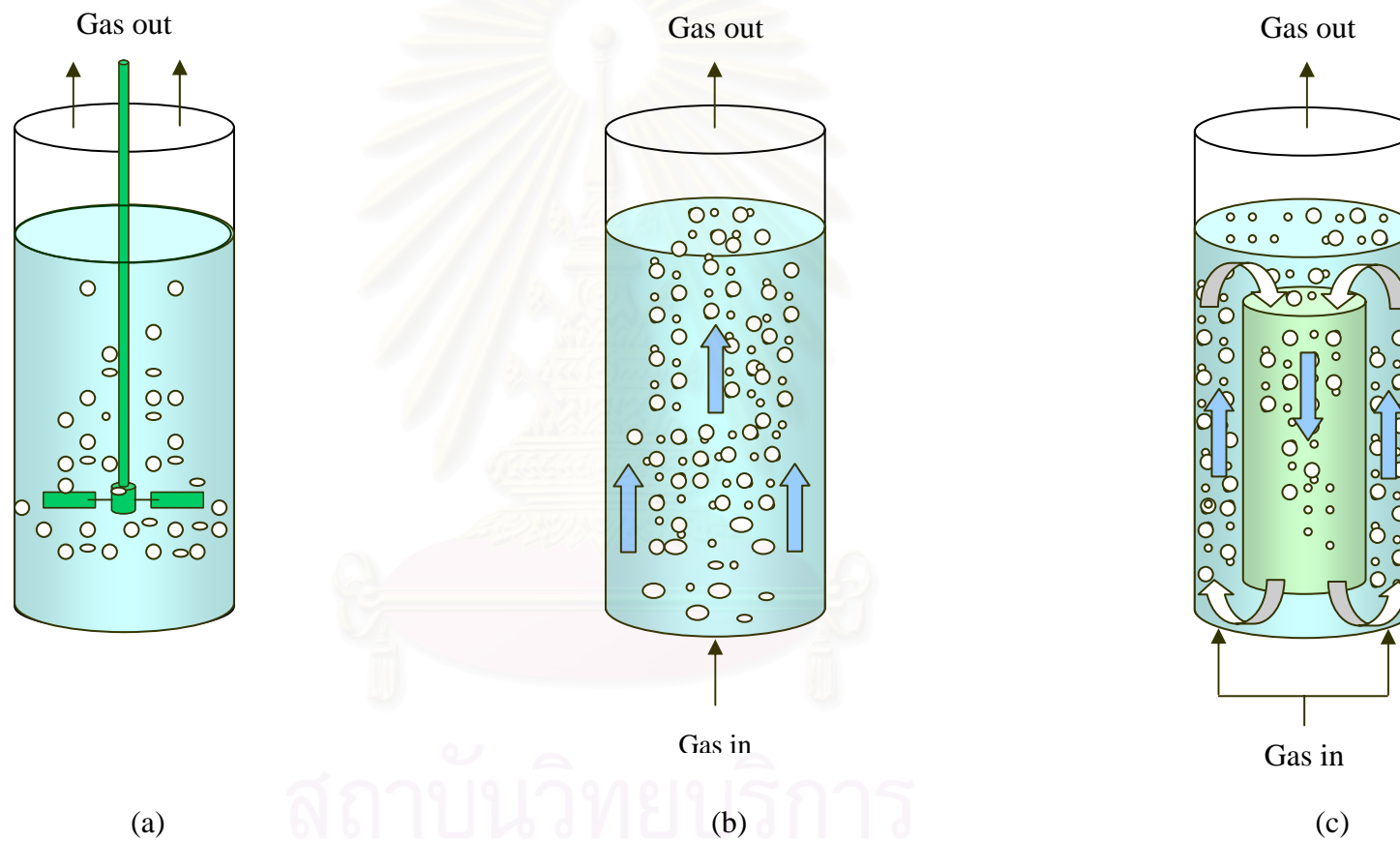


Figure 1.1 The type of gas-liquid contactors: (a) stirrer tank reactor, (b) bubble column, (c) airlift contactor

CHAPTER II

BACKGROUNDS & LITERATURE REVIEW

2.1 Airlift contactors

Airlift contactors (ALCs) consist of a liquid pool divided into two distinct zones. The different gas holdups in the aerated and unaerated zones cause different bulk densities of the fluid in these regions resulting in fluid circulation in the system (Chisti, 1989). The airlift contactors can be divided into two groups and three different regions as delineated below.

2.1.1 Type and configuration of airlift contactors

There are two basic classes of airlift contactors as shown in Figure 2.1:

- (1) Internal loop airlift contactors which is a simple bubble column split into a riser and a downcomer by an internal baffle (Figure 2.1 (a)-(c)).
- (2) External loop airlift contactors where riser and downcomer are two separated columns connected by horizontal tubes (Figure 2.1 (d)).

2.1.2 Three main regions of airlift contactors (Schematic flow directions shown in Figure 2.2)

Airlift contactors consist of three main sections:

(1) Riser: Gas is introduced into this section. Due to energy/momentum transfer, liquid flows co-currently with gas bubbles upwards along the length of the contactor.

(2) Gas-liquid separator: Most gas bubbles disengage from the liquid pool at this section. The degassed fluid becomes heavier than that in the riser and starts to move down into the downcomer.

(3) Downcomer: This section allows the downflow of liquid. Some small bubbles can also be dragged down the downcomer by the inertial force of the circulating liquid. The fluid recirculates back to the riser again at the bottom of the contactor.

Some stated that airlift contactors should consist of four main sections where the area that liquid flows from downcomer to riser is considered as an additional, bottom section. However, this section is usually very small compared to the other three sections and the effects of this section have so far not been visited. Further work in this regard is also currently under investigation in our research group.

2.2 Gas-liquid hydrodynamics and mass transfer

The aeration in airlift contactors causes turbulence and mixing in the system. However, due to the difference in gas distribution, the various compartments of the airlift contactors behave differently from each other both in terms of mass transfer and hydrodynamic performances. In fact, there are interrelationships between the various parameters and the behavior of the system as illustrated in [Figure 2.3](#). Details on hydrodynamic behavior and gas-liquid mass transfer characteristics of the airlift systems are described below.

2.2.1 Hydrodynamics behavior

2.2.1.1 Gas holdup

The volume fraction of the gas-phase in the gas-liquid dispersion is known as the gas void fraction or the gas holdup. The holdup affects the residence time of gas and the gas-liquid interfacial area which are important for gas-liquid mass transfer and therefore it is important that this quantity be examined for the operation of any gas-liquid contactors. The overall gas holdup (ε_o) can generally be calculated from:

$$\varepsilon_o = \frac{V_G}{V_G + V_L} \quad (2.1)$$

where V_G and V_L are the volumes of gas and liquid in the contactor, respectively.

Riser (ε_r) and downcomer gas holdups (ε_d) are related to the overall gas holdup (ε_o) from the following equation (assuming gas separator is resembled by the vertical extensions of riser and downcomer sections up to the liquid surface).

$$\varepsilon_o = \frac{A_r \varepsilon_r + A_d \varepsilon_d}{A_r + A_d} \quad (2.2)$$

Eq. (2.2) is derived through geometric parameters of reactors with uniform cross sectional riser and downcomer with the same height.

Often the gas holdups in the airlift contactors or other gas-liquid contactors are determined using empirical correlations to take into account the non-ideal behavior of the systems. For airlift cases, [Wongsuchoto \(2002\)](#) and [Limpanuphap \(2003\)](#) provided reviews on the available correlations regarding the gas holdups and other operating variables of the system. [Table 2.1](#) is an extension of the abovementioned review where additional literature during 2003-2005 was included. In general, gas holdups varied with superficial gas velocity but the extent of the gas holdup at certain specific gas velocity depended significantly on the configuration of airlift systems. Also properties of medium could impose dramatic deviation in the gas holdups.

2.2.1.2 Liquid velocity

The liquid circulation occurs due to two main causes. Firstly, the upward movement is induced from the energy/momentum balance from the input gas at the bottom of the contactor. Secondly, the differences in the fluid densities in riser and downcomer can also cause substantial liquid movement between the two sections. Generally, liquid velocity is measured in terms of linear liquid velocity defined as:

$$v_L = \frac{x_L}{t} \quad (2.3)$$

where x_L is the liquid path length and t is the average time for one complete movement. The superficial liquid velocity is the velocity calculated from the empty column (with no barrier) and therefore is different from the true linear velocity. The true velocity is always higher than superficial velocity as the area for the liquid movement is always blocked by the gas bubbles. The linear liquid velocities in riser, v_{Lr} , and in downcomer, v_{Ld} can be related to superficial velocity from:

$$v_{Lr} = \frac{u_{Lr}}{1 - \varepsilon_r} \quad (2.4)$$

and

$$v_{Ld} = \frac{u_{Ld}}{1 - \varepsilon_d} \quad (2.5)$$

There are various techniques to measure linear liquid velocity (v_{Lr} , v_{Ld}) such as a classic, color tracer injection method, where other electrolytic agents like KCl or acid and base tracers (HCl/NaOH solutions) can also be used as a tracer.

The superficial velocities are measured either in the riser (u_{Lr}) and the downcomer (u_{Ld}) where the relationship between the two quantities can be expressed using mass balance principle as:

$$u_{Lr}A_r = u_{Ld}A_d \quad (2.6)$$

This allows the estimation of one liquid velocity when the other is known.

Similar to gas holdups, liquid velocities were usually determined using empirical correlations to incorporate the non-ideal behavior of the systems. Table 2.1 summarizes some recent work regarding the estimate of liquid velocity in the airlift systems.

2.2.2 Gas-liquid mass transfer

Gas-liquid mass transfer rate is important particularly for the aerobic systems where the transfer of sparingly soluble oxygen could significantly limit the growth/reaction rate. In the gas-liquid contacting systems, the mass transfer between phases is often described by the Two-Film model where both liquid and gas films on both sides of the bubble could exert some mass transfer resistance (Figure 2.4). Often, the mass transfer resistance on the liquid side is significantly greater than that in the gas side, and the overall mass transfer resistance is controlled mostly by the resistance of the liquid film.

At steady-state mass transfer of molecular oxygen diffuses from gas phase across interface into bulk liquid phase can be postulates as (Seader and Henley, 1998):

$$N_A = \frac{(D_{AB})_G}{\delta_G} (p_{A_g} - p_{A_{gi}})_G = \frac{(D_{AB})_L}{\delta_L} (c_{A_i} - c_{A_b})_L \quad (2.7)$$

where N_A is molar flux of A (sparingly soluble species), $(D_{AB})_G$, $(D_{AB})_L$ are diffusivity in gas and liquid phase respectively. p_{A_g} and $p_{A_{gi}}$ are concentration of A in bulk gas and at interface and c_{A_b} , c_{A_i} are concentrations of A in bulk liquid and at interface, respectively.

In cases where the equilibrium can be explained by Henry's law, and k_g is considerably larger than k_L (as the gas phase diffusivities are vastly greater than those in liquids, i.e. $D_{\text{oxygen in air}} \simeq 10^4 \times D_{\text{oxygen in water at } 20^\circ\text{C}}$) (Bailey and Ollis, 1986), the overall flux expressed as the overall concentration driving force is:

$$N_A = k_L (c_A^* - c_{A_b}) \quad (2.8)$$

k_L is known as the overall mass transfer coefficient based on liquid phase concentration and c_A^* is equilibrium concentration with partial pressure in the bulk gas.

Often the gas-liquid mass transfer rate and the flux are related by:

$$aN_{O_2} = \frac{dc_{O_2}}{dt} \quad (2.9)$$

where a is the specific mass transfer area which is equal to the total mass transfer area divided by the dispersed volume in the system. Therefore the rate of oxygen mass transfer at steady-state can be written as:

$$\frac{dc_{O_2}}{dt} = k_L a (c_{O_2}^* - c_{O_2}) \quad (2.10)$$

where $k_L a$ is the overall volumetric mass transfer coefficient, $c_{O_2}^*$ and c_{O_2} is the equilibrium oxygen and dissolved oxygen concentration at any time t in the liquid, respectively.

The potential rate of mass transfer is typically reflected in the term $k_L a$ where the measurement of such quantity often follows the dynamic method as described in Section 3.3.4. In the case where the specific interfacial area (a) is known, the mass transfer coefficient, k_L , can simply be calculated from (Chisti, 1989):

$$k_L = \frac{k_L a}{a} \quad (2.11)$$

a can be obtained using the information on Sauter mean diameter (d_{Bs}) and gas holdup (ε) as follows:

$$a = \frac{6\varepsilon}{d_{Bs}(1-\varepsilon)} \quad (2.12)$$

A large number of literature demonstrated the relation between $k_L a$ and other operating/design variables. These have been reviewed by Wongsuchoto (2002), Limpanuphap (2003) and Tanthikul (2004). In general, the overall volumetric mass transfer coefficient varied with superficial velocity. Airlift configuration such as the ratio between the areas of downcomer and riser also played a significant part in controlling the mass transfer rate. Limpanuphap (2003) and Tanthikul (2004) also proved that the gas distributor and the medium properties significantly affected the behavior of the system.

2.3 Flow regimes

The movement of gas and liquid phases in the vertical tube leads to a number of flow patterns or regimes depending on the characteristics of mediums and vessel such as fluid properties, tube size and distribution of gas and liquid depending on gas velocity. [Teitel and Bornea \(1980\)](#) and [Kantarci et al. \(2005\)](#) classified four basic patterns of fluid flow based on liquid circulation and bubble characteristics such as coalescence and break-up as shown in [Figure 2.5](#). In general however, flow regimes in pneumatic contactors could be divided into two types: (i) homogeneous (bubbly-flow) and (ii) heterogeneous (churn-turbulent) bubbling regimes where the relationship between gas holdup and superficial gas velocity could be illustrated as depicted in [Figure 2.6](#), ([Snape et al., 1995](#), [Zahradnik et al., 1997](#), [Olmos et al., 2003](#) and [Tsao- Jen and Po-Chou, 2005](#)). Flow regimes affected the bubble size in the column and, as a result, influenced oxygen mass transfer rate from gas to liquid. In most cases, the bubble flow regime allowed a maximum amount of gas residing in the column ([Shah, 1983](#)), however, the mass transfer coefficient for this flow regime was rather low as there was little turbulence involved with the flow. Churn turbulence, on the other hand, although allowed gas bubbles to pass through rapidly which resulted in a rather low gas holdup, created a better mixing between gas and liquid which, in turn, led to a lower mass transfer resistance, or higher specific rate of mass transfer. The ultimate rate of mass transfer therefore significantly depended on operating conditions.

2.4 Bubble size distribution

2.4.1 Determination of bubble size distribution

There are several methods generally employed for the determination of interfacial area, for instance, the Danckwerts method which was based on the absorption of CO₂ in sodium or potassium carbonate–bicarbonate buffer solutions, dynamic gas disengagement method and photographic technique. In practice, bubble size is measured in terms of Sauter mean diameter, d_{Bs} , which refers to a diameter of a sphere with the same volume as the bubble:

$$d_{Bs} = \frac{\sum_{i=1} n_i d_{B,i}^3}{\sum_{i=1} n_i d_{B,i}^2} \quad (2.13)$$

where n_i is the bubble number having an equivalent sphere diameter, $d_{B,i}$ and d_B is the sphere diameter with the same volume as ellipsoidal bubble (see detail in [Section 3.3.1](#)).

The entire range of ascending bubbles velocity can be tentatively divided into four regions ([Treybal, 1980 and Kafarov, 1985](#)):

- 1) $d_B < 0.7$ mm: The bubbles behave like solid particles and their velocities are governed by Stokes' law which is depended on liquid properties and particle characteristic;
- 2) $0.7 \text{ mm} < d_B < 1.4$ mm: The bubbles retain the spherical shape but internal circulation appears, thus decreasing the stress on the interface. The ascent velocity exceeds the value calculated by Stokes' law;
- 3) $1.4 \text{ mm} < d_B < 6.0$ mm: The bubbles are no longer spherical and ascend in zig-zag manner. The resistance to their motion increase due to the hydrodynamic trail formation. A change in the bubble diameter does not have significant effect on the ascent velocity;
- 4) $d_B > 6$ mm: The bubbles are bowl-shaped. The limiting ascent velocity increases with the bubble diameter.

Most previous reports concentrated on the system without interaction between bubbles. In actual situation, bubbles occur in swarm and the interaction between them is utterly unavoidable. In these cases, the bubble size, especially in air-water systems, varies depending on contactor and distributor configurations. Mostly literatures demonstrated that higher gas flow rate often caused the bubble size to grow smaller in size and resulted in a log-normal size distribution. A larger diameter and a high number of annular sparger led to a larger bubble size, ([Wongsuchoto et al., 2003](#)). In the vicinity of gas sparger, an increase in gas flow rate often enlarged the bubble size whereas an increase in a number of holes resulted in the opposite result. Moreover, bubble size distribution near the sparger region was sensitive to the distance between holes (pinch), and a decreased pinch caused a reduction in bubble size, ([Polli et al., 2002](#)). As the bubbles traveled through the column to the top section, their sizes became smaller. This was due to the interaction between the bubbles which led to a breakup of the bubbles, and this was more pronounced at increasing gas velocity condition, ([Colella et al., 1999, Polli et al., 2002 and Wongsuchoto et al., 2003](#)).

In many industrial devices, bubbles are formed by forcing gas through an orifice into a pool of liquid. As the force is directed towards the center of the bubbles, the resulting bubble shape is normally sphere. As bubbles travel through the system, its size changes depending on liquid and gas properties which are, in turn, related to buoyant and surface forces. General equation for gas bubble growing at a circular orifice shown as (De Nevers, 1991):

$$d_b = \left[\frac{6d_o\sigma}{(\rho_l - \rho_g)g} \right]^{1/3} \quad (2.14)$$

where d_b is bubble diameter, d_o is orifice diameter, ρ_l , ρ_g are liquid density and gas density, respectively.

The bubble size distribution depended on medium physical properties such as density, surface tension, viscosity. In aqueous electrolyte systems, the interaction of bubbles at the orifice depended on the surface elastic value, E . This value was proportional to $E = \frac{4c}{DkT} \left(\frac{d\gamma}{dc} \right)^2$, when c is the solute concentration, D the interfacial thickness and γ the surface tension. A higher value of E (NaCl concentration above 0.1 M) inhibited bubble coalescence after leaving the orifice, producing smaller bubbles particularly at high gas flow rate, (Hofmeier et al., 1995 and Weissenborn et al., 1996). At low gas flow rate ($Q_G < 1$ ml/s), the bubble sizes in cationic and anionic surfactants were smaller than those in tap water because of dynamic surface tensions. On the other hand, at higher gas flow rate related to static surface tension that controlled by the power dissipated and break up and coalescence phenomena, (Painmanakul et al., 2005).

Moreover large bubble size formation was found in high viscosity medium for example as CMC (high surface tension), due to breakage and demotes coalescence. However in low viscosity for example as electrolytes was lower surface tension caused to smaller bubble formation, (Mouza et al., 2005).

2.4.2 Bubble size and gas-liquid mass transfer

Bubble size can be related to the gas-liquid mass transfer coefficient, k_L , using several reported correlations. For instance, the Frossling's equation stated that k_L varied with

the square root of bubble rise velocity (which was a function of bubble size) (Painmanakul et al., 2005):

$$k_L = 2\sqrt{\frac{D_{O_2}U_B}{\pi q}} \quad (2.15)$$

where U_B is bubble rise velocity, q is minor axes of ellipsoidal bubble and D_{O_2} is oxygen diffusivity, m^2/s . This equation was valid for the cases of rigid sphere bubbles with the size in the range from 0.1 - 2.0 mm. For larger bubbles ($d_B > 2.5$ mm), the Higbie's theory for mobile sphere could be applied:

$$k_L = \frac{D}{d_B}(2 + 0.6Re^{1/2}Sc^{1/3}) \quad (2.16)$$

where D is gas diffusivity, m^2/s . Note that this investigation was performed in a bubble column. Wongsuchoto et al. (2003), however, reported that the mass transfer coefficient in the airlift system was constant, independent of the aeration rate. The overall volumetric mass transfer coefficient was, on the other hand, increased as the specific interfacial area (a) increased with gas flow provided the flow was still in the churn turbulent regime.

2.5 Effects of geometry and liquid properties on airlift contactor performance

Liquid properties play a significant role in dictating the airlift system performance; for instance, the density of sea water depends on temperature, salinities and pressure. For airlift systems, as an increase in salinity leads to an increase in liquid density, this consequently affects the liquid circulation. Viscosity is a type of liquid property that measures the resistance of liquid motion; for example, lowering CMC (carboxy methyl cellulose) concentration often led to a higher liquid velocity in comparison with solutions with high CMC concentration, (Guo-Qing et al., 1995). As large bubbles were formed with the solution with low CMC, bubble rise velocity and liquid velocity were also high. Usually, surface tension (σ) is the attraction force between molecules in the liquid with the direction towards the center of the bubble. There are a number of literatures dealing with effects of configuration and medium on performance of airlift contactor and these are summarized in Table 2.2.

When gas is purged through the riser of the column, it causes the dissipation of energy and shear rate and the level of energy dissipation varied from location to location within the column. [Contreras et al. \(1999\)](#) operated the concentric airlift with different sizes and types of spargers in sea water system, and they showed that the largest dissipated energy was in the riser, followed by that in the gas separator, and the smallest in the downcomer, respectively. The shear rate behaved differently depending on the type of flow regime that occurred in the system, and mostly shear rate was ordered from large to small as the bottom, the gas separator, the riser, and the downcomer, respectively. Small orifices were also shown to create low shear force, ([Merchuk et al., 1998](#) and [Contreras et al., 1999](#)).

The overall mass transfer coefficient is a variable to demonstrate the efficiency of oxygen gas transfer from gas to liquid medium. This quality depends notably on the system geometry and liquid properties. In the uniform bubbly flow, spargers with smaller pores resulted in higher k_{La} than the system with large sparger pores, ([Contreras et al., 1999](#)). When compared between the various mediums, higher k_{La} was obtained from the system which created smaller bubbles, for instance, systems running with sea water would have higher k_{La} than that obtained with fresh water, ([Contreras, et al, 1999](#)). In addition, the airlifts running with a highly viscous carboxymethyl cellulose (CMC) solution exhibited much lower k_{La} than systems with lower viscosity, ([Guo-Qing et al., 1995](#) and [Vasconcelos et al., 2003](#)). Moreover, k_{La} in the gas separator was higher than those in riser and downcomer, ([Guo-Qing et al., 1995](#)). The addition of chemicals into the system could also change the level of k_{La} . For instance, in most biological systems, antifoam was added to prevent the excessive formation of foam which could deteriorate the cultivation. However, the addition of antifoam caused the liquid properties to change as it was aimed to decrease the surface tension of the liquid. This, unfortunately, reduced k_{La} of the system as the addition of antifoam would also promote the coalescence between bubble and reduced the mass transfer area, ([Al-Masry, 1999](#) and [Vasconcelos et al., 2003](#)). Apart from the liquid properties, literature showed that the geometry of the system such as the ratio between areas in downcomer and riser (A_d/A_r) in airlifts could notably affect the mass transfer rate, i.e. the airlifts with larger A_d/A_r usually encountered lower k_{La} than systems with smaller A_d/A_r , ([Wongsuchoto et al., 2003](#)). The influence of airlift geometry on the mass transfer rate has been extensively studied and the findings were completely summarized in [Wongsuchoto \(2003\)](#).

The gas holdup is the fraction of gas in the system. Mostly, the amount of gas holdup increased with gas flow rate, regardless of the type of mediums, (Guo-Qing et al., 1995, Snape et al., 1995 and Zahradnik et al., 1997). The effect of orifices in the gas sparger seems to have great effect on the gas holdup. As the orifice diameter decreased, smaller bubbles were formed which moved slower than large bubbles, and therefore the gas holdup increased. This effect was similar to that obtained in the case of increasing orifice numbers (whilst keeping the gas flow rate constant). Liquid properties exhibited significant effect on gas holdup too. Literature illustrated that higher viscosity mediums could accommodate higher gas holdup than mediums with lower viscosity, (Merchuk et al., 1998 and Limpanuphap, 2003). This was because viscosity caused the bubble to move more slowly and, as a result, each bubble remained in the system longer. In addition, viscosity seemed to show anti-coalescence for the contacting systems which, in certain circumstances particularly in the condition where the aeration rate was fast, slowed down the bubbles. For sugar solution, higher sugar concentration could only slightly accommodate gas holdup and caused a lower gas-holdup pneumatic system, (Guo-Qing et al., 1995 and Snape et al., 1995).

A number of literatures were dealt with the effects of NaCl and the results are summarized in Figure 2.6. It can easily be extracted from this figure that the addition of NaCl increased the gas holdup. The effect was strong at low NaCl concentration, and was faded away as the concentration became high. The effect of inhibited coalescence led the long stable homogeneous flow zone from this graph, (Merchuk et al., 1998 and Limpanuphap, 2003). This result is significant for the operation of airlift systems using sea water as liquid phase as often encountered in several aquaculture applications, (Krichnavaruk et al., 2005).

Table 2.1 Review on the investigations of liquid properties on the performance of pneumatic contactors

No.	Authors	Summary	Experimental conditions
1.	Chisti, 1989	<p>Bubble column:</p> $\varepsilon_{0.15 M NaCl} > \varepsilon_{water} > \varepsilon_{1\% SF sol.} > \varepsilon_{2\% SF sol.} > \varepsilon_{3\% SF sol.}$ $K_{La} 0.15M NaCl = K_{La} 1\% SF sol. > K_{La} 2\% SF sol. > K_{La} 3\% SF sol.$ <p>Airlift:</p> $\varepsilon_{0.15 M NaCl} > \varepsilon_{1\% SF sol.} > \varepsilon_{2\% SF sol.}$ $K_{La} 0.15M NaCl > K_{La} 1\% SF sol. > K_{La} 2\% SF sol.$	<p>Bubble column , Internal loop airlift reactor,annulus sparger</p> <p>Rectangular: $A_d/A_r = 0.614$</p> <p>gas - liquid or slurries (NaCl, Solka Floc cellulose fiber)</p> <p>$0 < u_{sg} < 30$ cm/s</p> <p>$0.17 < \eta < 9.06$ Pa.s or Pa.sⁿ</p> <p>Methods :</p> <p>Gas holdup: volume expansion or manometer</p>
2.	Popovic and Robinson, 1988	$\varepsilon_r = 0.465 (U_{sg})^{0.65} [1 + A_d/A_r]^{-1.06} (\eta_{eff})^{-0.103}$ $U_l = 0.23 (U_{sg})^{0.32} [A_d/A_r]^{0.97} (\eta_{eff})^{-0.39}$	<p>External loop airlift reactor</p> <p>System : Air - Non newtonian fluid and Viscous newtonian</p> <p>$0.11 < A_d/A_r < 0.44$</p> <p>$0.02 < \eta_{eff} < 0.5$ Pa.s</p> <p>$2.0 < U_{sg} < 26$ cm/s</p>
3.	Popovic and Robinson, 1989	$k_{La} = 2.14 \times 10^{-3} (U_{sg})^{0.52} [1 + A_d/A_r]^{-0.85} (\eta_{eff})^{-0.89}$	<p>External loop airlift reactor</p> <p>System : Air - Non newtonian fluid and Viscous newtonian</p>

No.	Authors	Summary	Experimental conditions
		Or $k_L a = 0.5 \times 10^{-2} (U_{sg})^{0.52} (D_L)^{0.5} [1 + A_d/A_r]^{-0.85} (\eta_{eff})^{-0.89} (\rho_L)^{1.03} (\sigma_L)^{-0.75}$	$0 < A_d/A_r < 0.44$ CMC: $0.02 < \eta_{eff} < 0.5$ Pa.s Sucrose: $\eta = 0.019$ Pa.s $2.0 < U_{sg} < 26$ cm/s $0.33 < D_L \times 10^9 < 2.53$ m ² /s $59 < \sigma_L \times 10^3 < 79$ N/m
4.	Philip et al., 1990	For viscous newtonian liquids; $\mathcal{E}_{lower\ viscosity} < \mathcal{E}_{higher\ viscosity}$ $U_{ID,water} > U_{ID,viscous\ newtonian\ liquid}$ For non newtonian liquids; No trend for gas hold up $U_{ID,water} > U_{ID,viscous\ newtonian\ liquid}$	Internal loop reactor , inner sparger circle cross section: $A_d/A_r = 1.78$ square cross section: $A_d/A_r = 3$ gas - fluid (olive oil, SAE, castor oil, sugar syrup, CMC, xanthan solution) $1.5 < U_{sg} < 11.7$ cm/s $0.115 < \eta < 2.85$ Pa.s or Pa.s ⁿ $0.03 < \sigma < 0.08$ N/m

No.	Authors	Summary	Experimental conditions
5.	Snape et al., 1992	<p>Aqueous sugar solutions;</p> <p>$\varepsilon_{\text{lower concentration}} > \varepsilon_{\text{higher concentration}}$</p> <p>$U_{l,\text{lower concentration}} > U_{l,\text{higher concentration}}$</p> <p>Aqueous electrolyte solutions;</p> <p>$\varepsilon_{\text{lower concentration}} < \varepsilon_{\text{higher concentration}}$</p>	<p>Methods :</p> <p>Gas holdup: visual observation</p> <p>Liquid velocity: metal detectors</p> <hr/> <p>External loop airlift reactor</p> <p>$v = 65 \text{ dm}^3, A_d/A_r = 1.33$</p> <p>$15.7 < U_{sg} < 22 \text{ cm/s}$</p> <p>$0.000887 < \eta_{\text{electrolyte}} < 0.000962 \text{ Pa.s or Pa.s}^n$</p> <p>$0.00101 < \eta_{\text{sucrose solution}} < 0.00141 \text{ Pa.s or Pa.s}^n$</p> <p>$57.3 < \sigma_{\text{electrolyte}} < 69.8 \text{ N/m}$</p> <p>$60.5 < \sigma_{\text{sucrose solution}} < 69.5 \text{ N/m}$</p> <p>Air - aqueous electrolyte system</p> <p>(NaCl,KCl,Na₂SO₄,MgSO₄,CaCl₂) 0.01- 0.2 M</p> <p>Air - sugar solution system (0.5-8 % v/w)</p> <p>Methods:</p> <p>gas holdup: visual observation</p>

No.	Authors	Summary	Experimental conditions
6.	Zhao et al., 1994	$k_{La} \text{ air lift} < k_{La} \text{ bubble column}$ $\varepsilon \text{ air lift} < \varepsilon \text{ bubble column}$ $k_{La} \text{ liquid} > k_{La} \text{ highly viscous liquid}$ $\varepsilon \text{ liquid} > \varepsilon \text{ highly viscous liquid}$	liquid velocity: conductivity pulse technique using KCl Bubble column , Internal loop airlift reactor, inner sparger $A_d/A_r = 1.8$ gas - fluid fluid : water, sugar (40%,97%), olive oil, SAE (20,40,50), castor oil, CMC (0.1%,3.5%, 0.75%, 1.5%) $0.78 < U_{sg} < 6.5$ cm/s $0.001 < \eta < 1.26$ Pa.s or Pa.s ⁿ $0.03 < \sigma < 0.07$ N/m
7.	Guo-Qing et al., 1995	Airlift reactor: $\varepsilon_{Gr, 4\% \text{ wtCMC}} < \varepsilon_{Gr, 3\% \text{ wtCMC}} < \varepsilon_{Gr, 2\% \text{ wtCMC}} < \varepsilon_{Gr, 1\% \text{ wtCMC}} < \varepsilon_{Gr, \text{ water}}$ $\varepsilon_{Gd, 2\% \text{ wtCMC}} < \varepsilon_{Gd, 3\% \text{ wtCMC}} < \varepsilon_{Gd, 4\% \text{ wtCMC}} < \varepsilon_{Gd, 1\% \text{ wtCMC}} < \varepsilon_{Gd, \text{ water}}$ $v_{L, 4\% \text{ wtCMC}} < v_{L, 3\% \text{ wtCMC}} < v_{L, 2\% \text{ wtCMC}} < v_{L, 1\% \text{ wtCMC}} < v_{L, \text{ water}}$ $t_{c, \text{ water}} < t_{c, 1\% \text{ wtCMC}} < t_{c, 2\% \text{ wtCMC}} < t_{c, 3\% \text{ wtCMC}} < t_{c, 4\% \text{ wtCMC}}$	Medium: carboxymethyl cellulose (CMC) -water
8.	Pironti et al., 1995	$\varepsilon \text{ high siliceous sand} < \varepsilon \text{ low siliceous sand}$	Internal loop airlift reactor , central sparger

No.	Authors	Summary	Experimental conditions
			$A_d/A_r = 3.44$ System : Air - slurry (siliceous sand) $121 < C_{siliceous\ sand} < 230 \text{ Kg/m}^3$ $0 < U_{sg} < 25 \text{ cm/s}$ Methods: Gas holdup: pressure transmitters connected to a data acquisition system
9.	Snape et al., 1995	External-loop airlift reactor: aqueous saccharose solutions : $\epsilon_{4\% \text{ wt}} > \epsilon_{0.5\% \text{ wt}} = \epsilon_{\text{tab water}} > \epsilon_{8\% \text{ wt}}$ $V_{Ld\ 1.0\% \text{ wt}} > V_{Ld\ 2.0\% \text{ wt}} > V_{Ld\ 4.0\% \text{ wt}} > V_{Ld\ \text{tab water}} > V_{Ld\ 8.0\% \text{ wt}}$ electrolyte solutions : $\epsilon_r \text{ KCl} > \epsilon_r \text{ NaCl} > \epsilon_r \text{ Na}_2\text{SO}_4 > \epsilon_r \text{ water}$	Two perforated plates, hole diameter 0.5 and 1.6 mm Medium: aqueous saccharose solutions 0.5 – 8.0 %wt and electrolyte solutions of NaCl, KCl, CaCl ₂ , Na ₂ SO ₄ and MgSO ₄ 0.01 and 0.2 kmol/m ³ Salt concentration: $\text{MgSO}_4 < \text{BaCl}_2 < \text{Na}_2\text{SO}_4 < \text{CaCl}_2 < \text{NaCl} < \text{KCl} < \text{KI}$ $0.028 < u_g < 0.198 \text{ m/s}$
10.	Hwang and Cheng., 1997	Airlift contactor: ring gas sparger $\epsilon_{gr}: 0.1 > 0 \text{ (water)} > 0.25 > 0.5 > 0.8 \text{ wt\% CMC (small, low velocity bubble)}$ $\epsilon_{gd}: 0.1 > 0 \text{ (water)} > 0.25 > 0.8 > 0.5 \text{ wt\% CMC (low bubble rise velocity)}$ $\epsilon_{gO}: 0 \text{ (water)} \sim 0.1 > 0.25 > 0.5 > 0.8 \text{ wt\% CMC}$ $V_{lr}: 0 \text{ (water)} > 0.1 > 0.25 > 0.5 > 0.8 \text{ wt\% CMC}$ $V_{ld}: 0 \text{ (water)} > 0.1 > 0.25 > 0.5 > 0.8 \text{ wt\% CMC}$	Medium: three phase with CMC ($\tau = KY^n = \mu_{app} Y$), gas, polystyrene particles Assume: polystyrene ~ liquid phase

No.	Authors	Summary	Experimental conditions
		$\varepsilon_{gd} = 0.00174 Q_g^{0.735} \left(\frac{A_d}{A_r} \right)^{-0.378} \mu_h^{-0.388} H_d^{0.125} \times (1 + \varepsilon_g)^{-2.060}$ <p>when $\varepsilon_g = \varepsilon_{gr} = \varepsilon_{gd}$</p>	
11.	Zahradnik et al., 1997	<p>ε_G: $d_o = 1.6 \text{ mm} < d_o = 0.5 \text{ mm}$ in all conditions</p> <p>$d_o = 0.5 \text{ mm}$: $\varepsilon_{G,\text{distilled}} < \varepsilon_{G,0.2\%} < \varepsilon_{G,1.0\%} = \varepsilon_{G,0.5\%}$</p> <p>$d_o = 1.6 \text{ mm}$: $\varepsilon_{G,\text{distilled}} < \varepsilon_{G,0.2\%} < \varepsilon_{G,1.0\%} = \varepsilon_{G,0.5\%}$</p> <p>$d_o = 0.5 \text{ mm}$: $\varepsilon_{G,\mu=110\text{mPas}} < \varepsilon_{G,\mu=30\text{mPas}} < \varepsilon_{G,\mu=19\text{mPas}} < \varepsilon_{G,\mu=8.2\text{mPas}} < \varepsilon_{G,\mu=3\text{mPas}} < \varepsilon_{G,\text{distilled}}$</p>	<p>Ethanol 0.2 -1.0 wt%</p> <p>Saccharose solutions 30-55 wt%</p>
12.	Al-Masry and Abasaed, 1998	<p>Xantan gum :</p> $\varepsilon_r = 0.9856 (U_{sg})^{0.8747} (\eta_{eff})^{0.0577}$ $k_{La} = 0.0032 (U_{sg})^{0.7271} (\eta_{eff})^{-0.5282}$ <p>CMC :</p> $\varepsilon_r = 0.3245 (U_{sg})^{0.9032} (\eta_{eff})^{-0.0925}$ $k_{La} = 0.0032 (U_{sg})^{0.8797} (\eta_{eff})^{-0.6966}$ <p>Adding antifoam :</p>	<p>External loop airlift reactor</p> <p>$A_d/A_r = 1$</p> <p>System : Air – Non lectroma fluid (xanthan gum and CMC)</p> <p>Antifoam agent : silicone polymer</p> <p>$0.0663 < \sigma_{xanthan\ gum} < 0.0696 \text{ N/m}$</p> <p>$0.0590 < \sigma_{CMC} < 0.0688 \text{ N/m}$</p> <p>$0.2 < U_{sg} < 6 \text{ cm/s}$</p> <p>Methods:</p>

No.	Authors	Summary	Experimental conditions
		$\varepsilon_{\text{xanthan gum solution}} > \varepsilon_{\text{water}}$ $D_{b,\text{xanthan gum solution}} < D_{b,\text{water}}$ $U_{l,\text{xanthan gum solution}} < U_{l,\text{water}}$ $k_{La,\text{xanthan gum solution}} < k_{La,\text{water}}$ Air – cmc system :	Gas holdup: using a differential pressure cell and u-tube manometer Liquid velocity: electromagnetic flowmeter K_{La} : DO meter both riser and downcomer (bigger bubbles)
13.	Al-Masry, 1999	$\varepsilon_{\text{silicone}} < \varepsilon_{\text{water}}$ $U_{l,\text{silicone}} < U_{l,\text{water}}$ $k_{La,\text{silicone}} < k_{La,\text{water}}$	External loop airlift reactor $A_d/A_r = 0.25, 1$ System : Air - water Antifoam agent : silicone polymer $0.036 < \sigma < 0.046$ N/m $0 < U_{sg} < 25$ cm/s Methods: Gas holdup: using a differential pressure cell and u-tube

No.	Authors	Summary	Experimental conditions
			manometer Liquid velocity: electromagnetic flowmeter K_{La} : DO meter
14.	Van Baten et al., 2003	Bubble columns: computational fluid dynamics (CFD) model $V_{L, 0.1di} < V_{L, 0.38di} < V_{L, 1di}$ $\varepsilon_{, 1.0di} < \varepsilon_{, 0.38di} < \varepsilon_{, 0.1di}$ $k_{La, 1di} < k_{La, 0.38di} < k_{La, 0.1di}$ $\varepsilon_{r, 1.0di} < \varepsilon_{r, 0.38di} < \varepsilon_{r, 0.1di}$ $V_{r, 0.1di} < V_{r, 0.38di} < V_{r, 1.0di}$	Medium: air–water system with diameter 0.1, 0.38 and 1m $0.01 < u_g < 0.08$ m/s
15.	Rodrigues and Rubio, 2003	Clear acrylic column: $0.1 < d_B < 0.5$ mm $d_{B, 30 \text{ mg/l}} < d_{B, 20 \text{ mg/l}} < d_{B, 10 \text{ mg/l}} < d_{B, 5 \text{ mg/l}}$ higher Saturation pressure, higher sauter mean diameter	air–tap water system $0.8 < Q_g < 1.0$ l/min Surfactant concentration range 0–30 mg/l (but lower surface tension from $72.6 < \sigma < 61.3$ mN/m)
16.	Vasconcelos et al., 2003	Bubble column and rectangular airlift contactors: orifices perforated plate Airlift: $k_{La, 0.0016} < k_{La, 0.0031} < k_{La, 0.0048} < k_{La, 0.0065} < k_{La, 0.0083}$ Lower antifoam concentration, higher k_{La}	antifoam solutions of 0.5–100 ppm orifice diameter 0.5 – 3 mm

No.	Authors	Summary	Experimental conditions
		$k_{L, 0.0016, 0.5 \text{ mm}} \cong k_{L, 0.0016, 3 \text{ mm}}$ $k_{L, 0.0083, 0.5 \text{ mm}} < k_{L, 0.0083, 3 \text{ mm}}$ Bubble column: $k_{La, 0.0016} < k_{La, 0.0031} < k_{La, 0.0048} < k_{La, 0.0065} < k_{La, 0.0083}$ $k_{L, 0.022 \text{ m/s}, 0.1 \text{ ppt}} < k_{L, 0.022 \text{ m/s}, 0.5 \text{ ppt}} < k_{L, 0.022 \text{ m/s}, \text{ water}}$ Lower liquid height, higher k_{La}	$0.0016 < u_g < 0.0083 \text{ m/s}$
17.	Wongsuchoto et al., 2003	Airlift contactors: $d_{B, \text{ top}} < d_{B, \text{ middle}} < d_{B, \text{ bottom}}$ Larger size with increased number of orifices k_{La} increased with u_{sg} but decreased with increasing A_d/A_r	$0.067 < A_d/A_r < 1.0$ $5 < \text{Number of orifices} < 14$
18.	Wongsuchoto and Pavasant, 2004	Annulus sparged internal loop airlift contactor: $V_{Lr, \text{ cal}} < V_{Lr, \text{ measured}}$ in all condition of $V_{Lr, 0.067} < V_{Lr, 1.540}$ V_{Ld} no trend $A_d/A_r, 0.067 Q_{Ld} < Q_{L, \text{ dn}} < Q_{L, \text{ up}}$ $A_d/A_r, 0.431 Q_{Ld}, Q_{L, \text{ dn}} < Q_{L, \text{ up}}$ $A_d/A_r, 0.988 Q_{L, \text{ dn}} < Q_{Ld} < Q_{L, \text{ up}}$ $A_d/A_r, 1.540 Q_{L, \text{ dn}} < Q_{Ld} < Q_{L, \text{ up}}$	$0.067 < A_d/A_r < 1.540$

No.	Authors	Summary	Experimental conditions
		$Q_{Lr,dn}/Q_{Lr,up}: A_d/A_r, 1.540 < A_d/A_r, 0.988 < A_d/A_r, 0.431 < A_d/A_r, 0.067$	
19.	Azher et al., 2005	<p>Square split-rectangular airlift bioreactor: single-orifice nozzle</p> <p>ε_{gr} propanol: 0.1% > 0.075% > 0.05% > 0.01% > 0%</p> <p>ε_{gd} propanol: 0.01% > 0.05% > 0.075% > 0.1% > 0%</p> <p>$\varepsilon_{gO, water}$ < methanol 0.05% < propanol 0.05% < butanol 0.05%</p> <p>$k_L a_L$: 0% > methanol 0.05% > propanol 0.05% > butanol 0.05%</p> <p>$k_L a_L$ propanol: 0% > 0.01% > 0.05% > 0.075% > 0.1%</p>	<p>Medium: air-water as added propanol from 0.01 to 0.1% (v/v)</p> <p>σ: butanol < propanol < metanol</p> <p>0.01 < u_{sg} < 0.085 m/s</p>
20.	Felice, 2005	<p>External airlift reactors:</p> <p>Air-water: $\Delta P_D/\Delta P_{exp} * 100, H_{1m} < \Delta P_D/\Delta P_{exp} * 100, H_{2m}$</p> <p>$Q_{L, H_{2m}} > Q_{L, H_{1m}}$</p> <p>Air-water-solid: $Q_{L, 0.6 kg} < Q_{L, 0.3 kg}$</p> <p>$\Delta P_D/(\Delta P_D + \Delta P_C) * 100, H_{1m} < \Delta P_D/(\Delta P_D + \Delta P_C) * 100, H_{2m}$</p>	Medium: air, tap water, glass spheres
21.	Gourich et al., 2005	<p>Split-rectangular airlift contactor: a single-orifice with 3.5 mm diameter</p> <p>in all cases: $\varepsilon_{gd} = 0.94\varepsilon_{gr} - 0.016$ $\varepsilon_g = 1.277U_{gr}^{1.06}$</p> <p>$K_L a_L = 1.45U_{gr}^{1.28}$, $K_L a_L = (0.6038s^{-1})\varepsilon_g$</p>	<p>Medium: air-water and solid(polystyrene)-water</p> <p>0.01 < u_g < 0.08 m/s</p>

No.	Authors	Summary	Experimental conditions
22.	Painmanakul et al., 2005	<p data-bbox="595 384 1384 405">Glass bubble column: using silicone elastomer glue membrane sparger</p> <p data-bbox="595 437 927 458">d_B cationic, d_B anionic < d_B tap water</p> <p data-bbox="595 469 1167 489">a tap water < a anionic < a cationic between 1.5 and 10 1/m</p> <p data-bbox="595 521 1301 542">$k_L a$ anionic, $k_L a$ cationic < $k_L a$ tap water between 0.00035 and 0.003 1/s</p> <p data-bbox="595 590 902 611">k_L anionic, k_L cationic < k_L tap water</p>	<p data-bbox="1480 384 2114 405">Medium: σ Tap water > σ Anionic surfactant (Sodium laurylsulfate 110 mg/l)</p> <p data-bbox="1480 437 2114 496">>σ Cationic surfactant (ammonium bromine) > σ Anionic surfactant (Sodium laurylsulfate 1900 mg/l) > σ Cationic surfactant (Lauryl dimethyl benzyl)</p> <p data-bbox="1480 521 1816 542">0.3 < gas flow rate < 3.5 ml/s</p>

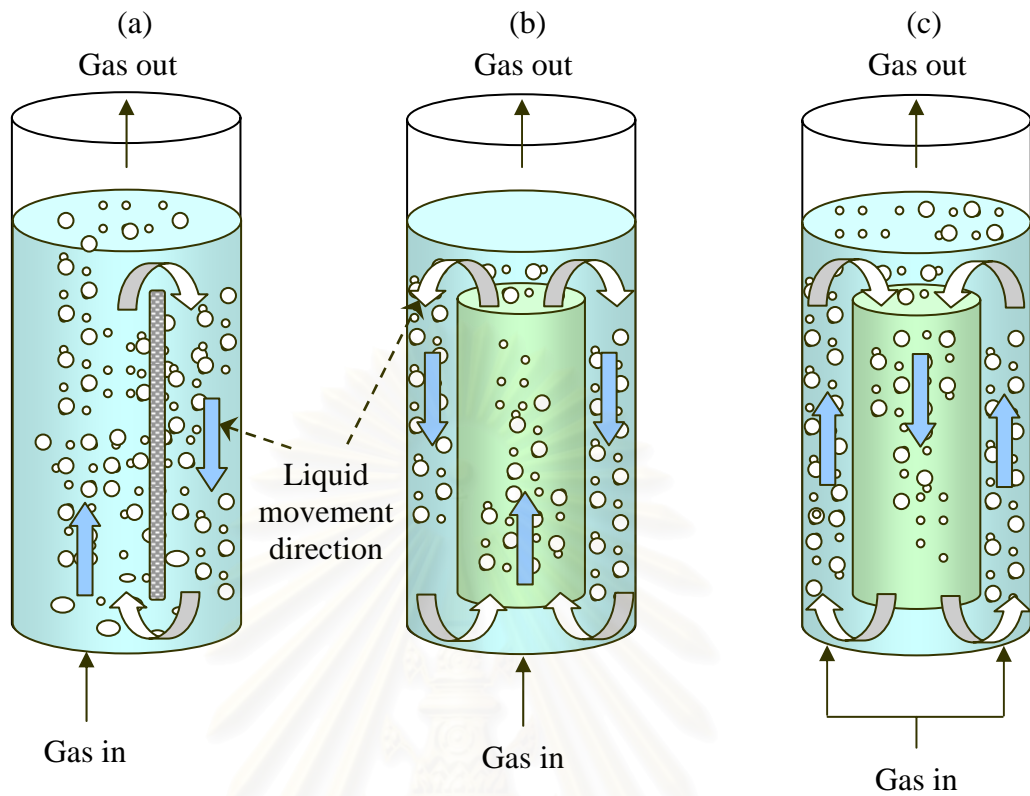
Table 2.2 Review on various liquid properties on hydrodynamic performance in pneumatic contactors

Substances	Properties	References
1. Alcohol	$\varepsilon_{gO,water} < \varepsilon_{gO,methanol} < \varepsilon_{gO,propanol} < \varepsilon_{gO,butanol}$ (σ : butanol < propanol < methanol < water) :long carbon chain with high hydrophobicity & co-response with bubble diameter) Low aeration rate: linear $k_L a_L$ Low oxygen transfer: high alcohol concentration contradict with theory Increase gas holdup: increasing alcohol concentration Reduced different between riser and downcomer gas holdup Decrease driving force on liquid circulation	Azher et al., 2005
2. Anionic surfactant (sodium carbonate–bicarbonate buffer with sodium arsenite, SLS)	$k_L = K_2 u_G^{0.5}$, $k_L = K_3 \sigma^{1.35}$, $k_L = K_4 \sigma^{1.35} u_G^{0.5}$ A (interfacial area) \uparrow with $\downarrow \sigma$ (surface tension), \uparrow surfactant concentration $ad_c = K_5 \cdot Re^{0.98} \cdot Sc^{0.57} \cdot Fr^{0.09} \cdot Bo^{-0.70} \left(\frac{d_p}{d_c} \right)^{-0.19}$	Vázquez et al., 2000
3. Carboxymethyl cellulose (CMC) non-Newtonian fluid	$\varepsilon_{Gr} = 44.4 J_{Gr}^{0.841} \mu_{ap}^{-0.135}$ $\varepsilon_{Gd} = 29.7 J_{Gr}^{0.935} \mu_{ap}^{-0.107}$ both gas holdup depended strongly on J_{Gr} $Q_L = J_{Ld} A_d = J_{Lr} A_r = V_{Ld} \left(1 - \frac{\varepsilon_d}{100} \right) A_d$ Liquid velocity increased: increasing gas velocity and decreasing apparent viscosity $k_L a = 3.43 \times 10^{-2} J_{Gr}^{0.524} \mu_{ap}^{-0.255}$	Guo-Qing et al., 1995

Substances	Properties	References
	<p>CMC property: $\tau = K\Upsilon^n = \mu_{app}\Upsilon$</p> <p>Low aeration rate: linear gas holdup with gas flow rate</p> <p>High aeration rate: increase slightly gas holdup (bubble coalescence)</p> <p>High CMC: decrease gas holdup (large bubble form at high viscosity)</p> <p>Increasing gas flow rate: increase liquid velocity but slightly increase with high gas flow rate (higher friction factor)</p> <p>Increasing CMC concentration: decrease liquid velocity</p> $\varepsilon_{gd} = 0.00174 Q_g^{0.735} \left(\frac{A_d}{A_r} \right)^{-0.378} \mu_h^{-0.388} H_d^{0.125} \times (1 + \varepsilon_g)^{-2.060} \text{ when } \varepsilon_g = \varepsilon_{gr} = \varepsilon_{gd}$	Hwang and Cheng, 1997
4. Electrolyte solution	<p>Increase $k_L a$: increasing gas flow rate in cationic and anionic but smaller than water σ and surface coverage ratio (se) for predicting the k_L values</p> <p>Higher surface tension: higher bubble diameter and lower interfacial area (a)</p> <p>Faster absorption kinetics in anionic surfactant than caionic</p> <p>Increase stability on homogeneous regime (non-coalescence bubble)</p> <p>Riser gas holdup depend on ionic-strength</p>	Painmanakul et al., 2005 Snape et al.,1995
5. Salinity	<p>Stronger in-coalescence effect in sea water than NaCl</p> <p>ε_r: sea water > NaCl 38 > 30 > 20 > 10 > 0 kg/m³</p> $k_L a_L = 0.1633(\varepsilon)^{1.0187} (J_{Lr})^{-0.6187}$ $k_L a_L = C \sqrt{D_L} \frac{6\varepsilon}{d_b(1-\varepsilon)} \left(\frac{E_D}{V_D \mu_L} \right)^{1/4}$ $k_L a_L = C \sqrt{D_L} \left(\frac{6\varepsilon}{d_b(1-\varepsilon)} \right)^{5/4} \left(\frac{2H\gamma}{t_c} \right)^{1/4}$	Merchuk et al., 1998 Contreras et al, 1999

Substances	Properties	References
6. Saccharose solution	Decrease gas holdup: increasing saccharose concentration (increasing viscosity) Increase aeration rate: increase gas holdup but the driving force for liquid circulation remains constant or even decreases (increasing bubble entrainment)	Snape et al., 1995

Internal loop airlift contactors



External loop airlift contactor

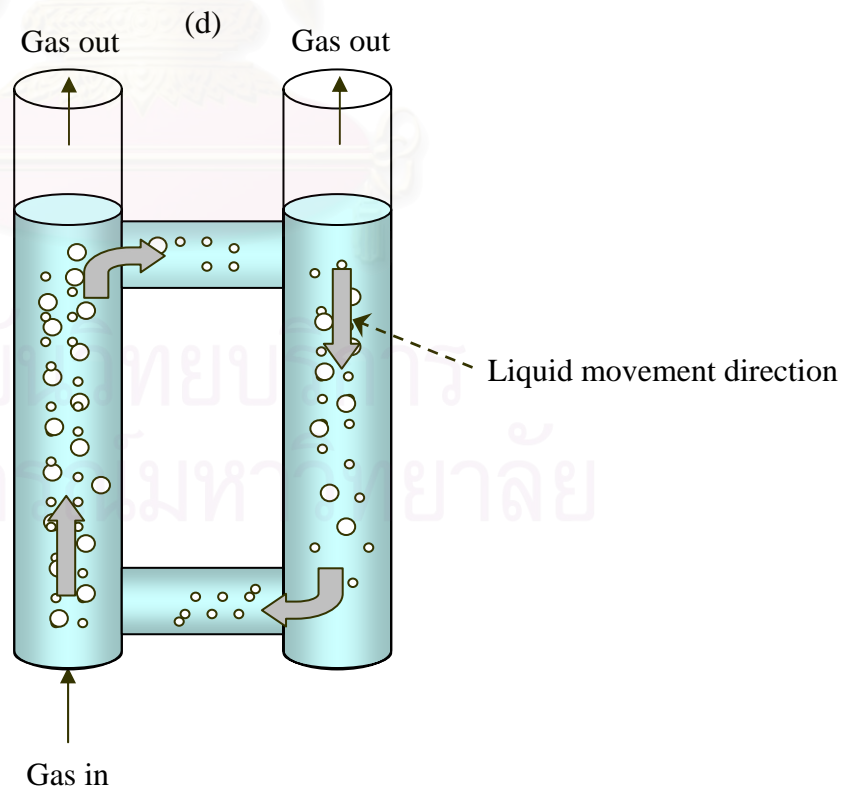


Figure 2.1 Two configurations of ALCs: (a) split cylinder internal loop ALC (b) and (c) concentric internal loop ALCs (d) external loop ALC

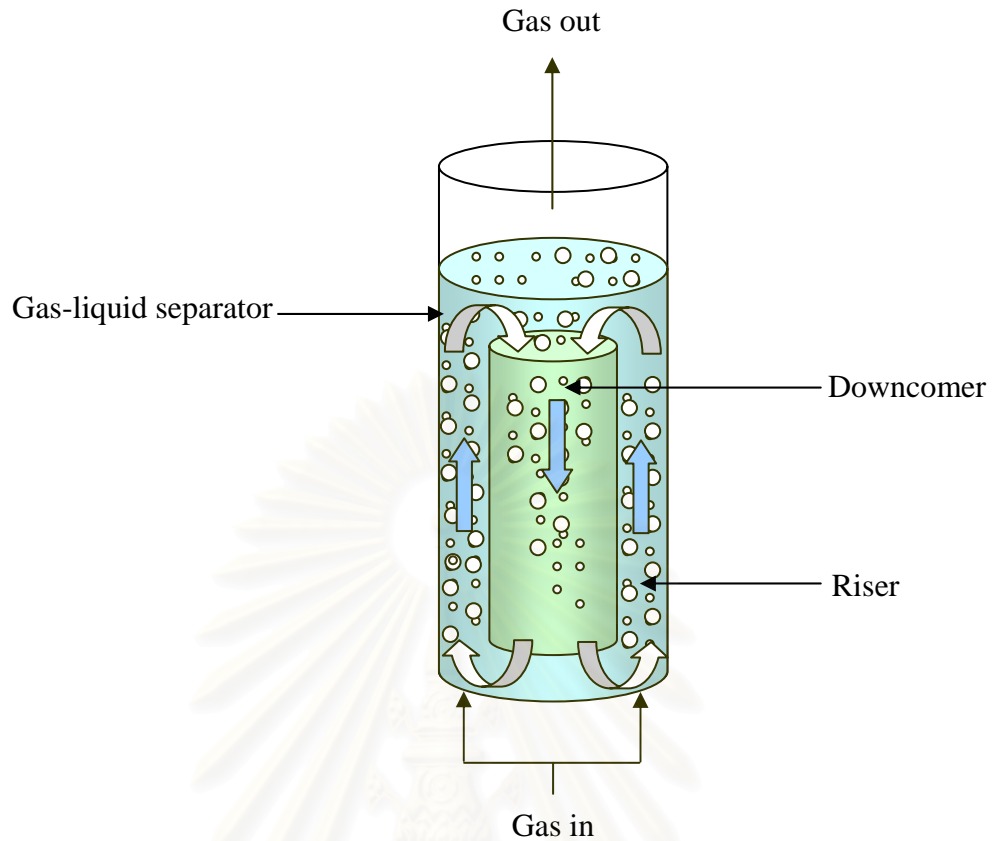


Figure 2.2 Schematic flow directions in airlift system

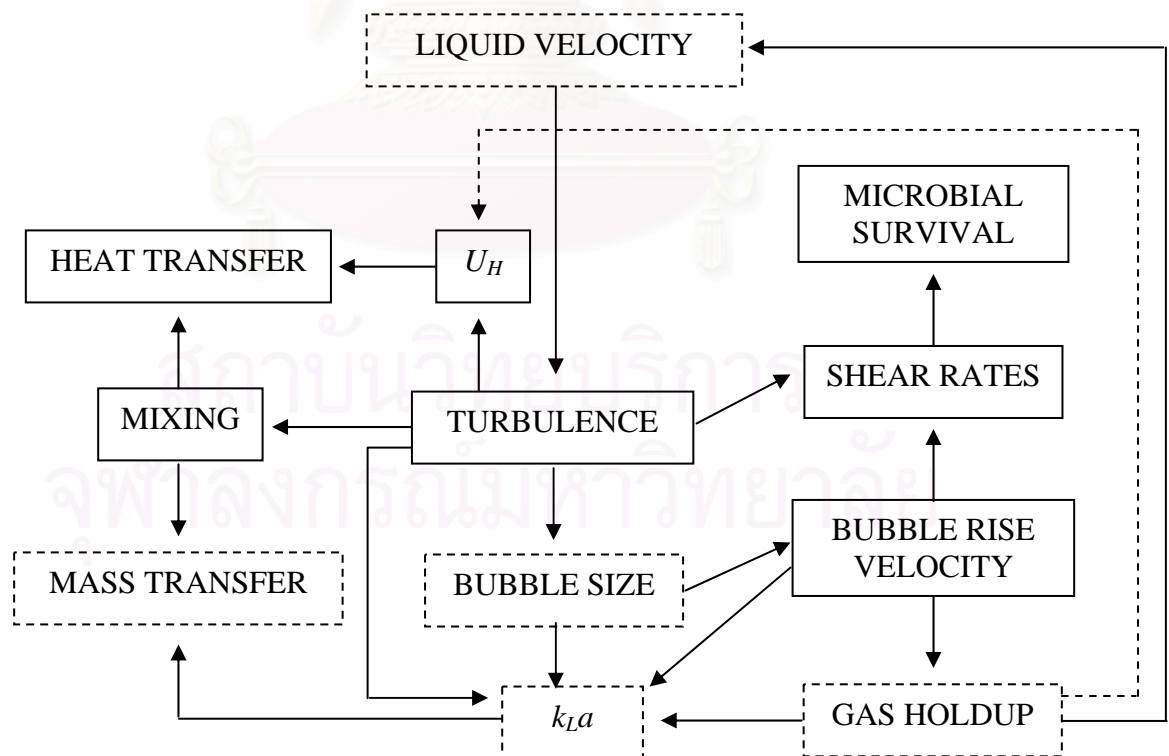


Figure 2.3 Interrelationship between bioreactor performance characteristics

(Chisti, 1989)

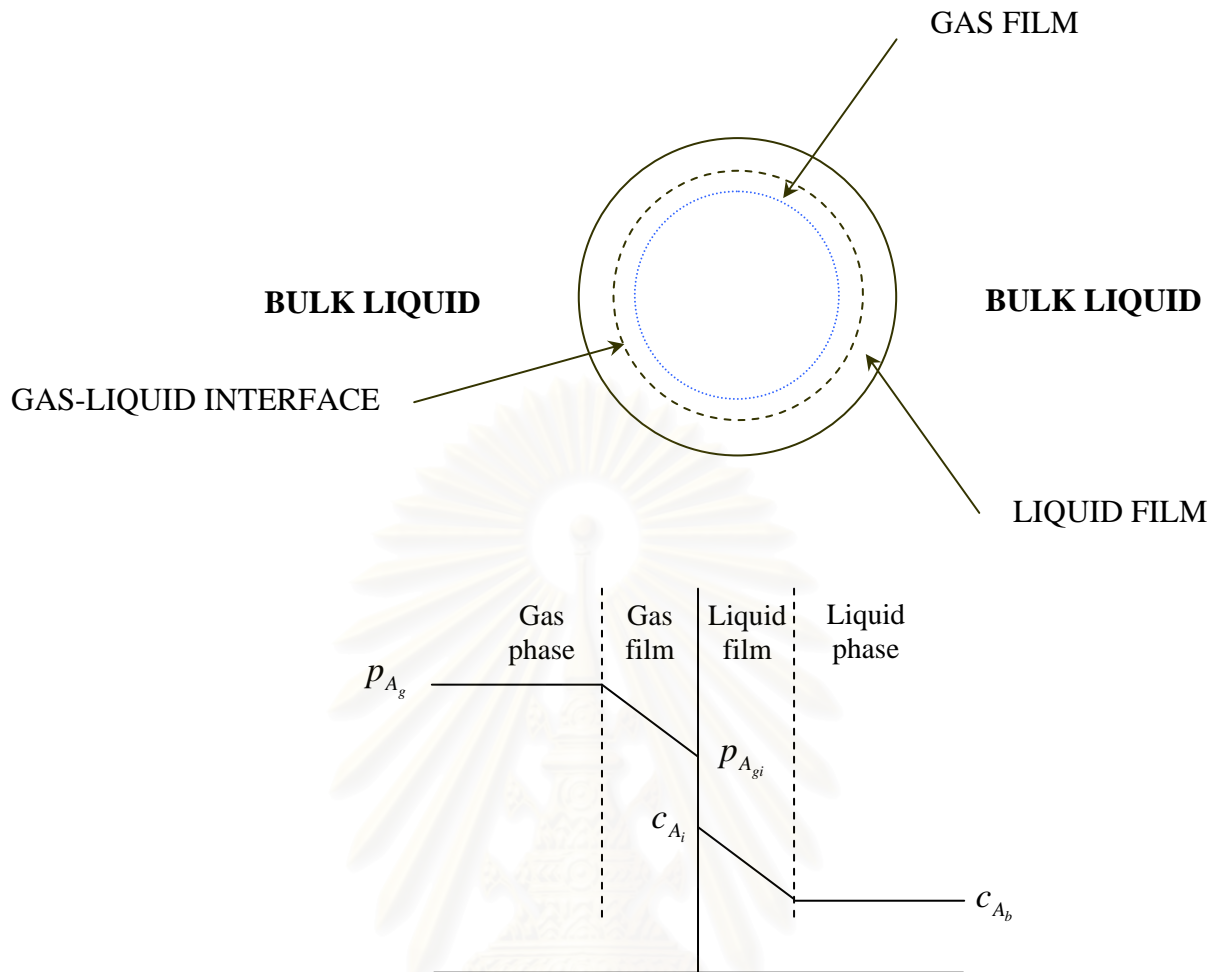


Figure 2.4 Oxygen transport path from the bubble to the bulk liquid and various regions where transport resistance encountered (Seader and Henley, 1998)

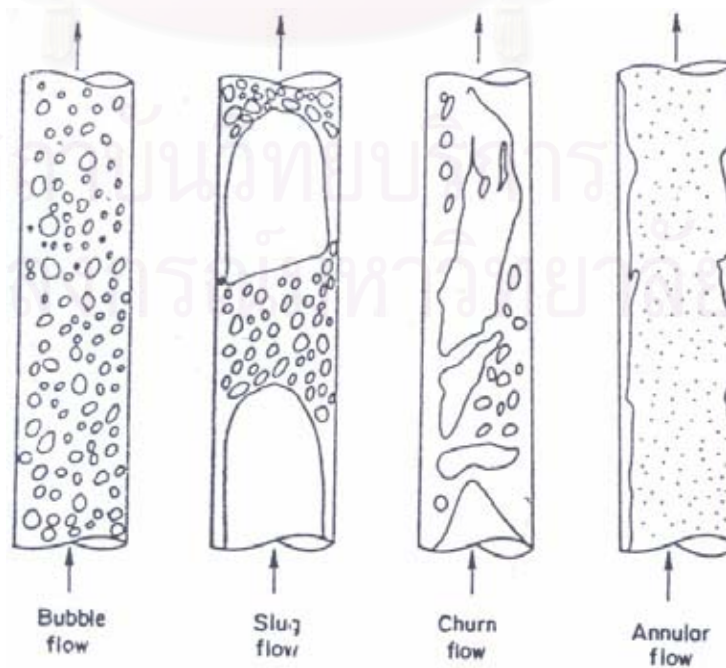


Figure 2.5 Flow regimes in vertical flow (Teitel and Bornea, 1980 and Azbel and Nicholas, 1983)

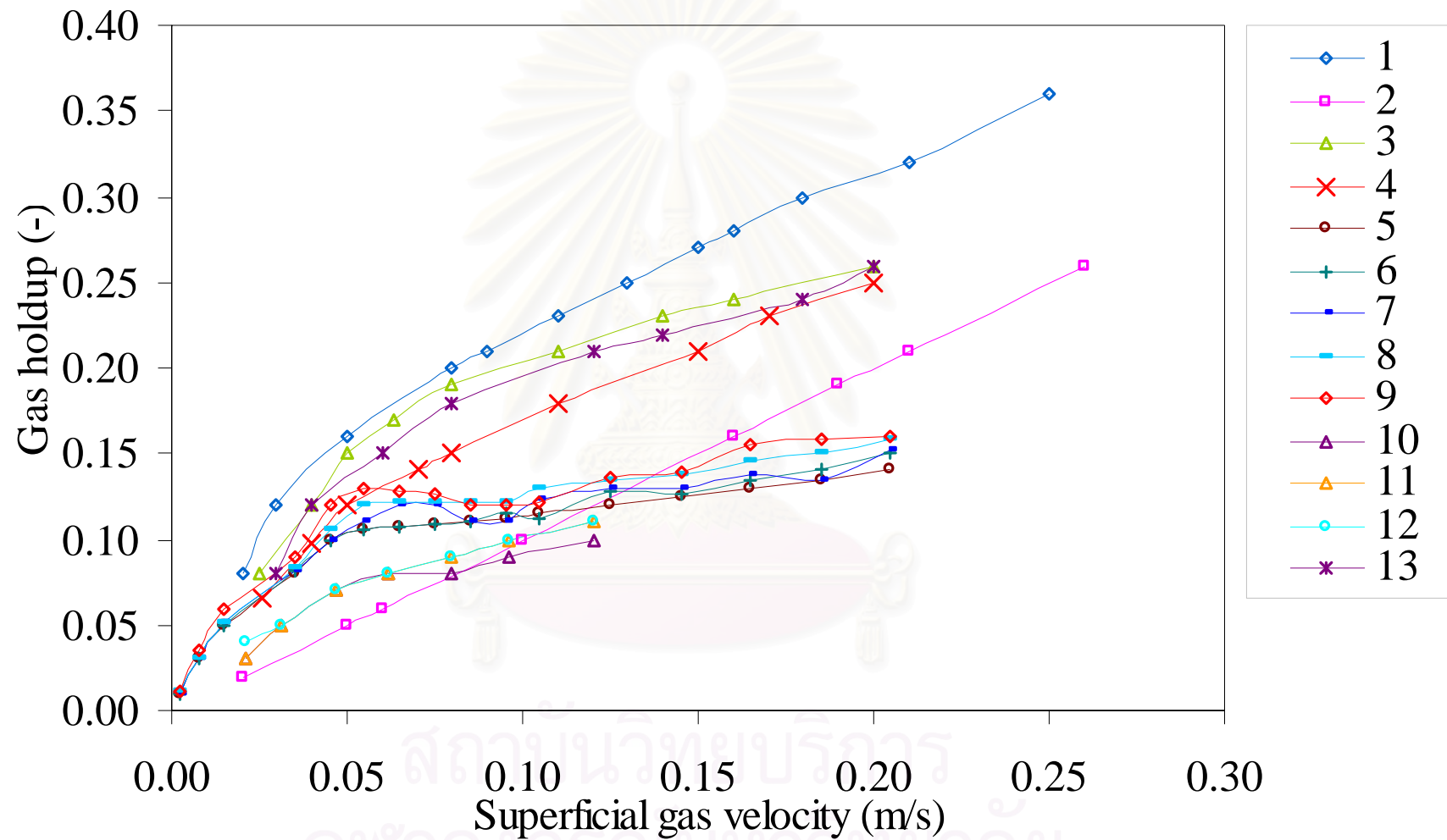


Figure 2.6 Effect of NaCl solution on gas holdup in various types of reactor

Nomenclature of **Figure 2.6**

No.	Authors	Condition
1	Zahradnik et al., 1997	Bubble column, $d_o = 0.16$ mm, NaCl = 0.145 mol/l
2	Zahradnik et al., 1997	Bubble column, $d_o = 0.5$ mm, NaCl = 0.145 mol/l
3	Zahradnik et al., 1997	External-loop airlift contactor, $d_o = 0.5$ mm, NaCl = 0.145 mol/l
4	Zahradnik et al., 1997	External-loop airlift contactor, $d_o = 0.16$ mm, NaCl = 0.145 mol/l
5	Merchuk et al., 1998	Porous sintered glass 60 μ m airlift, 10 kg/m ³
6	Merchuk et al., 1998	Porous sintered glass 60 μ m airlift, 20 kg/m ³
7	Merchuk et al., 1998	Porous sintered glass 60 μ m airlift, 30 kg/m ³
8	Merchuk et al., 1998	Porous sintered glass 60 μ m airlift, 38 kg/m ³
9	Merchuk et al., 1998	Porous sintered glass 60 μ m airlift, sea water
10	Limpanuphap 2003	Annular airlift contactor, $d_o = 1$ mm, 15 ppt
11	Limpanuphap 2003	Annular airlift contactor, $d_o = 1$ mm, 30 ppt
12	Limpanuphap 2003	Annular airlift contactor, $d_o = 1$ mm, 45 ppt
13	Snape et al., 1995	External loop airlift, NaCl = 0.15 kgmol/m ³

CHAPTER III

MATERIAL & METHODS

3.1 Experimental setup

A schematic diagram of experimental system employed in this work is shown in Figure 3.1. The airlift contactor consists of a concentric internal loop airlift contactor (ALC) with the main column height of (H) of 150 cm and an inside diameter of 13.7 cm. A draft tube (100 cm height, H_{dt}) is inserted centrally inside the main column. Both concentric columns are made from transparent acrylic plastic to allow visual observation for the bubble size characteristics and to record the movement of the color tracer for liquid velocity measurement. The ratio between downcomer and riser cross sectional areas (A_d/A_r) is altered by changing the draft tube diameter (D_{dt} in Figure 3.2) to new draft tubes with dimensions as shown in Table 3.1. Each draft tube is located at 10 cm above the base of the contactor. The gas is dispersed through the porous sparger installed at the base of the main column where the gas flow rate is regulated in the range from 0 to 8 cm/s by a calibrated rotameter. A dissolved oxygen (DO) meter (JENWAY model 9300) is used to measure dissolved oxygen in the dispersion for the estimation of the mass transfer rate. The experiment is performed as a gas-liquid system with water or sea water as liquid phase and air as gas phase. The sea water is prepared using sea salt and a refractometer is used to measure the level of salinity (OPTIK Handheld Refractometers). During the experiment, the medium is pumped continuously into the column until the liquid level is 3 cm above the draft tube after which air is supplied into the system. The system is then left running for a certain period of time to ensure a steady state operation before taking further measurement.

3.2 Experimental procedures

3.2.1 Bubble characteristics measurement

The measurements of bubble size and distribution are performed only in the riser of the internal loop ALC using a direct observation with photographic technique method. The bubble sizes are measured at three levels along the height of the column as shown in the parameter h_i in Table 3.2. The number of bubble sizes for each measurement is more than 200 bubbles. The correction of the size due to curve of the contactor is performed based on the scale attached to the draft tube. The experimental steps are detailed as follows:

Procedure

1. Fill tap water into the concentric column until the liquid level (H_L) reaches 3 cm above the top of the draft tube
2. Turn on the lamp to illuminate the observation-desired point
3. Open valve to continuously disperse compressed air from an air compressor through the annular sparger to the column
4. Adjust superficial velocity (u_{sg}) to the desired value by using calibrated rotameter
5. Record images of the bubbles at three different heights as shown in Table 3.1
6. Calculate the bubble size by using Equation 3.1
7. Repeat Steps 1 to 6 with other new geometric and/or operating parameters

3.2.2 Gas holdup measurement

The overall gas holdup is determined by the volume expansion method. The gas holdup in the annular section is determined by the manometric method. The experimental steps are detailed as follows:

Procedure

1. Fill tap water into the concentric column until the liquid level (H_L) is 3 cm above the top of the draft tube
2. Open valve to continuously disperse compressed air from an air compressor through the sparger to the column
3. Adjust superficial velocity (u_{sg}) to the desired value by using calibrated rotameter

4. Read the liquid dispersion height (H_D) to evaluate the overall gas holdup in the airlift contactor
5. Measure the pressure difference between the two positions (ΔP) in the annular section using the attached water manometer to evaluate the riser gas holdup. The calculation is then performed according to Equations 3.5 and 3.13. However, the gas holdup in the draft tube cannot be measured directly so downcomer gas holdup is calculated following Equation 3.16.

3.2.3 Liquid velocity

The measurement is done by a dye tracer method with detail as follows:

Procedure

1. Fill tap water into the concentric column until the liquid level (H_L) reaches the level 3 cm above the top of the draft tube
2. Open valve to continuously disperse compressed air from an air compressor through the sparger to the column
3. Inject dye tracer directly into the measuring port to measure riser liquid velocity and inject into the measuring beginning position to measure downcomer. The motion of the dye tracer is visually observed and a stopwatch is used to measure the time between the two positions.
4. Calculate riser and downcomer liquid velocity following Equations 3.17 and 3.18
5. Repeat Steps 1 to 4 with other geometric and/or operating parameters

3.2.4 Mass transfer coefficient measurement

The overall volumetric mass transfer coefficient ($k_L a$) is determined by using the dynamic gassing method (Bailey and Ollis, 1986). A dissolved oxygen (DO) meter (JENWAY model 9300) is used to measure and record the changes in dissolved oxygen concentration in a batch of water. The experimental steps are detailed as follows:

Procedure

1. Fill tap water into the concentric column until the liquid level (H_L) is 3 cm above the top of the draft tube

2. Disperse nitrogen gas through the base of the contactor to the column for removing dissolved oxygen from the water in the column
3. Immerse the dissolved oxygen probe into the water in the column as shown in Figure 3.1 for measuring the dissolved oxygen concentration in the water by dissolved oxygen meter to ensure that all of the oxygen has been removed
4. Stop the nitrogen gas flow when the dissolved oxygen concentration reaches zero
5. Distribute compressed air from an air compressor continuously through the sparger into the column using rotameter as calibrated superficial velocity
6. Record the dissolved oxygen concentration with respect to time during air is distributed into the column until the water is saturated with oxygen.
7. Calculate mass transfer coefficient following Equation 3.19
8. Repeat Steps 1 to 6 with other geometric and/or operating parameters

3.3 Experimental Analysis

3.3.1 Bubble size calculation

For ellipsoidal bubbles, the major and the minor axes (p and q) of the bubble images are measured as shown in Figure 3.3. The equivalent diameter of a sphere with the same volume as the ellipsoidal bubble is calculated by:

$$d_B = (p^2 q)^{1/3} \quad (3.1)$$

Mostly in practice, a distribution of bubble sizes are measured by Sauter mean diameter which refers to a diameter of a sphere. The ratio of the volume to surface of the same sphere is given by:

$$d_{Bs} = \frac{\sum_{i=1} n_i d_{B,i}^3}{\sum_{i=1} n_i d_{B,i}^2} \quad (3.2)$$

where n_i is the occurrence frequency of the sphere bubbles diameter, $d_{B,i}$.

3.3.2 Gas holdup calculations

3.3.2.1. Overall gas holdup

The overall gas holdup is determined by using a volume expansion technique. The expanded dispersion volume represents the gas volume in the system according to the following equation:

$$V_o = V_D - V_L \quad (3.3)$$

where V_o = expanded gas volume or overall gas volume (cm^3)

V_D = dispersed liquid volume (cm^3)

V_L = unaerated liquid volume (cm^3)

The fluid volume can be calculated from cross sectional area of the column (A) and fluid height (H) in these equations:

$$V = AH \quad (3.3a)$$

$$V_D = AH_D \quad (3.3b)$$

$$V_L = AH_L \quad (3.3c)$$

where A = cross sectional area of the column (cm^2)

H_D = dispersed liquid height (cm)

H_L = unaerated liquid height (cm)

Moreover the overall gas hold up can be calculated by:

$$V_o = \varepsilon_o AH_D \quad (3.3d)$$

where ε_o = gas fraction in the expanded fluid volume

From Eqs (3.2), (3.2a), (3.2b), (3.2c) and (3.2d);

$$\varepsilon_o AH_D = AH_D - AH_L \quad (3.4)$$

$$\varepsilon_o = \frac{(H_D - H_L)}{H_D} \quad (3.5)$$

where ε_o = overall gas holdup (-)

H_D = dispersed liquid height (cm)

H_L = unaerated liquid height (cm)

The unaerated liquid height and dispersion height can be measured from Section 3.2.2 and then the overall can be calculated.

3.3.2.2. Riser gas holdup

For the annular sparged airlift contactor, the riser gas holdup is estimated by measuring the pressure difference between two measuring ports of the column.

Firstly,
$$\Delta P_{\text{column}} = \Delta P_{\text{manometer}} \quad (3.6)$$

$$\rho g \Delta H = \rho_L g \Delta Z \quad (3.7)$$

$$(\rho_L \varepsilon_L + \rho_g \varepsilon_g) g \Delta H = \rho_L g \Delta Z \quad (3.8)$$

Neglecting the wall friction loss and $\rho_L \gg \rho_g$, the gas holdup can be calculated from the following equations:

$$(\rho_L \varepsilon_L) g \Delta H = \rho_L g \Delta Z \quad (3.9)$$

$$\varepsilon_L = \frac{\rho_L g \Delta Z}{\rho_L g \Delta H} \quad (3.10)$$

since
$$\varepsilon_L = 1 - \varepsilon_G \quad (3.11)$$

so
$$1 - \varepsilon_G = \frac{\rho_L g \Delta Z}{\rho_L g \Delta H} \quad (3.12)$$

finally,
$$\varepsilon_r = 1 - \frac{\Delta P}{\rho_L g \Delta H} \quad (3.13)$$

where ΔP = pressure difference of defined liquid level in manometer ($\text{g/cm} \cdot \text{s}^2$)

ΔH = height of defined liquid level in the column (cm)

ΔZ = height of liquid level in the manometer (cm)

ρ_G = gas density (g/cm^3)

ρ_L = liquid density (g/cm^3)

g = gravitational acceleration (cm/s^2)

3.3.2.3. Downcomer gas holdup

It is assumed that the gas holdup in the top section is approximately equal to in the riser. The downcomer gas holdup can then be calculated from the overall and the riser gas holdups. The relationship between the gas holdups in different parts of an airlift contactor can be written as:

$$\varepsilon_o = \frac{H_{dt} A_r \varepsilon_r + H_{dt} A_d \varepsilon_d + (H_D - H_{dt})(A_r + A_d) \varepsilon_t}{H_D (A_r + A_d)} \quad (3.14)$$

Substituting $\varepsilon_t = \varepsilon_r$ into Equation 3.14 yields:

$$\varepsilon_o = \frac{H_{dt}A_d\varepsilon_d + (H_D A_d + H_D A_r - H_{dt}A_d)\varepsilon_r}{H_D(A_r + A_d)} \quad (3.15)$$

or

$$\varepsilon_d = \frac{\varepsilon_o H_D (A_r + A_d) - (H_D A_d + H_D A_r - H_{dt} A_d) \varepsilon_r}{H_{dt} A_d} \quad (3.16)$$

where ε_o = overall gas hold up (-)

ε_r = gas holdup in riser (-)

ε_d = gas holdup in downcomer (-)

ε_t = gas holdup in gas-liquid separator (-)

A_d = cross-sectional area of downcomer (cm²)

A_r = cross-sectional area of riser (cm²)

3.3.3 Liquid velocity

The liquid velocities both in riser and downcomer are measured by tracer injection method where the measured times which the color uses for traveling between any two fixed positions is used for the calculation:

$$v_r = \frac{x_r}{t_r} \quad (3.17)$$

$$v_d = \frac{x_d}{t_d} \quad (3.18)$$

where v = liquid velocity (cm/s)

x = distance between any two fixed position (cm)

t = time for any two fixed position (s)

3.3.4 Volumetric mass transfer coefficient calculation

The volumetric mass transfer coefficient ($k_L a$) is determined by using the dynamic method. The time profile of dissolved oxygen concentration in the solution is measured and recorded until equilibrium concentration. We can calculate $k_L a$ from slope of this equation:

$$\ln \frac{(c^* - c_o)}{(c^* - c_L)} = k_L a t \quad (3.19)$$

where c^* = saturated oxygen concentration (mg/l)

c_o = initial oxygen concentration (mg/l)

c_L = oxygen concentration in liquid phases (mg/ l)

k_La = overall volumetric mass transfer coefficient (1/s)

t = time profile (s)



สถาบันวิทยบริการ
จุฬาลงกรณ์มหาวิทยาลัย

Table 3.1 Ratio of downcomer to riser cross sectional area in this work

Draft tube	Symbol	D_i (cm)	D_{io} (cm)	A_d/A_r (-)
Draft tube 1	DT1	3.4	4	0.067
Draft tube 2	DT2	7.4	8	0.443
Draft tube 3	DT3	8.4	9	0.661
Draft tube 4	DT4	9.4	10	1.008

Remarks

D_i = inside draft tube diameter (cm)

D_{io} = outer draft tube diameter (cm)

A_d/A_r = ratio of down comer cross sectional area and riser cross sectional area (-)

Table 3.2 Locations of digital video camera for bubble size measurement

Section	Height from the bottom end of the draft tube (h_i) (cm)
Top section (h_1)	90
Middle section (h_2)	50
Bottom section (h_3)	10

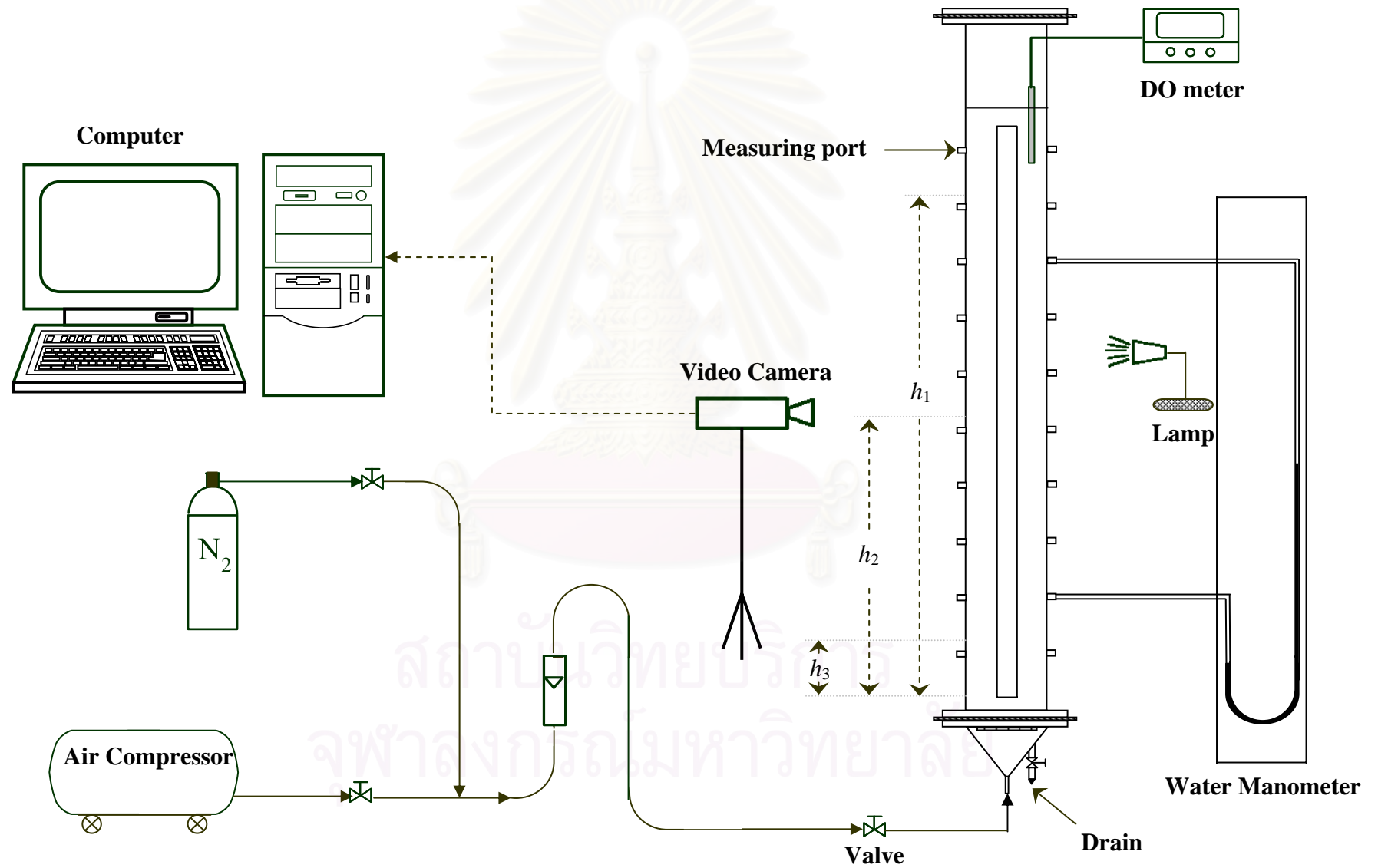


Figure 3.1 Schematic diagram of the concentric internal loop airlift contactor employed in this work

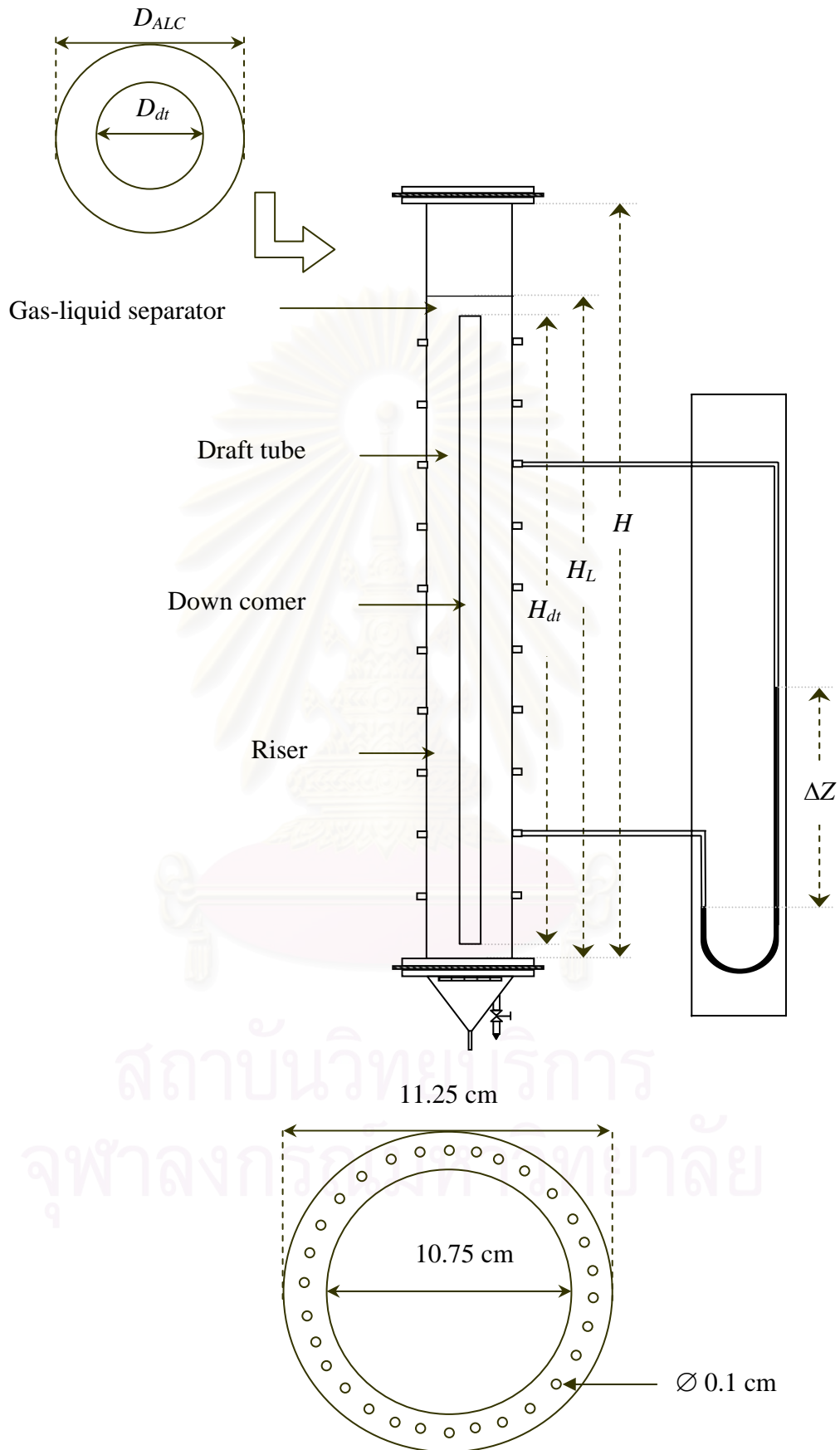


Figure 3.2 Configuration of airlift contactor and annular sparger in this work

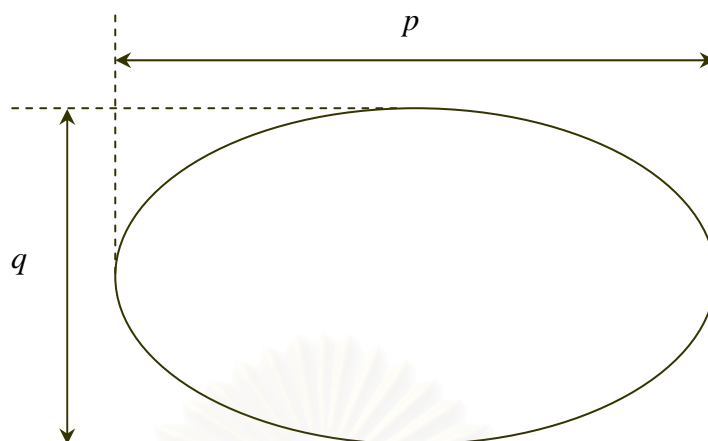
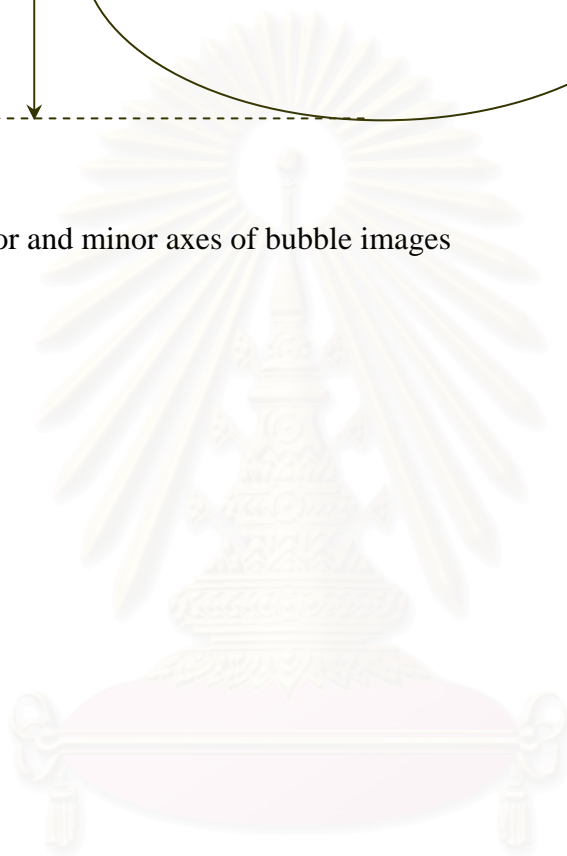


Figure 3.3 Major and minor axes of bubble images



สถาบันวิทยบริการ
จุฬาลงกรณ์มหาวิทยาลัย

CHAPTER IV

RESULTS & DISCUSSION

4.1 Error compensation in photographic technique

The measurement of the bubble sizes was performed along the height of the airlift contactor (three axial locations). The radial variation in the bubble size was not observed as the cross sectional area of the riser (between inner and outer columns) was rather small which was approximately in the same order of magnitude with the bubble size. Therefore precise measurement along radial direction was not possible. There were errors from the reading of the bubble size due to curvature of the column surface, and this was encountered by placing an object with known size along the radial direction in the column and the pictures of such object were taken for size compensation. Note that the error due to the curvature of the column surface was approximately $\pm 15\%$ (Wongsuchoto 2002). With the limitation of the photographic technique, the bubble size in downcomer was not possibly observed. Examples of the figures of bubble sizes taken from this work are illustrated in [appendix B](#).

4.2 Effect of salinity on average bubble size

Figure 4.1 illustrates that, at low range of u_{sg} (< 0.02 m/s), the effect of salinity on bubble size was not obvious and bubble sizes were in the range of 6.0 to 7.5 mm in all ALC systems. At higher u_{sg} , the effect of salinity on bubble size became more apparent where the bubble size appeared to be smaller in the saline solution than that in fresh water. This was in contrast with the fact that saline solution possesses a stronger surface tension and viscosity than water and the bubble size in such solution should be larger than in water. However, the effect of electrolyte on surface tension gradient at the interface (Marangoni effect) was reported not to be adequate to regulate the bubble size (Marrucci, 1969, Prince and Blanch, 1990(a)), and therefore the effects of salinity on bubble size were mainly due to its ionic properties. This finding was in good agreement with several past reports which stated that electrolyte solutions inhibited bubble coalescence and retarded bubble riser velocity which then caused the bubble size to be smaller than that in water (Marrucci and Nicodemo, 1967, Lessard and Zieminski, 1971, Prince and Blanch, 1990(a), Prince and Blanch, 1990(b), Weissenborn and Pugh, 1996, Tse et al., 2003 and Malysa et al., 2005).

Types and concentration of electrolyte can impose different effects on bubble coalescence, for instance, [Lessard and Zieminski, 1971](#) ordered efficiency of coalescence in various electrolytes as follows: $\text{MgSO}_4 < \text{MgCl}_2 < \text{CaCl}_2 < \text{Na}_2\text{SO}_4 < \text{LiCl} < \text{NaCl} < \text{NaBr} < \text{KCl}$.

There are two types of forces or pressures dealing with the coalescence or breakup of the bubbles. The first one is the Laplace pressure which promotes bubble coalescence from the drainage of the liquid film located in between the two adjacent bubbles. This pressure depends on the reciprocal of the bubble radius. However, if the Laplace pressure is too strong, bubbles coalesce very rapidly and this caused instability of the bubbles. Therefore, at this condition, bubble breakage dominates in the system. The other type of force is repulsive force. Electrolytes such as salt increased the repulsive hydration force by enhancing water structure due to hydrogen bond at the interface leading to a more stable bubble than that in the fresh water system. This formation of repulsive force balances the Laplace pressure, inhibiting bubble coalescence ([Tsang et al, 2004](#)). The two forces can be written in a mathematical form as follows:

$$\Delta P = \frac{\sigma}{r_p} - \Pi \quad (4.1)$$

when σ is surface tension, r_p is radius of intersection of three films called the Plateau border channel and the ratio between the surface tension and radius of intersection or $\left(\frac{\sigma}{r_p}\right)$ is equal to Laplace pressure. Π is the disjoining pressure which is the summation of various forces between ions interaction at the gas and liquid interface according to Equation (4.2).

$$\Pi = \Pi_{vdw} + \Pi_{DL} + \Pi_{hyd} \quad (4.2)$$

where Π_{vdw} is attractive Van der Waals force, Π_{DL} is the dielectric double layer force or repulsive force and Π_{hyd} is short-range repulsive or hydration force. An attractive van der Waals force (Π_{vdw}) was weak force attraction and caused from the polarization of molecules into dipoles, and can be expressed mathematically as in Equation (4.3). A dielectric double layer (Π_{DL}) was the repulsive force caused from confinement of the ion charge at gas-liquid interface. A hydration forces was short-range repulsive force (Π_{hyd}) resulting from the formation of the water molecules near charged surfaces as in Equation (4.4),

$$\Pi_{vdw} = \frac{-A}{6\pi h^3} \quad (4.3)$$

$$\Pi_{hyd} = \left(\frac{W}{\lambda} \right) \exp(-h/\lambda) \quad (4.4)$$

where A is the Hamaker constant which is equal to 10^{-20} J, h the film rupture thickness, λ the decay length of the hydration interaction, mostly takes the value of about 8.5 nm, and W the pre-exponential constant ≈ 6 mN/m (Tsang et. al., 2004). The film rupture thickness or h was reported to be a function of salinity by Cain and Lee (1985) which were equal to 114.7, 106.8, 98.8, and 90.9 for the water with salinity levels of 0, 15, 30, and 45 ppt, respectively. In the same work (Cain and Lee, 1985), it was reported that the dielectric double layer force (Π_{hyd}) was negligible compared with the hydration force and should be disregarded from the calculation. Moreover, Van der Waals attraction was generally reported to be relatively small and was also negligible compared with the hydration force (Marrucci, 1969, Prince and Blanch, 1990(a)). Therefore Equation (4.1) is reduced to

$$\Delta P = \frac{\sigma}{r_p} - \Pi_{hyd} \quad (4.5)$$

The pressure difference, ΔP , in Equation (4.1) was important in controlling the level of bubble coalescence or bubble breakage in the system. ΔP is low for the condition with inhibiting bubble coalescence, and high for the bubble coalescence promoting conditions. Nevertheless, as mentioned above, a much higher ΔP would result in a breakup of bubbles (Hartland 2004). A summary of these forces acting on the bubbles in the airlift systems is given in Table 4.1.

Let's define the parameter ΔP_C which is the range of ΔP that results in the bubble coalescence. The conditions with smaller ΔP lead to the inhibition of bubble coalescence, whilst higher ΔP than this would cause bubble breakage, and in both cases, this results in smaller bubble sizes. From the results obtained in this work (Table 4.2), it was clear that the bubble size in the water system was the largest (ΔP in water = approx. 20 N/m² for the whole range of u_{sg} employed in this work). This was due to the absence of repulsive force to balance the Laplace pressure. With the presence of salinity, the repulsive force became stronger. However, it was illustrated that this repulsive force was not strong enough to bring ΔP down. In contrast, the Laplace pressure in the presence of salinity seemed to be quite large which could be the result from the increasing surface tension. This resulted in

ΔP having a much value than 20 N/m^2 . Therefore bubbles tended to break in such condition.

In the airlift with A_d/A_r of 0.067 running with 45 ppt salinity, ΔP was about 43-75 N/m^2 at $u_{sg} > 0.02 \text{ m/s}$ and therefore bubble breakup was expected. The bubble size in this case was quite small, at 0.001-0.002 m (see Figure 4.1). Figure 4.3 illustrates that when the A_d/A_r was altered (from 0.067 to 0.661), the condition in the system changed, and despite using the same level of u_{sg} , the system running with 45 ppt salinity had ΔP of 12-25 N/m^2 and larger bubbles (0.005-0.006 m) than that at lower A_d/A_r were observed.

Figure 4.3 illustrates the relationship between pressure driving forces and the average bubble size in all airlift systems employed in this work. It seemed that ΔP that gave the largest bubble size was in the range from 15–20 N/m^2 . A lower ΔP would inhibit bubble coalescence and therefore the bubble size was slightly lower than that at ΔP of 15-20 N/m^2 . At high ΔP , the bubble size became quite small which suggested that bubble breakup was quite significant in controlling the bubble size distribution inside the system. Hence, for this work, ΔP_C lies at the range of 15-20 N/m^2 .

4.3 Effect of superficial velocity

Figure 4.1-4.2 demonstrates that Sauter mean diameter of the bubbles decreased with increasing of superficial gas velocity at all salinity levels. This finding agreed well with the reported data in the airlift systems operated with various types of liquid (Colella et al., 1999, Contreras et al., 1999, Polli et al., 2002 and Wongsuchoto et al., 2003). The bubble sizes were regulated by the level of pressure difference in the airlift system as described above. At low range of gas flow rate ($< 0.02 \text{ m/s}$) as shown in Figure 4.3, the pressure difference was in the range of 15-20 N/m^2 . Therefore this range of ΔP enhanced bubble size. At a higher range of superficial gas velocity ($> 0.02 \text{ m/s}$), the ΔP was higher than 20 N/m^2 which promoted the breakup of the bubbles. In addition, at this high gas throughput conditions, the airlift contained a relatively high gas hold-up which also enhanced the chance of bubbles collision and breaking up.

4.4 Local bubble size distribution in airlift systems

Figure 4.4 illustrates examples of the bubble size distribution curves obtained from the various sections of the ALC system operated with saline water at 30 ppt and with draft tube # DT3 ($A_d/A_r = 0.661$). As a general trend, bubble size was quit large, in the range of

6.0-8.2 mm at low superficial velocity. When the system was operated with higher gas throughput, bubbles became smaller in size and the variation in bubble size became bimodal distribution where there were two main bubble sizes present at the same time (2 and 6.5 mm). At high gas throughput, bubble size became small and the distribution illustrated that there was only one main bubble size in the system at this condition (2 mm). Bubble size did not seem to be smaller when the superficial velocity became higher than 0.036 m/s. This finding was for the system operated with water at salinity of 30 ppt, and it agreed well with the report by [Wongsuchoto et al., 2003](#) who carried out the experiment in fresh water systems that bubble no longer changed its size distribution $u_{sg} > 0.05$ m/s. The difference was that the airlift operated with saline solution had smaller bubble sizes than those with fresh water.

4.5 Axial bubble size distribution in airlift contactors

The axial bubble size distribution was obtained by taking photographs of bubbles in the airlift at different heights. Bubble distribution frequency was then formulated for each sampling point, and the results were shown in [Figure 4.4](#). In the top and middle sections, the distribution changed from uni-modal to multi-modal curve at $u_{sg} \approx 0.019$ m/s whereas the bottom section saw this change at $u_{sg} \approx 0.029$ m/s. The breakage of the bubbles at high gas throughput was caused by higher amount of energy dissipation and turbulent which promoted more interaction between bubbles. The results suggested, therefore, that there was a higher level of turbulence in the top and middle sections than that in the bottom. The Sauter mean diameters of bubbles in the three sections in the airlift system with A_d/A_r of 0.661 are illustrated in [Figure 4.5](#). This revealed that bubble size in the bottom section was slightly larger than in those in the other sections, particularly at a lower range of u_{sg} (< 0.04 m/s) examined in this work. At a higher u_{sg} range, the effect of column height on the bubble size was not obvious and the sizes of bubbles were approximately the same throughout the length of the airlift. The same finding was found for the system running with tap water as described in [Wongsuchoto et al. \(2003\)](#).

4.6 Effect of the ratio between downcomer and riser cross-sectional areas on bubble size

To investigate the effect of the ratio between the downcomer and riser cross-sectional areas (A_d/A_r), the experiment was conducted in the airlift contactors running with sea

water at 30 ppt with four different draft tube sizes as detailed in [Table 3.1](#) and the average bubble sizes are shown in [Figure 4.6](#). At a low range of u_{sg} (< 0.015 m/s), no significant differences in bubble size were observed in all systems. At u_{sg} greater than 0.015 m/s, the differentiation of the bubble sizes in the systems with different draft tube sizes became more obvious, i.e. the bubble size was larger with increasing draft tube size (d_{Bs} , DT4 $>$ DT3 $>$ DT2 $>$ DT1). In other words, the bubble size was larger in the system with smaller riser cross sectional area. It was possible that turbulence in the system with smaller riser area was stronger than those with larger riser areas, and the chance of bubbles being coalesced at this high turbulent regime was relatively high. [Figure 4.6](#) also illustrates that the effect of A_d/A_r on bubble size was more obvious at the bottom section, and not as much in the middle and top sections. As stated earlier, the level of turbulence in the middle and top sections of the airlift with the size used in this work was stronger than that in the bottom section. With similar level of turbulent intensity in the top part of the various airlift systems, bubble sizes in this section were not significantly regulated by A_d/A_r . Unlikely, the bottom section was operated at lower turbulent intensity where the airlift with different A_d/A_r might exert noticeable levels of turbulence intensities. This resulted in a distinguishable bubble sizes as observed in [Figure 4.6](#). This finding was also similar to the performance of airlift contactor operated with fresh water as reported in [Wongsuchoto et al. \(2003\)](#).

4.7 Overall volumetric mass transfer coefficient (k_La) in the airlift systems operating with sea water

The overall volumetric mass transfer coefficient (k_La) was calculated from [Equation \(3.19\)](#). The change in the overall volumetric mass transfer coefficient (k_La) with superficial gas velocity and salinity level was shown in [Figure 4.7](#). This illustrated that k_La increased with superficial gas velocity but decreased with an increase in salinity. As an overall observation, salinity seemed to have adverse effects on k_La and the system with fresh water always imposed a higher k_La than those running with sea water. The effect of salinity on k_La was quite complicated. At low range of u_{sg} (< 0.03 m/s), the effect of salinity did not seem to be significant, however, the effect became more pronounced at high aeration rate ($u_{sg} > 0.03$ m/s) and k_La was the highest at 30 ppt followed by those at 15 and 45 ppt, respectively.

This $k_L a$ quantity composed two main parameters, i.e. “ k_L ” or overall mass transfer coefficient, and “ a ” or specific interfacial area. Generally k_L was reported to be a function of turbulence, liquid properties and bubble size. As the salinity did not have notable effect on liquid properties, k_L should be controlled only by turbulence and bubble size. The two film theory suggested that k_L was more regulated by the shear rate at the gas-liquid interface which was controlled by the slip velocity or the difference in the bubble and liquid velocity. However, the estimate of k_L required the use of certain empirical correlation whereby the coefficients needed to be obtained from experimental data. These parameter fittings would be described shortly after the calculation of specific area.

The specific interfacial area (a) was estimated using Equation (4.6):

$$a = \frac{6\varepsilon_g}{d_{Bs}(1 - \varepsilon_g)} \quad (4.6)$$

where $\varepsilon_{g,r}$ is the riser gas holdup and d_{Bs} Sauter mean diameter which is defined as:

$$d_{Bs} = \frac{\sum n_i d_{B,i}^3}{\sum n_i d_{B,i}^2} \quad (4.7)$$

where n_i is the occurrence frequency number of the sphere bubbles diameter, $d_{B,i}$. The two parameters significant for the determination of the specific mass transfer area were average bubble size (Figure 4.2) and gas holdup. Figure 4.8 illustrates that the effect of salinity on gas holdups in the system was only marginal and the specific area should only vary with bubble size. As discussed earlier, the bubble size in sea water was smaller than that in fresh water and became smaller with an increase in superficial gas velocity. Therefore the specific interfacial areas obtained in the systems at all salinity levels were higher than that in the fresh water system.

It was primarily assumed that the gas holdup was uniform throughout, both in axial and radial directions. The estimates of specific interfacial area (a) in the airlift system with $A_d/A_r = 0.661$ at various salinities is displayed in Figure 4.9. This finding revealed that effect of salinity on specific area was only marginal at low range of superficial gas velocity ($u_{sg} < 0.028$ m/s), and became more significant at higher u_{sg} . The largest gas-liquid surface area was obtained from the airlift operating with saline water at 15 ppt, followed by those at 30 and 45 ppt. This corresponded well with the information on the effect of salinity on bubble size in Figure 4.2.

Now that once the information on $k_L a$ and a became known, the overall mass transfer coefficient or k_L could simply be calculated by dividing $k_L a$ with a and the results are given in Figure 4.10.

4.8 Estimate of $k_L a$

The mass transfer rate for entire contactor was proposed in the terms of the overall volumetric mass transfer coefficient $(k_L a)_T$ and could be calculated from sum of the mass transfer rates in riser and downcomer section as follows:

$$(k_L a)_T = \frac{(k_L a)_r V_{L,r} + (k_L a)_d V_{L,d}}{V_{L,T}} \quad (4.8)$$

where $V_{L,r}$ is the volume of liquid in riser, $V_{L,d}$ the volume of liquid in downcomer and $V_{L,T}$ the volume of total liquid. $(k_L a)_r$ and $(k_L a)_d$ were obtained from $k_{L,r}$ multiplied by $a_{L,r}$ and $k_{L,d}$ multiplied by $a_{L,d}$.

As a was obtained from the measurement, the estimate of $k_L a$ requires only the estimation of k_L . As mentioned above, the mass transfer coefficient, k_L was reported as a function of liquid properties and bubble size, (Higbie, 1935, Calderbank, 1967., Bailey and Ollis, 1986). The determination of mass transfer coefficient, k_L was summarized in Skelland, 1974, Welty 1984, Stanley, 1998, and Painmanakul et. al., 2005. Equation (4.9) is usually to estimate k_L . Hence, the dimensionless relationship between Sherwood number (Sh) in Equation (4.10), Schmidt number (Sc), Grashof number (Gr) and Reynold number (Re) could be formulated as follows:

$$Sh = a + bGr^c Sc^d + eRe^f Sc^h \quad (4.9)$$

Generally, Grashof number, Gr , represents the mass transfer by natural convection or free rise velocity whilst Reynolds number, Re , is the mass transfer form forced convection:

$$Sh = \frac{k_L d_{Bs}}{D_L} \quad (4.10)$$

$$Gr = \frac{d_{Bs}^3 \rho_l \Delta \rho g}{\mu_l^2} \quad (4.11)$$

$$Re = \frac{d_{Bs} v_s \rho_l}{\mu_l} \quad (4.12)$$

The velocity and bubble diameter used in the calculation of Reynolds number were the slip velocity, v_s , and Sauter mean diameter, d_{Bs} . The slip velocity in riser, $v_{s,r}$ was calculated as a function of the terminal rise velocity of a single bubble, u_∞ , which were related to hindering effects from neighboring bubbles in the riser section. Information on bubble sizes was then employed to estimate the slip velocity of the gas bubbles in the system using the following equation (Marrucci, 1965; Wallis, 1969):

$$v_{s,r} = \frac{u_\infty}{(1 - \varepsilon_{g,r})} \quad (4.13)$$

where u_∞ is the terminal bubble riser velocity which can be calculated using the correlation proposed by Jamialahmadi et al., 1994,

$$u_\infty = \frac{(1/8)((\rho_l - \rho_g) / \mu_l) g d_{Bs}^2 ((3\mu_l + 3\mu_g) / (2\mu_l + 3\mu_g)) \sqrt{2\sigma / d_{Bs} (\rho_l + \rho_g) + g d_{Bs} / 2}}{\sqrt{[(1/8)((\rho_l - \rho_g) / \mu_l) g d_{Bs}^2 ((3\mu_l + 3\mu_g) / (2\mu_l + 3\mu_g))]^2 + 2\sigma / d_{Bs} (\rho_l + \rho_g) + g d_{Bs} / 2}} \quad (4.14)$$

The parameters $a - h$ in Equation (4.9) was then determined from experiments.

Equation 4.9 must be used to predict $k_{L,r}$ and $k_{L,d}$, and in doing so, the slip velocities or terminal rise velocities in both riser and downcomer must be known (from Equations 4.13 and 4.14) for the calculation of Reynolds number. As the photographic technique could only be used to measure the bubble size in riser, bubble size in downcomer was not known and the determination of slip velocity in downcomer was not possible. However, the average bubble size in downcomer ($d_{B,d}$) could be estimated from the downcomer liquid velocity, $u_{L,d}$, by assuming that the liquid must have velocity equaled to the terminal velocity to be able to drag the bubble down into the downcomer, or

$$v_{s,d} = u_{L,d} \quad (4.15)$$

Once the terminal velocity was known, the Levich equation (Levich, 1962) as shown in Equation (4.15) was proposed for the calculation of bubble size:

$$d_{B,d} = \frac{1.8}{g} \left(\frac{u_{L,d}}{2} \right)^2 \quad (4.16)$$

Assume that there was no variation of bubble size along the radial and axial directions in downcomer:

$$d_{Bs,d} = d_{B,d} \quad (4.17)$$

The $a_{L,d}$ was calculated from substitution of $d_{Bs,d}$ from Equation (4.17) and $\varepsilon_{g,d}$ from the experiment in Equation (3.16).

The parameters $a-h$ in Equation 4.9 were evaluated using non-linear parameter fittings using all the results available in this work, and the results are given in Table 4.3 (noted that these parameters were obtained from the solver function in the MS Excel 97 where the objective was a minimal error between experimental and simulation data). For the case of tap water, the results from parameter fitting were reasonably close to those proposed from Wongsuchoto et al. (2003) (as shown in the last row of Table 4.3). The fittings for the saline water gave somewhat different results from that for pure water in that the terms Reynolds number was not involved in the pure water system, but it was, to certain extent, for the saline water systems. This meant that the mechanism controlling the mass transfer coefficient in pure water was only the natural convection whereas the force convection as represented by the Reynolds term also was significant in the system operated with saline water. Figure 4.11 illustrates the comparison between the calculated and experimental $k_L a$ of the airlift contactor operated with various saline solutions.

Table 4.1 Estimation values of disjoining pressures (Π) in different salinity levels

Salinity (ppt)/Type	h^a (nm)	Van der waals attraction (N/m^2)	Electrostatic repulsion (N/m^2)	Hydration repulsion (N/m^2)	Total pressure (Π) (N/m^2)
0	114.7	-0.35	0	0.97	0.62
15	106.8	-0.44	0	2.47	2.03
30	98.8	-0.55	0	6.29	5.74
45	90.9	-0.71	0	16.01	15.30

^a Film rupture thickness estimated from Cain and Lee's experiment in 1985.

Table 4.2 Estimation value of pressure driving forces for bubble coalescence in various conditions

Salinity (ppt)/Condition	Draft tube	u_{sg} (m/s)	ΔP (N/m^2)	Salinity (ppt)/Condition	Draft tube	u_{sg} (m/s)	ΔP (N/m^2)
0	0.067	0.008	19.96	30	0.443	0.011	18.61
		0.012	20.32			0.016	18.38
		0.018	19.97			0.025	20.77
		0.022	20.97			0.031	23.93
		0.030	20.71			0.041	35.08
0	0.661	0.035	20.80	30	0.661	0.048	52.97
		0.013	22.58			0.013	16.13
		0.019	22.24			0.019	16.94
		0.029	22.27			0.029	19.84
		0.036	23.11			0.036	27.14
15	0.067	0.048	25.21	30	1.001	0.048	37.62
		0.056	29.62			0.056	54.34
		0.008	17.13			0.016	17.86
		0.012	20.20			0.023	16.61
		0.018	26.68			0.035	19.43
15	0.661	0.022	33.54	45	0.067	0.044	20.39
		0.030	39.59			0.058	27.72
		0.035	56.92			0.068	41.34
		0.013	20.13			0.008	7.50
		0.019	21.96			0.012	12.25
30	0.067	0.029	27.24	45	0.661	0.018	21.01
		0.036	45.72			0.022	44.44
		0.048	59.46			0.030	72.61
		0.056	69.01			0.035	122.15
		0.008	16.16			0.013	5.28
30	0.661	0.012	17.84	45	0.661	0.019	5.29
		0.018	30.55			0.029	5.92
		0.022	46.93			0.036	13.58
		0.030	71.21			0.048	26.47
		0.035	97.57			0.056	40.00

Table 4.3 Parameter values from the initial establishment of k_L correlation in Equation (4.9)

$$Sh = a + bGr^c Sc^d + e Re^f Sc^h$$

Condition	Parameter							R ²
	<i>a</i>	<i>b</i>	<i>c</i>	<i>d</i>	<i>e</i>	<i>f</i>	<i>h</i>	
0 ppt	0.41	1.05	0.48	0	0	0	0	0.91
15 ppt	0.41	1.04	0.16	0.3	0.13	0.46	0.06	0.81
30 ppt	0.41	1.04	0.16	0.3	0.13	0.46	0.06	0.82
45 ppt	0.41	1.04	0.16	0.3	0.13	0.46	0.06	0.82
0 ppt (Wongsuchoto et al., 2003)	0.5	1.07	0.47	0	0	0	0	0.92

สถาบันวิทยบริการ
จุฬาลงกรณ์มหาวิทยาลัย

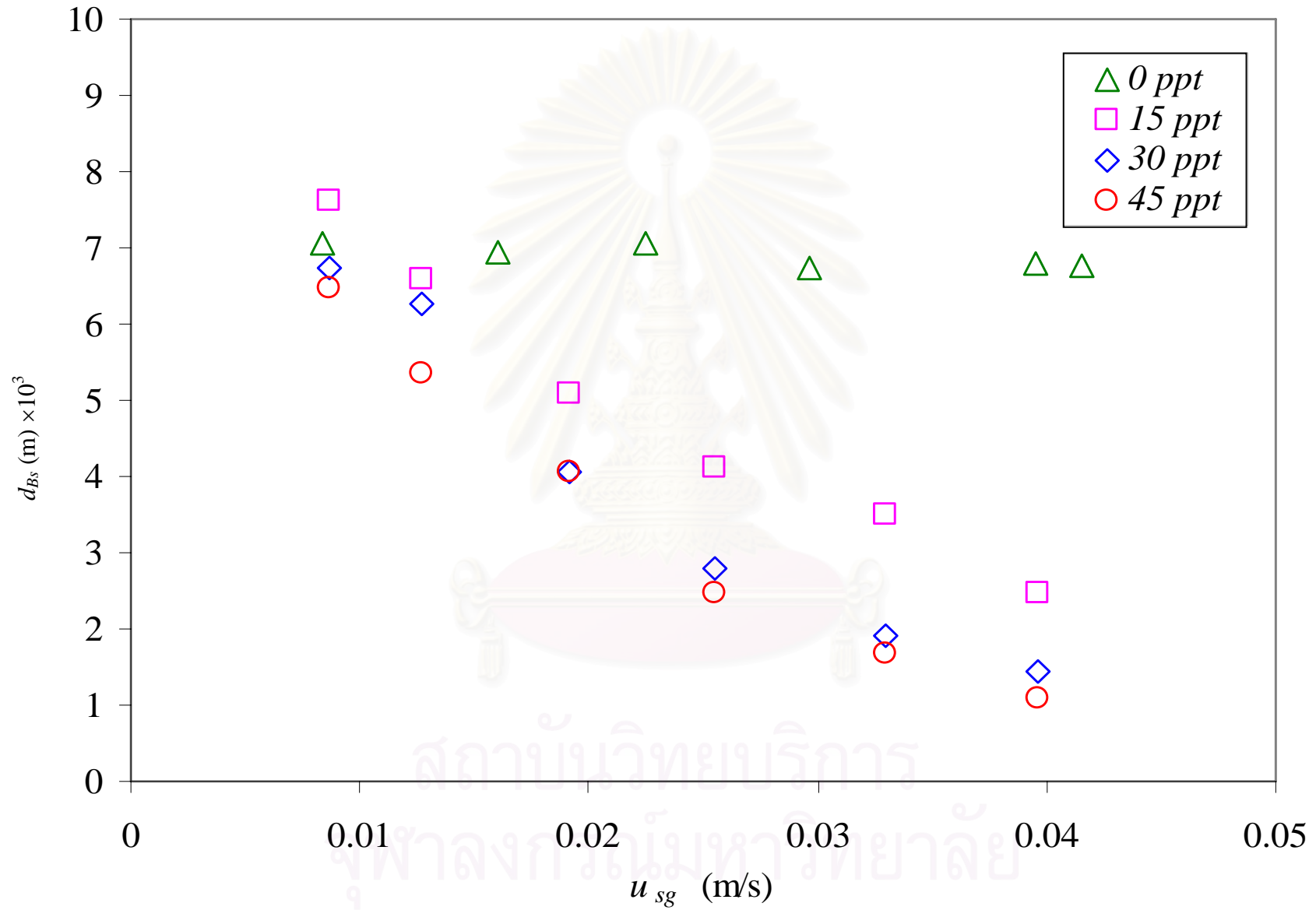


Figure 4.1 Bubble sizes in ALC running at different salinity levels ($A_d/A_r = 0.067$)

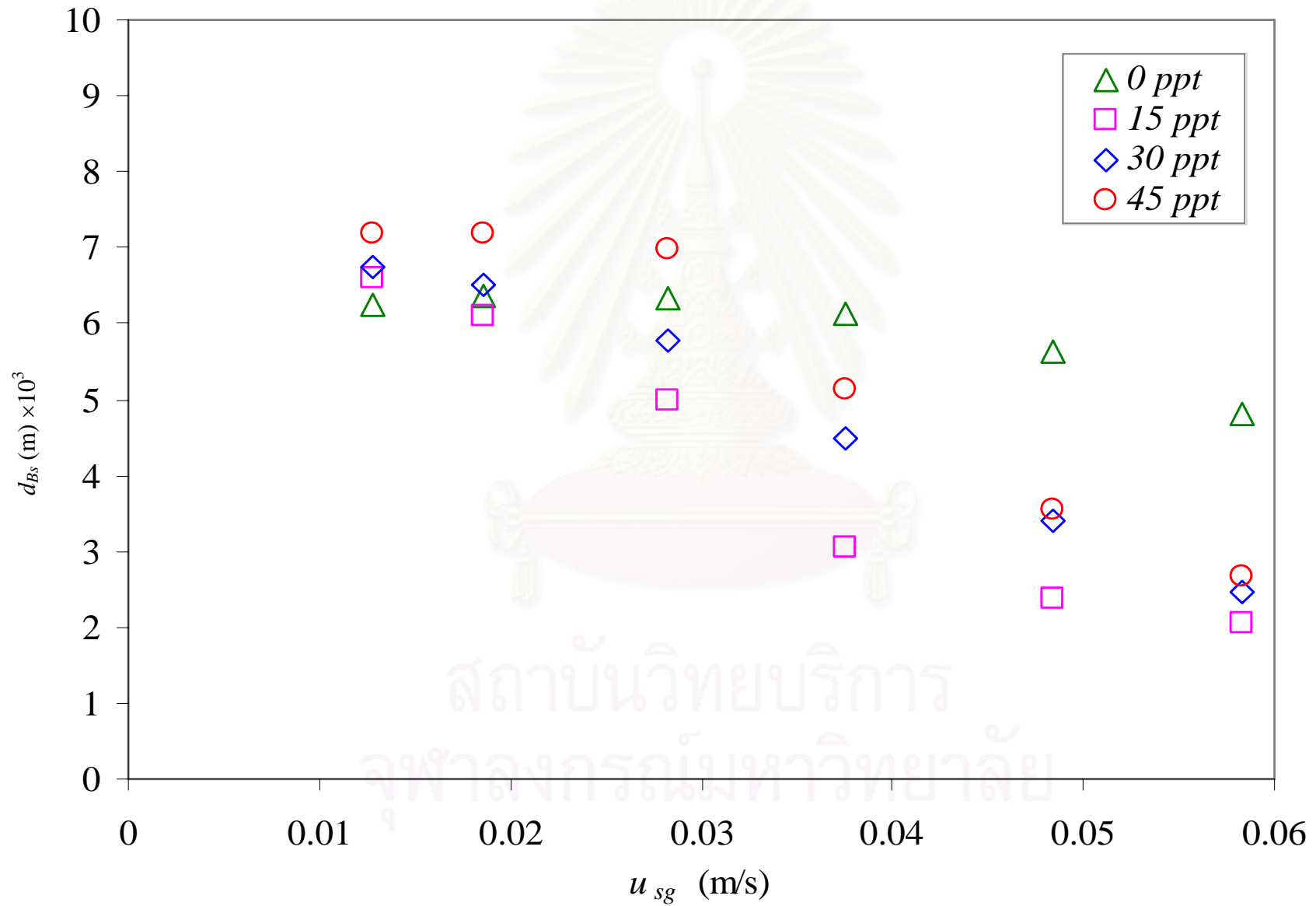


Figure 4.2 Bubble sizes in ALC running at different salinity levels ($A_d/A_r = 0.661$)

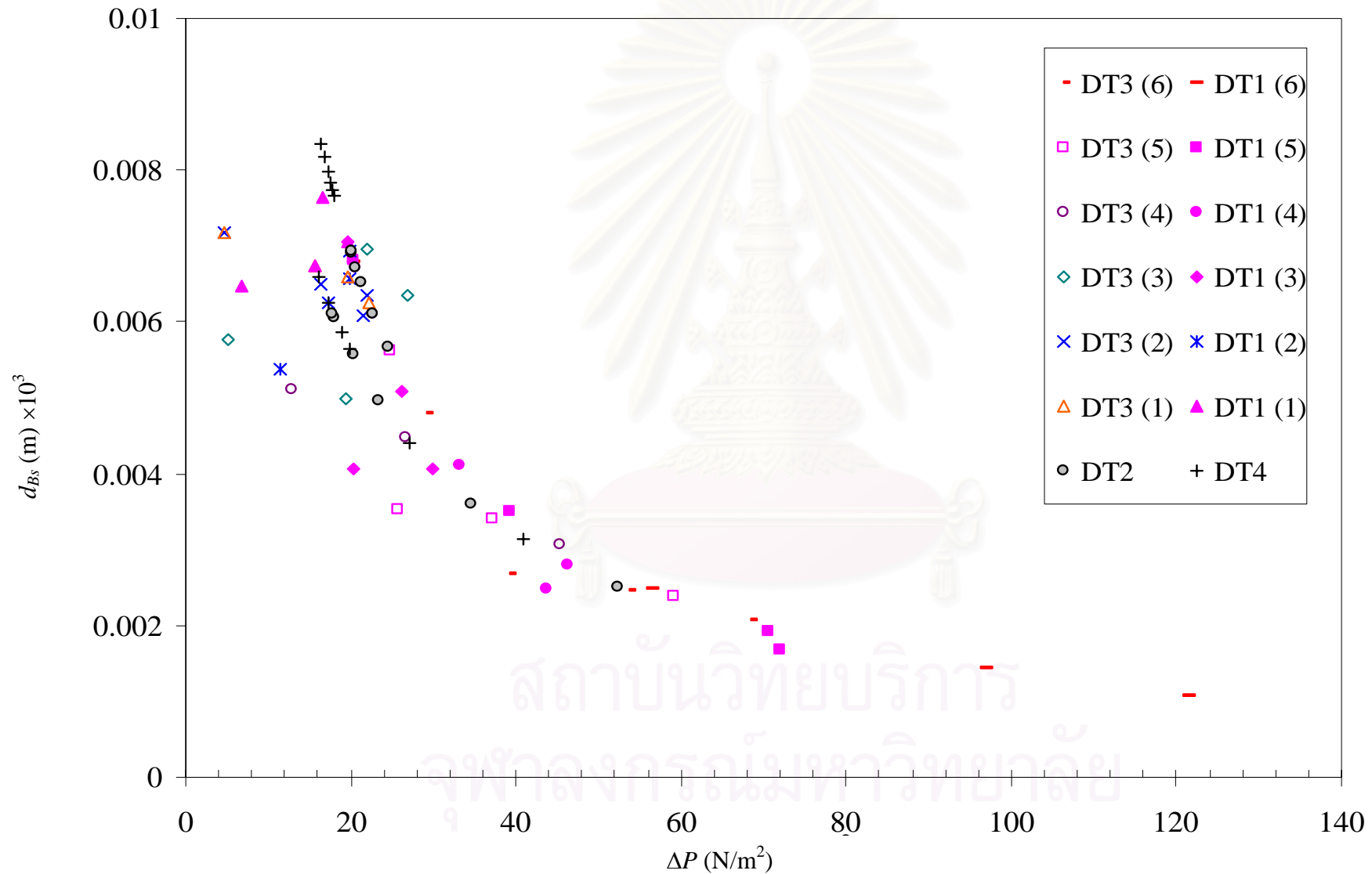


Figure 4.3 Pressure difference in ALC running at different draft tube sizes ($A_d/A_r = 0.067$ - 0.661) and superficial gas velocity in blanket

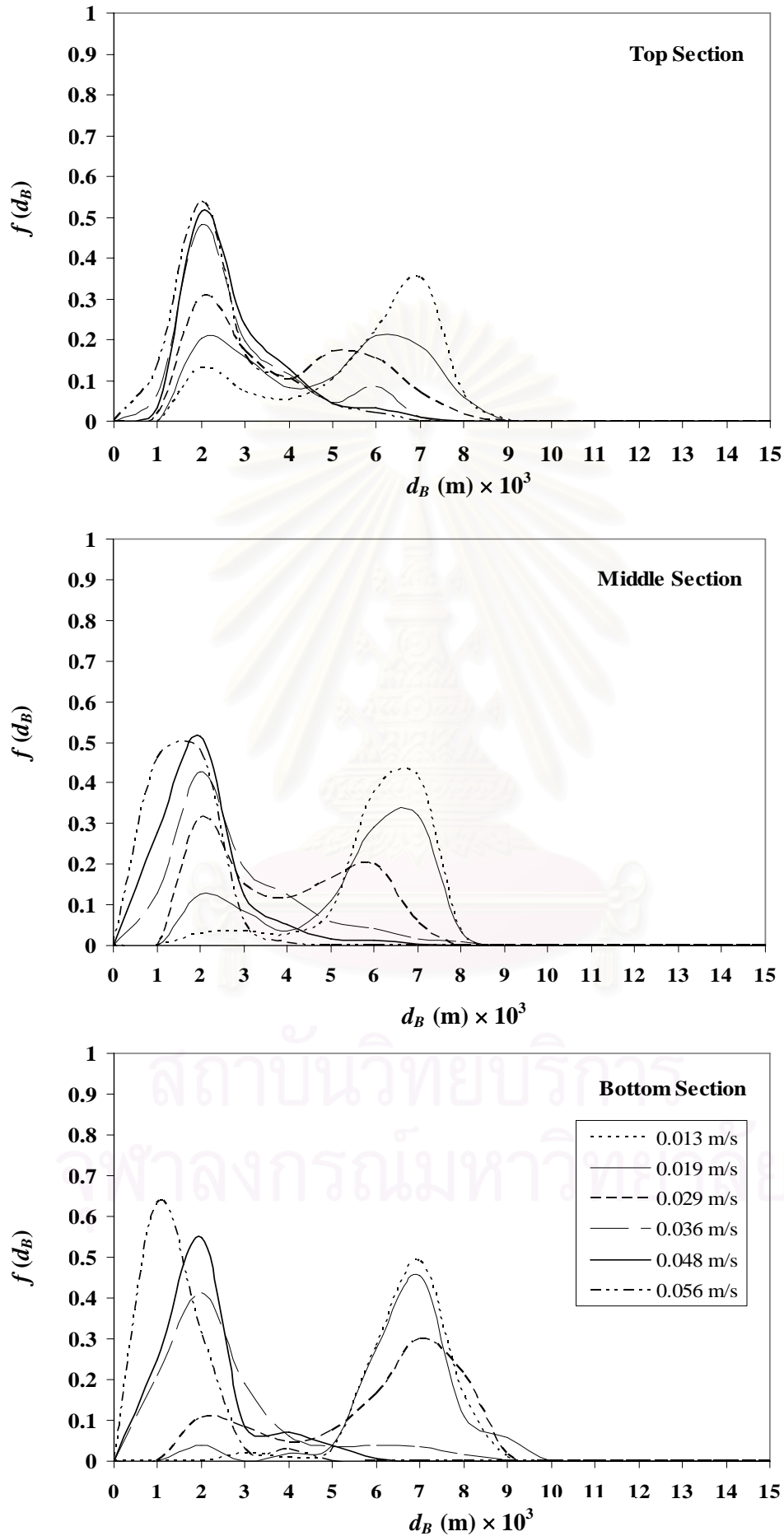


Figure 4.4 Frequency distribution of bubble sizes at various superficial gas velocities in ALC with $A_d/A_r = 0.661$ (salinity = 30 ppt)

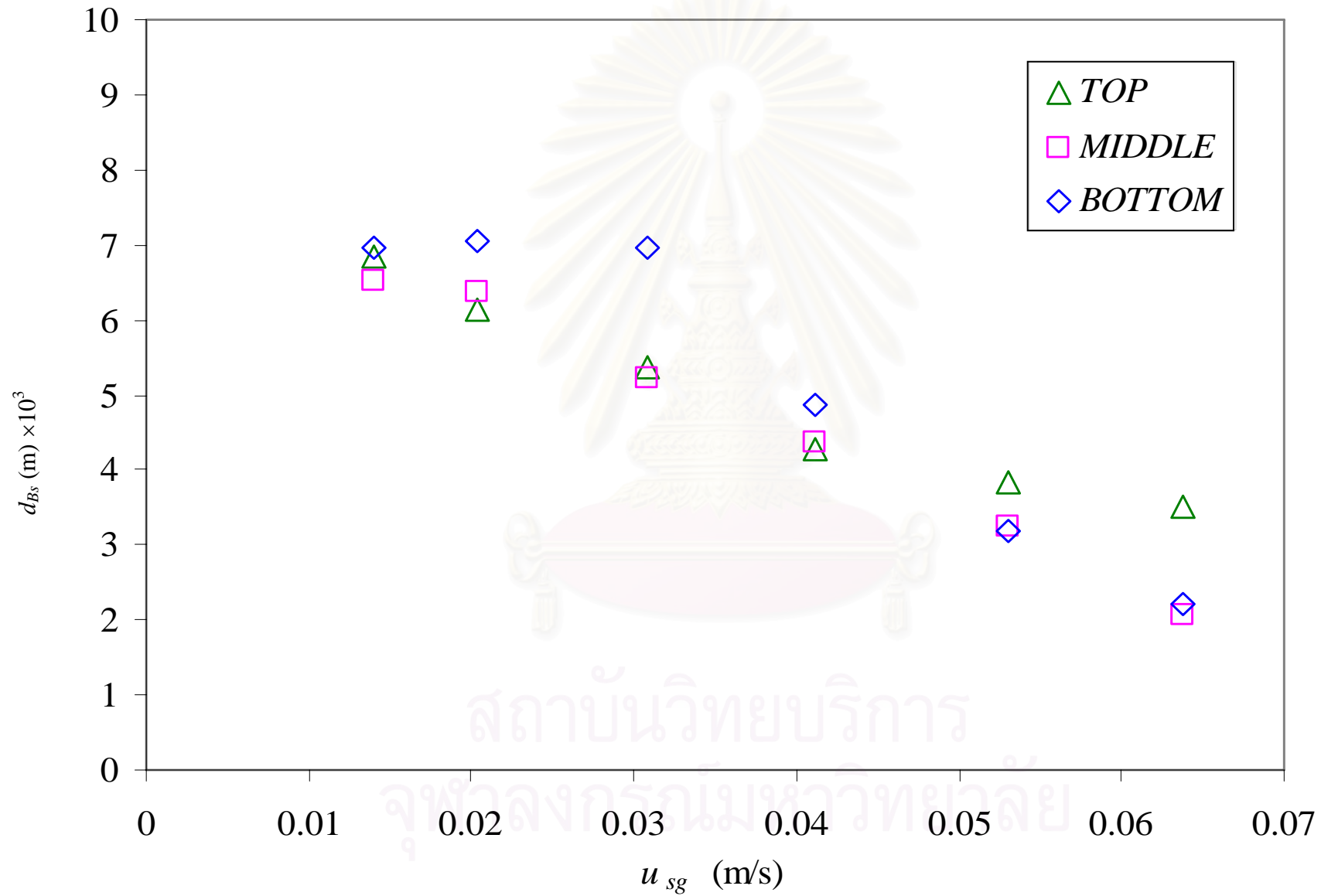


Figure 4.5 Bubble size at different locations in ALC with $A_d/A_r = 0.661$ (salinity = 30 ppt)

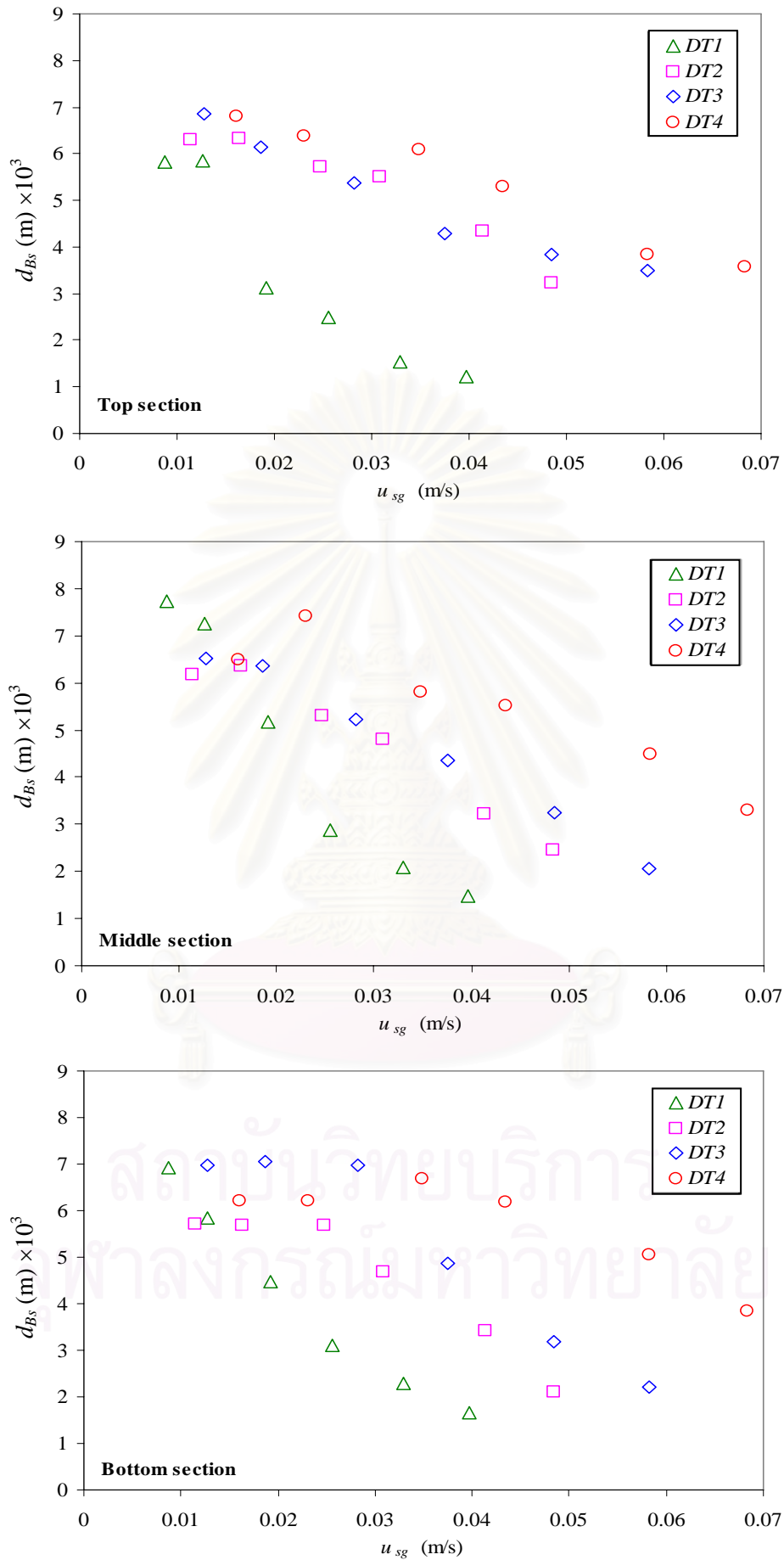


Figure 4.6 Bubble sizes at different draft tube sizes (DT1 = $A_d/A_r = 0.067$, DT2 = $A_d/A_r = 0.443$, DT3 = $A_d/A_r = 0.661$ and DT4 = $A_d/A_r = 1.01$) in ALCs (salinity = 30 ppt)

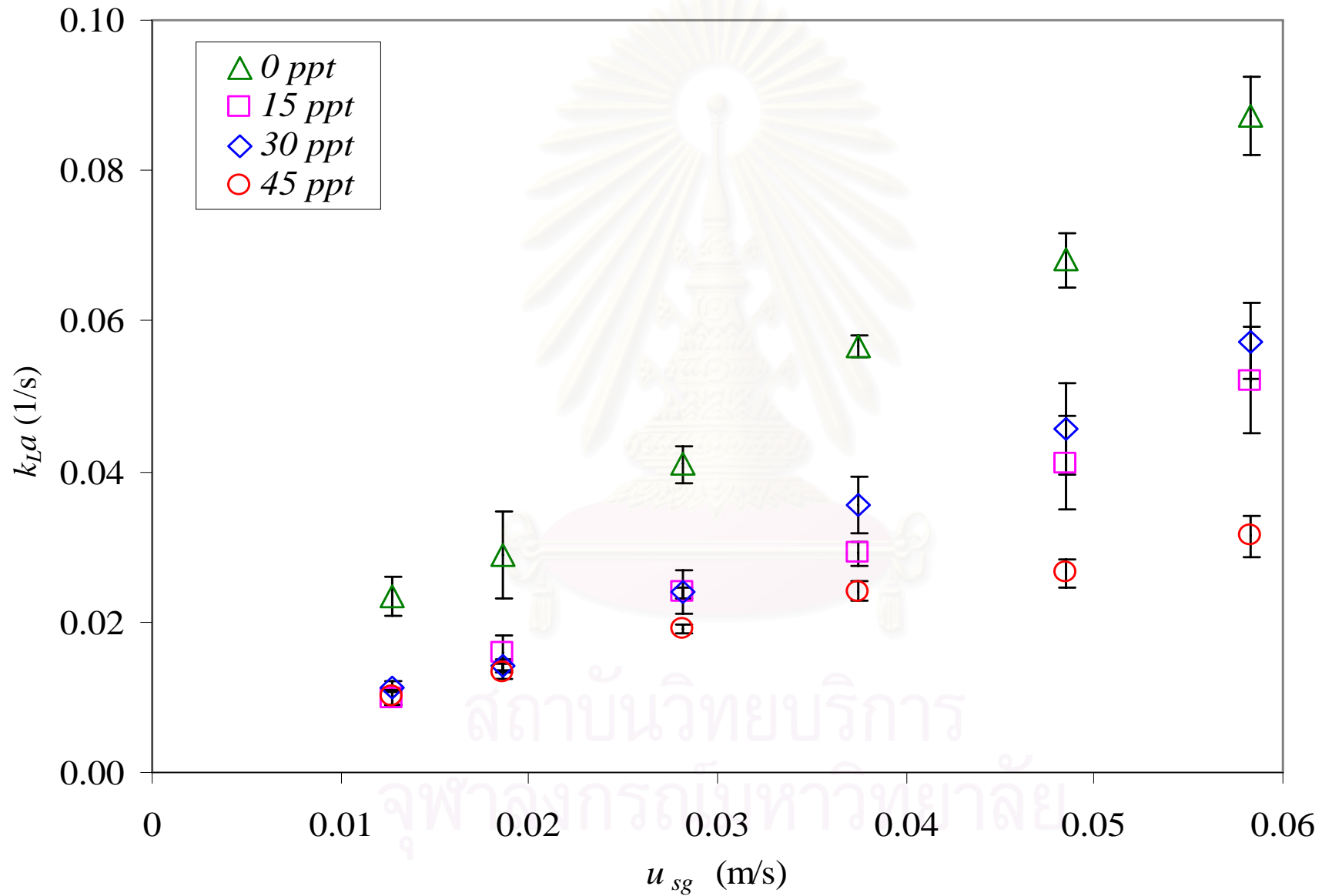


Figure 4.7 Overall volumetric mass transfer coefficient at different salinity levels (salinity = 0, 15, 30 and 45 ppt) in ALC ($A_d/A_r = 0.661$)

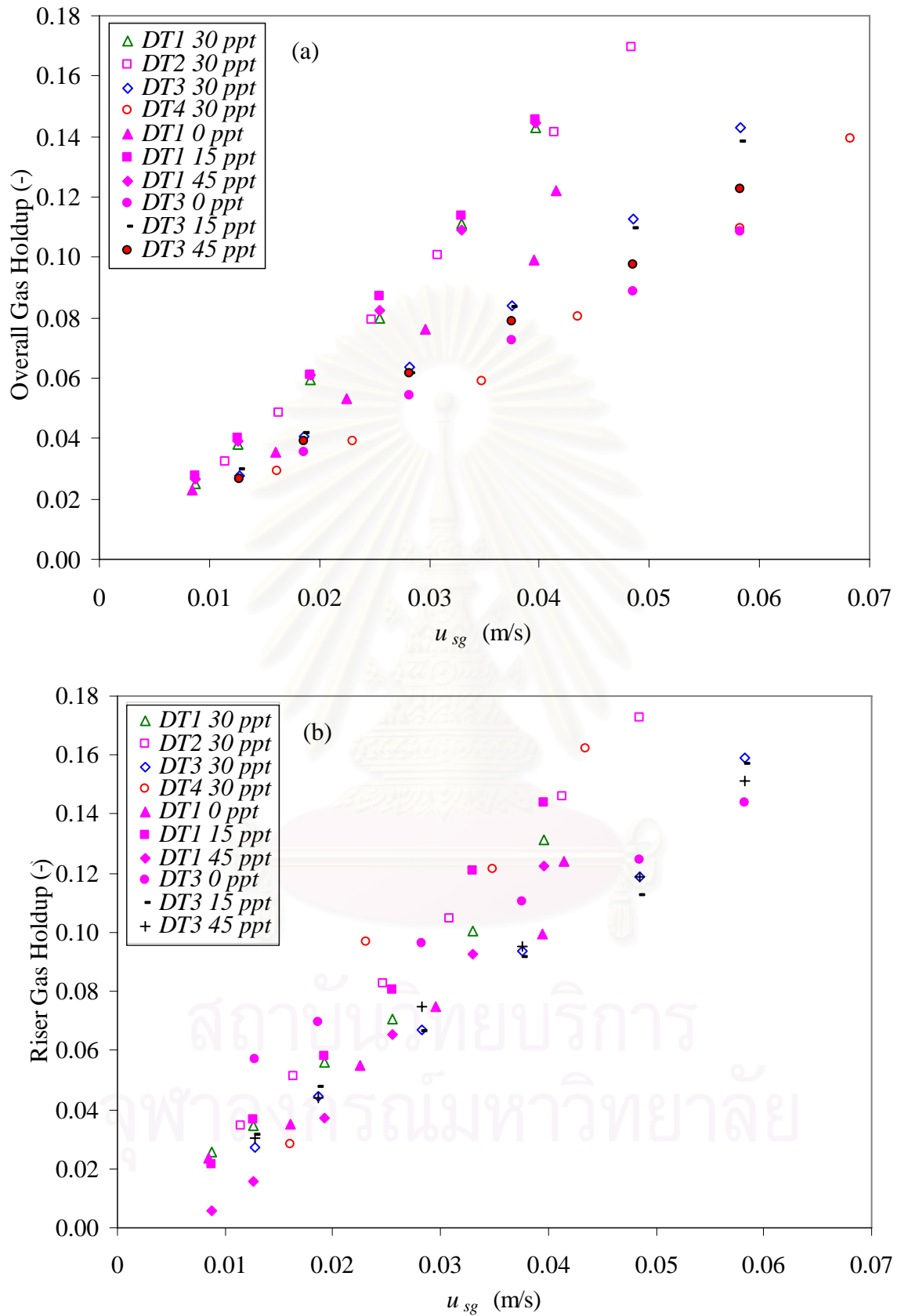


Figure 4.8 Effects of superficial gas velocity, u_{sg} on (a) overall gas holdup and (b) riser gas holdup with different draft tube sizes (DT1 = $A_d/A_r = 0.067$, DT2 = $A_d/A_r = 0.443$, DT3 = $A_d/A_r = 0.661$ and DT4 = $A_d/A_r = 1.01$)

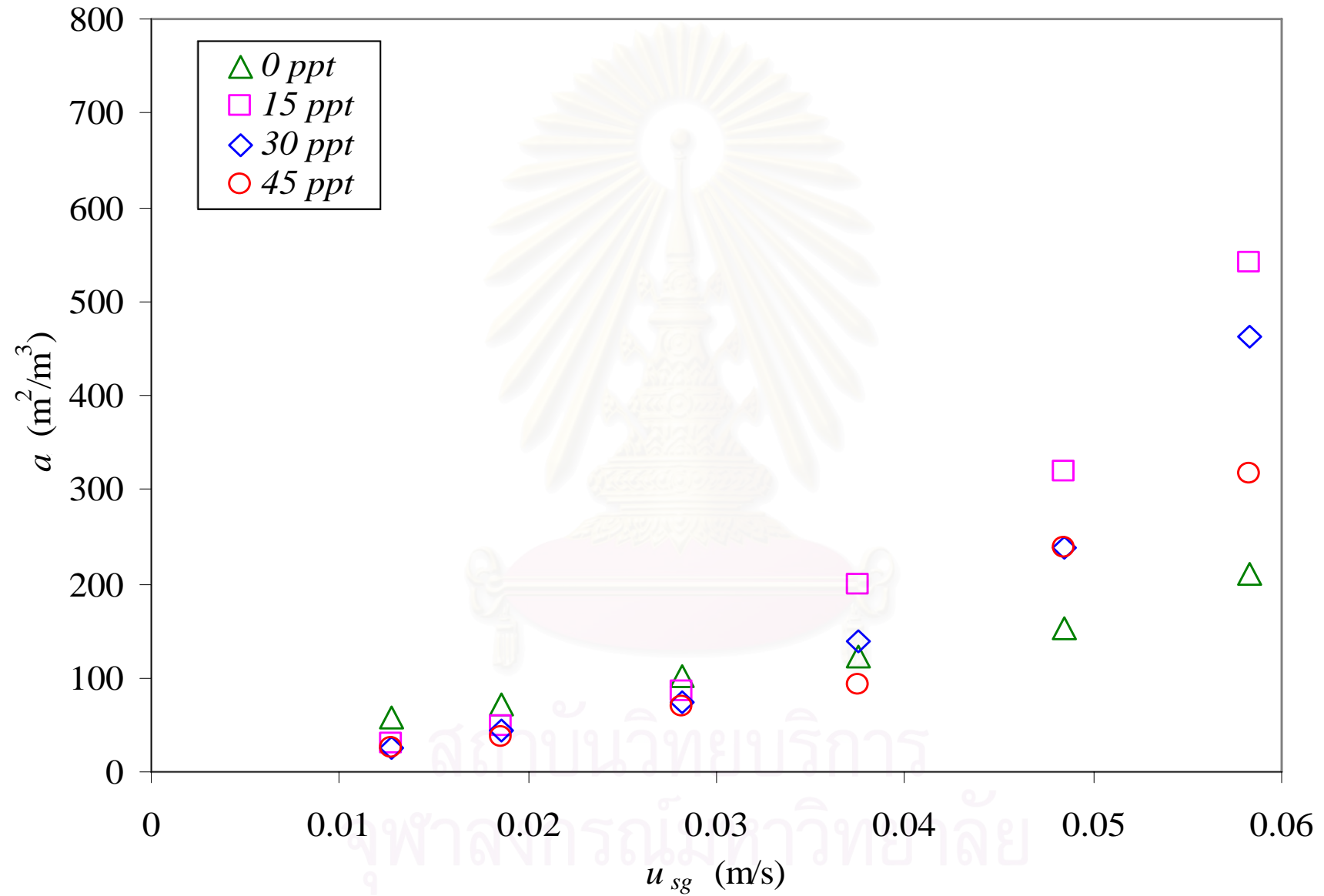


Figure 4.9 Specific interfacial area at different salinity levels (salinity = 0, 15, 30 and 45 ppt) in ALC ($A_d/A_r = 0.661$)

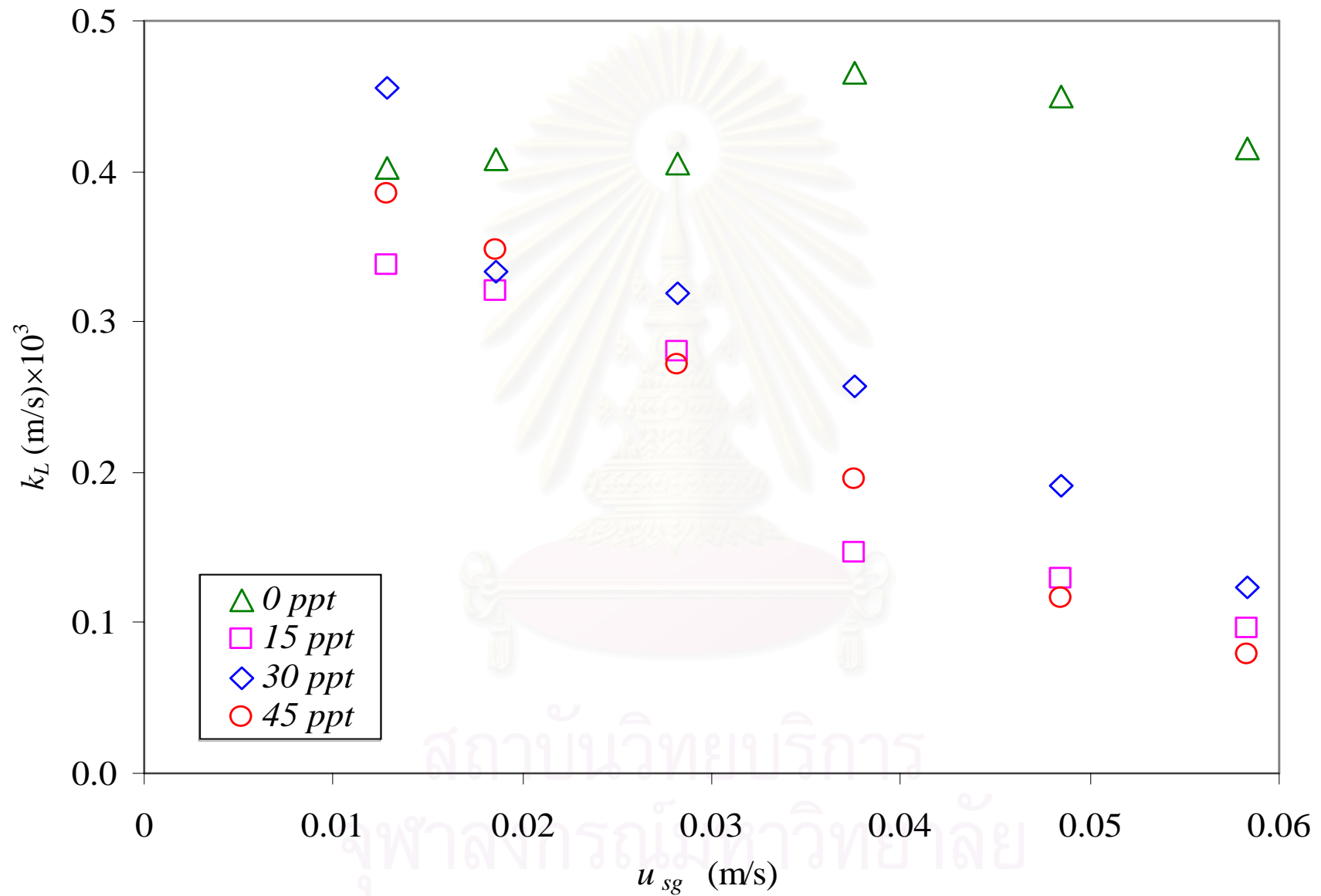


Figure 4.10 Effects of superficial gas velocity, u_{sg} on overall specific mass transfer coefficient, k_L

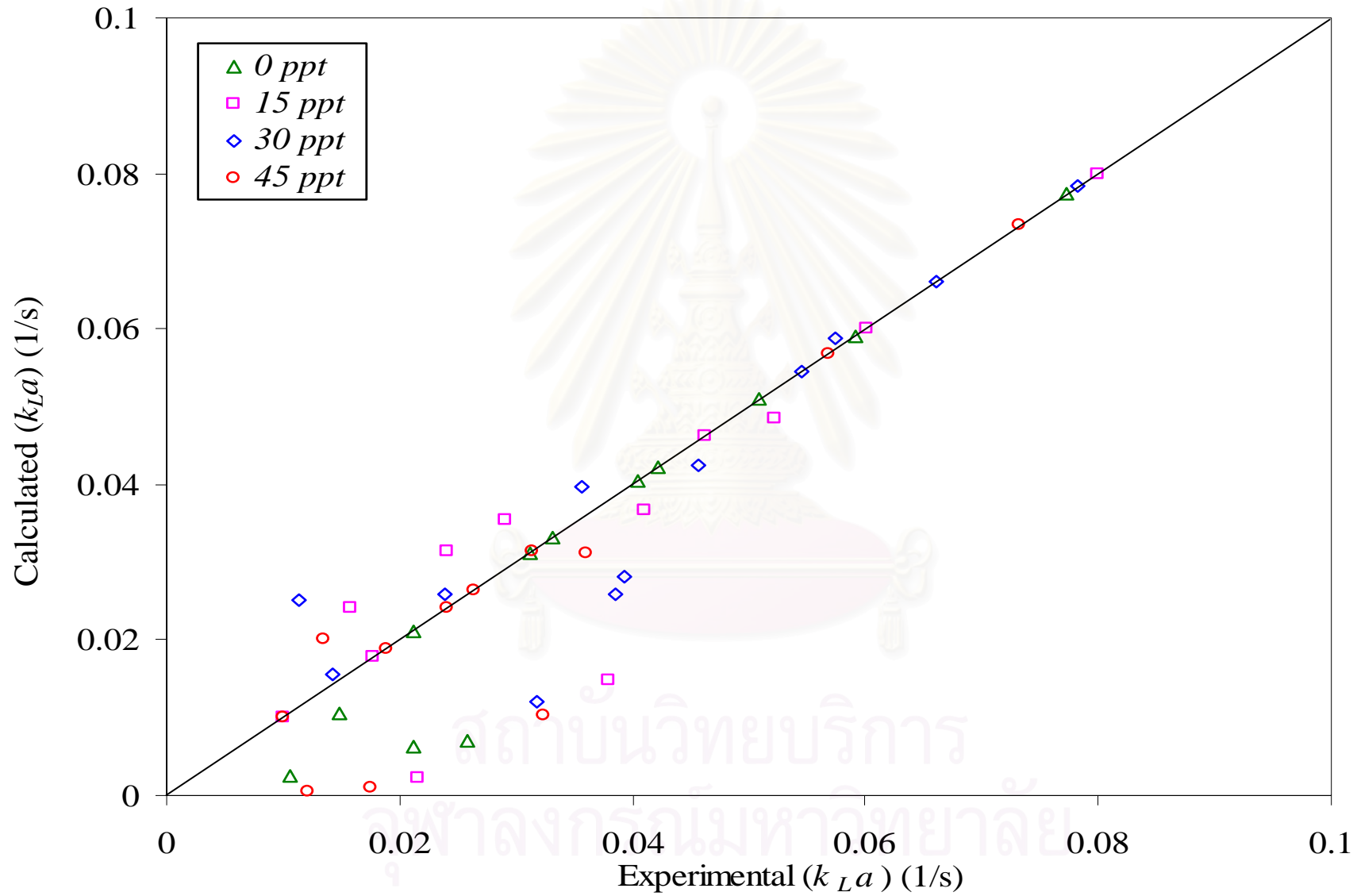


Figure 4.11 Comparison of (k_{La}) from experiment and (k_{La}) estimated by Equation (4.9) at different salinity levels (salinity = 0, 15, 30 and 45 ppt)

CHAPTER V

CONCLUSIONS & RECOMMENDATIONS

5.1 Achievements & Contributions

The finding from this work (as summarized in Table 5.1) revealed the effect of salinity on the performance of the airlift contactors both in terms of hydrodynamic properties and the mass transfer characteristics. It became clearer how the bubble size distributed within the airlift systems. The influence of salinity on liquid properties was described which could then be used to explain the mechanism of bubble coalescence and bubble breakup. Detail on bubble size alone is extremely important in predicting the rate of gas-liquid mass transfer rate in such airlift systems. This is not to mention the data on the liquid circulation which will facilitate the design of other biological systems in which the cell circulation is necessary for a good contact with fresh or re-fresh medium.

It was interesting to find out that the bubble size in the saline water was smaller than that in the fresh water systems, as salinity enhanced the surface tension which should give a larger bubble size. However, due to the balance of Laplace and ionic pressures, opposite results were observed. It was therefore expected to have a higher gas-liquid mass transfer rate in the saline solution. Nevertheless, it is worth mentioning that the saturated level of dissolved oxygen in saline water (7.57 mg/L at 15ppt, 6.95 mg/L at 30 ppt, and 6.38 mg/L at 45 ppt) is much lower than that in fresh water (8.24 mg/L).

Applications in saline water systems are variable and some will need knowledge on the operation of airlift such as the cultivation of single cell algae or diatom. Examples include the cultivation of *Chaetoceros calcitrans* which is the feed for shrimp larvae culture. Information obtained from this work can facilitate the future design of such system to have better circulation of the culture and to control the level of gas holdup in the various sections of the airlift systems.

Table 5.1 Summation of characteristics in airlift contactor with different salinity levels

Parameter	DT1 = 0.067	DT3 = 0.661	at 30 ppt
d_{Bs}	0 > 15 > 30 > 45 ppt	0 > 45 > 30 > 15 ppt	DT4 > 3 > 2 > 1
$\varepsilon_{g,o}$	15 > 45 > 30 > 0 ppt	15 > 30 > 45 > 0 ppt	DT1 > 2 > 3 > 4
$\varepsilon_{g,r}$	15 > 0 > 30 > 45 ppt	0 > 45 > 30 > 15 ppt	DT4 > 2 > 1 > 3
$\varepsilon_{g,d}$	45 > 30 > 15 > 0 ppt	30 > 15 > 45 > 0 ppt	DT1 > 2 > 3 > 4
	$\varepsilon_{g,d} > \varepsilon_{g,o} > \varepsilon_{g,r}$	$\varepsilon_{g,r} > \varepsilon_{g,o} > \varepsilon_{g,d}$	
$v_{l,riser}$	45 > 30 > 15 > 0 ppt	15 > 30 > 45 > 0 ppt (no sharply)	DT1 > 2 > 3 > 4
$v_{l,downcomer}$	45 > 15 > 30 > 0 ppt	0 > 15 > 30 > 45 ppt (no sharply)	DT3 > 2 > 1 > 4
k_{La}	30 > 15 > 45 > 0 ppt	0 > 30 > 15 > 45 ppt	DT1 > 2 > 3 > 4
k_L	0 > 15 > 30 > 45 ppt	0 > 30 > 45 > 15 ppt	DT1 > 2 > 3 > 5

5.2 Limitations & Recommendations

The ultimate goal of most reaction engineering is to be able to design the system that suits the need of industry. With this primary goal, this work is set out as a preliminary investigation what awaits the scale up to pilot and industrial levels. However, the design of the airlift systems or other pneumatic contactors is difficult in that the bubble size cannot be enlarged with the same scale as the reactors. Next proposals should then be directed towards the investigation of the behavior of a larger airlift system where a few design criteria should be employed as a design basis, such as the ratio between diameter and height, the ratio between downcomer and riser cross sectional area. Perhaps there will be some other dimensionless parameters which could be used with confidence in the scale up of such airlift contactors. Also configuration of airlift systems can be modified into a variety of designs, e.g. external loop airlift systems, expanded top airlift reactor, etc. This variation of the system configuration should also be visited.

References

- Al-Masry W. A., 1999. Effects of antifoam and Scale-up on Operation of Bioreactors. Chemical Engineering and Processing 38: 197-201.
- Al-Masry W. A., and Abasaed A.E., 1998. On the Scale-up of External Loop Airlift reactors: Newtonian systems. Chemical Engineering Science 53: 4085-4094.
- Azbel S. D., and Nicholas P., 1983. Cheremisinoff, Fluid Mechanics and Unit operations. Ann Arbor Science Publishers.
- Azher E. N., Gourich B., Vial C., Bellhaj M. S., Bouzidi A., Barkaoui M., and Ziyad M., 2005. Influence of Alcohol Addition on Gas Hold-Up, Liquid Circulation Velocity and Mass Transfer Coefficient in a Split-Rectangular Airlift Bioreactor. Biochemical Engineering Journal 23: 161–167.
- Bailey J. E., and Ollis D. F., 1986. Biochemical Engineering Fundamentals. Chemical Engineering Series: McGraw-Hill.
- Calderbank P. H., 1967. Mass Transfer in Fermentation Equipment, in: N. Blakebrough (Ed.), Biochemical and Biological Engineering Science, Vol. 2, Academic Press, New York, 1967, pp. 102–180.
- Cain W. F., and Lee C. J., 1985. A Techque for Studing the Drainage and Rupture of Unstable Liquid Films Formed between Two Captive Bubbles. Journal of Colloid and Interface Science 106: 70-85.
- Chisti, and Moo-Young M., 1988. Hydrodynamics and Oxygen Mass Transfer in a Pneumatic Bioreactor Devices. Biotechnol. Bioeng. 31: 487–494.
- Chisti M. Y., 1989. Airlift bioreactors. NY: Elsevier Science Publishing.
- Colella D., Vinci D., Bagatin R., Masi M., and Bakr A. E., 1999. A Study on Coalescence and Breakage Mechanisms in three Different Bubble Columns. Chemical Engineering Science 54: 4767-4777
- Contreras A., Garcia F., Molina E., and Merchuk J. C., 1999. Influence of Sparger on Energy Dissipation, Shear Rate, and Mass Transfer to Sea Water in a Concentric-tube Airlift Bioreactor. Enzyme and Microbial Technology 25: 820-830.
- Couvert A., Roustan M., and Chatellier P., 1999. Two-phase Hydrodynamic Study of a Rectangular Airlift Loop Reactor with an Internal Baffle. Chem. Eng. Sci. 54: 5245–5252.

- De Nevers N., 1991. Fluid Mechanics for Chemical Engineers. International Edition. McGraw-Hill, Inc.
- Felice R. D., 2005. Liquid Circulation Rates in Two- and Three-Phase External Airlift Reactors. Chemical Engineering Journal 109: 49–55.
- Gourich B., Azher N. E., Bellhaj M. S., Delmas H., Bouzidi A., and Ziyad M., 2005. Contribution to the Study of Hydrodynamics and Gas–Liquid Mass Transfer in a Two- and Three-Phase Split-Rectangular Airlift Reactor. Chemical Engineering and Processing 44: 1047–1053.
- Guo-Qing L., Shou-Zhi Y., Zhao-Ling C., and Jia-Yong C., 1995. Mass Transfer and Gas-Liquid Circulation in an Airlift Bioreactor with Viscous Non-Newtonian Fluid. The Chemical Engineering Journal 56: B101-B107.
- Hartland Stanley, 2004. Surface and Interface Tension: Measurement, Theory, and Applications. Surfactant Science Series: 119. New York; Basel: Marcel Dekker.
- Higbie R., 1935. Rate of Absorption of a Pure Gas into a still Liquid during short Period of Exposure. Trans. Am. Inst. Chem. Eng. 31: 365–389.
- Hofmeier U., Yaminsky V. V., and Christenson H. K., 1995. Observations of Solute Effects on Bubble Formation. Journal of Colloid and Interface Science 174: 199-210.
- Hwang S.-J., and Cheng Y.-L., 1997. Gas Holdup and Liquid Velocity in Three-Phase Internal-Loop Airlift Reactors. Chemical Engineering Science 52: 3949-3960.
- Jamialahmadi M., Branch C., and Müller-Steinhagen, 1994. Terminal Bubble Rise Velocity in Liquid. Trans. Inst. Chem. Eng. Part A 72: 119-122.
- Kaewpintong K., 2004. Cultivation of *Haematococcus pluvialis* in Airlift Bioreactor. Master's Thesis, Department of Chemical Engineering, Graduate School, Chulalongkorn University.
- Kafarov V., 1985. Fundamental of Mass Transfer Gas-Liquid, Vapour-Liquid and Liquid-Liquid System, Second Edition. Mir Publisher Moscow.
- Kantarci N., Borak F., and Ulgen K. O., 2005. Review: Bubble column reactors. Process Biochemistry 40: 2263–2283.
- Krichnavaruk et al., 2005. Effects of Perforated Plates on Mass Transfer and Hydrodynamic Behavior in the Internal Loop Airlift Contactor. Mass's Thesis,

Department of Chemical Engineering Graduate School, Chulalongkorn University.

- Lessard R. R. and Zieminiski A. S., 1971. Bubble Coalescence and Gas Transfer in Aqueous Electrolytic Solutions. Ind. Eng. Chem. Fundam 10: 260-269.
- Levich V. G., 1962. *Physicochemical Hydrodynamics*. Prentice-Hall, Englewood Cliffs, NJ.
- Limpanuphap A., 2003. Hydrodynamics and mass transfer in internal loop airlift contactor with sea water. Master's Thesis, Department of Chemical Engineering, Graduate School, Chulalongkorn University.
- Loataweesup W., 2002. Cultivation of a Diatom Chaetoceros calcitrans in Airlift Bioreactor. Master's Thesis, Department of Chemical Engineering, Graduate School Engineer.
- Malysa K., Krasowska M., and Krzan M., 2005. Influence of Surface Active Substances on Bubble Motion and Collision with Various Interfaces. Advances in Colloid and Interface Science 114-115: 205-225.
- Marrucci G., 1965. Rising Velocity of a Swarm of Spherical Bubbles. Ind. Eng. Chem. Fundam 4: 224–225.
- Marrucci G. and Nicodemo L., 1967. Coalescence of Gas Bubbles in Aqueous Solution of Inorganic Electrolytes. Chemical Engineering Science 22: 1257-1265.
- Marrucci G., 1969. A Theory of Coalescence. Chemical Engineering Science 24: 975-985.
- Merchuk J. C., Contreras A., Garcia F., and Molina E., 1998. Studies of Mixing in a Concentric Tube Airlift Bioreactor with Different Spargers. Chemical Engineering Science 53: 709-719.
- Mouza A. A., Dalakoglou K. G. and Paras V. S., 2005. Effect of Liquid Properties on the Performance of Bubble Column Reactors with Fine Pore Spargers. Chemical Engineering Science 60: 1465-1475.
- Olmos E., Gentric C., and Midoux N., 2003. Numerical Description of Flow Regime Transitions in Bubble Column Reactors by a Multiple Gas Phase Model. Chemical Engineering Science 58: 2113 – 2121.

- Painmanakul P., Loubère K., Hebrard G., Mietton-Peuchot M., and Roustan M., 2005. Effect of Surfactants on Liquid-Side Mass Transfer Coefficients. Chemical Engineering Science 60: 6480 – 6491.
- Philip J., Proctor J. M., Niranjana K., and Davidson J. F., 1990. Gas Hold-Up and Liquid Circulation in Internal Loop Reactors Containing Highly Viscous Newtonian and Non-Newtonian Liquid. Chemical Engineering Science 45: 651-644.
- Pironti F. F., Medina V. R., Calvo R., and Saez A. E., 1995. Effect of Draft Tube Position on the Hydrodynamics of a Draft Tube Slurry Bubble Column. The Chemical Engineering Journal 60: 155-160.
- Pollia M., Stanislaw M. D., Bagatin R., Bakr E. A., and Masi M., 2002. Bubble Size Distribution in the Sparger Region of Bubble Columns. Chemical Engineering Science 57: 197–205.
- Popovic M., and Robinson C. W., 1988. External Circulation Loop Airlift Bioreactors: Study of the Liquid Circulating Velocity in Highly Viscous Non Newtonian Liquids. Biotechnology and Bioengineering 32: 301-312.
- Popovic M. K., and Robinson C. W., 1989. Mass Transfer Studies of External-Loop Airlifts and a Bubble Column. AIChE Journal 35: 393-405.
- Prince Michael, J. and Blanch Harvey, W., 1990. Transition Electrolyte Concentrations for Bubble Coalescence. AIChE Journal 36: 1425-1429. (a)
- Prince Michael, J. and Blanch Harvey W., 1990. Bubble coalescence and Break-up in Air-sparged Bubble Column. AIChE Journal 36: 1485-1499. (b)
- Rodrigues R. T., and Rubio J., 2003. New Basis for Measuring the Size Distribution of Bubbles. Minerals Engineering 16: 757–765.
- Seader J. D., and Henley E. J., 1998. Separation Process Principles. John Wiley & Sons, Inc.
- Shah Y. T., 1983. Handbook of Fluids in Motion. Ann Arbor Science.
- Skelland A. H. P., 1974. Diffusional Mass Transfer, Wiley, New York.
- Snape J. B., Fialova M., Zahradnik J., and Thomas N. H., 1992. Hydrodynamic Studies in an External Loop Airlift Reactor Containing Aqueous Electrolyte and Sugars Solutions. Chemical Engineering Science 47: 3387-3394.

- Snape J. B., Zahradnik J., Fialova M., and Thomas N. H., 1995. Liquid-Phase Properties and Sparger Design Effects in an External-Loop Airlift Reactor. Chemical Engineering Science 50: 3175-3186.
- Stanley M., 1998. An Introduction to Mass and Heat Transfer, Wiley, New York.
- Tanthikul N., 2004. Hydrodynamics and Mass transfer Behavior in Multiple draft tube Airlift Contactors. Master's Thesis, Department of Chemical Engineering, Graduate School, Chulalongkorn University.
- Tchobanoglous G., Burton F., and Stensel D. H., 2003. Wastewater Engineering. Boston: Mc Graw Hill.
- Teitel Y., and Bornea D., 1980. Modelling Flow Pattern Transitions for Steady Upward Gas-Liquid Flow in Vertical Tubes. AIChE Journal 26: 345-354.
- Treybal R. E., 1980. Mass Transfer Operations, McGraw-Hill, New York.
- Tsang Y. H., Young-Ho K. and Donald L. K., 2004. Bubble-size Dependence of the Critical Electrolyte Concentration for Inhibition of Coalescence. Journal of Colloid and Interface Science 275: 290-297.
- Tsao-Jen L., and Po-Chou C., 2005. Studies on Hydrodynamics of an Internal-loop Airlift Reactor in Gas Entrainment Regime by Particle Image Analyzer. Chemical Engineering Journal 108: 69–79.
- Tse L. K., Martin T., McFarlane M. C., and Nienow W. A., 2003. Small Bubble Formation via a Coalescence dependent Break-up Mechanism. Chemical Engineering Science 58: 275-286.
- Van Baten J. M., Ellenberger J., and Krishna R., 2003. Hydrodynamics of Internal Air-Lift Reactors: Experiments versus CFD. Simulations Chemical Engineering and Processing 42: 733-742.
- Vasconcelos J. M. T., Rodrigues J. M. L., Orvalho S. C. P., Alves S. S., Mendes R. L., and Reis A., 2003. Effect of Contaminants on Mass Transfer Coefficients in Bubble Column and Airlift Contactors. Chemical Engineering Science 58: 143- 1440.
- Vázquez G., Cancela M. A., Riverol C., Alvarez E., and Navaza J. M., 2000. Application of the Danckwerts Method in a Bubble Column Effects of Surfactants on Mass Transfer Coefficient and Interfacial Area. Chemical Engineering Journal 78: 13–19.
- Wallis G. B., 1969. One Dimensional Two-Phase Flow, McGraw-Hill, New York.

- Welty J. R., Wicks C. E., and Wilson R. E., 1984. Fundamentals of Momentum, Heat, and Mass Transfer, Wiley, New York.
- Weissenborn P. K., and Pugh R. J., 1996. Surface Tension of Aqueous Solutions of Electrolytes: Relationship with Ion Hydration, Oxygen Solubility, and Bubble Coalescence. Journal of Colloid and Interface Science 184: 550–563.
- Wongsuchoto P., 2002. Bubble Characteristics and Liquid Circulation in Internal Loop Airlift Contactors. Doctoral's Thesis, Department of Chemical Engineering, Graduate School, Chulalongkorn University.
- Wongsuchoto P., Charinpanitkul T., and Pavasant P., 2003. Bubble Size Distribution and Gas-liquid Mass Transfer in Airlift Contactors. Chemical Engineering Journal 92: 81-90.
- Wongsuchoto, P. and Pavasant, P. 2004. Internal Liquid Circulation in Annulus Sparged Internal Loop Airlift Contactors. Chemical Engineering Journal 100: 1-9.
- Zahradnik J., Fialova M., Ruzicka M., Drahos J., Kastanek F., and Thomas N. H., 1997. Duality of the Gas-liquid Flow Regimes in Bubble Column Reactors. Chemical Engineering Science 52: 3811-3826.
- Zhao M., Niranjana K., and Davidson J. F., 1994. Mass Transfer to Viscous Liquids in Bubble Column and Air-Lift Reactors: Influence of Baffles. Chemical Engineering Science 49: 2359-2369.



APPENDICES

สถาบันวิทยบริการ
จุฬาลงกรณ์มหาวิทยาลัย

Appendix A

Table A-1 Physical properties of liquid phase

Liquid phase	Surface tension $\times 10^3$	Viscosity $\times 10^3$ (kg/m.s)	density $\times 10^{-3}$ (kg/m ³)
Tap water	72.6	1.28	0.996
Sea water at 15 ppt	73.1	1.44	1.005
Sea water at 30 ppt	73.7	1.47	1.016
Sea water at 45 ppt	73.9	1.49	1.027

Note: The salinity levels were measured by OPTIK Handheld Refractometer.

The density of solution was measured by pycnometer (UL/Y ADAPTER, MIDDLE BORO, MA 02346 U.S.A., Brook field ENGINEERING LABS INC) and rotation with 100 rpm at 26.5°C.

The surface tension was measured with KRUSS K10T (Du Noüy Ring).

Table A-2 Liquid phase used in this work

Key	Liquid phase
0 ppt	Tap water
15 ppt	Sea water at 15 ppt
30 ppt	Sea water at 30 ppt
45 ppt	Sea water at 45 ppt

Table A-3 Solubility of dissolved oxygen in liquid phase

(Tchobanoglous et al., 2003)

Liquid phase	Dissolved oxygen concentration (mg/l)
Tap water	8.24
Sea water at 15 ppt	7.57
Sea water at 30 ppt	6.95
Sea water at 45 ppt	6.38

Table A-4 Operating conditions for each ALC system

ALCs	Superficial gas velocity (m/s)					
	①	②	③	④	⑤	⑥
DT1	0.008	0.012	0.018	0.022	0.030	0.035
DT2	0.011	0.016	0.025	0.031	0.041	0.048
DT3	0.013	0.019	0.029	0.036	0.048	0.056
DT4	0.016	0.023	0.035	0.044	0.058	0.068
Symbol	————	-----	-----	————	-----



สถาบันวิทยบริการ
จุฬาลงกรณ์มหาวิทยาลัย

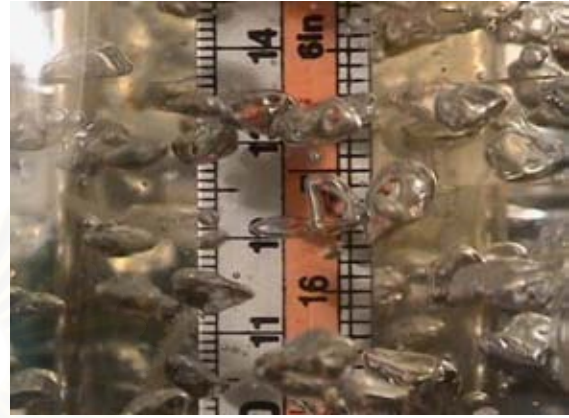
Appendix B

Bubble Pictures in ALCs running with different Draft Tube Sizes ($A_d/A_r = 0.067-1.008$) and different Salinity levels (15-45 ppt)

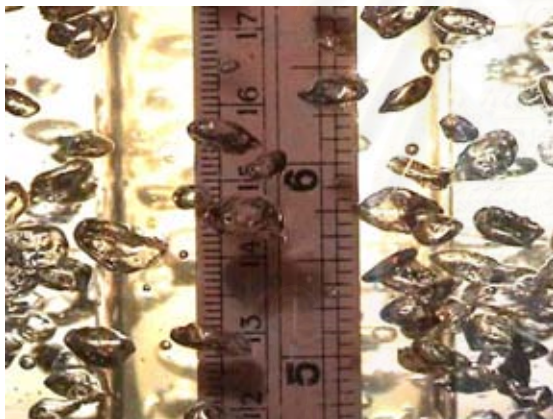
B-1 15 ppt with $A_d/A_r = 0.067$



a) Superficial Gas Velocity = 0.008 m/s
Top Section



a) Superficial Gas Velocity = 0.012 m/s
Top Section



b) Superficial Gas Velocity = 0.008 m/s
Middle Section



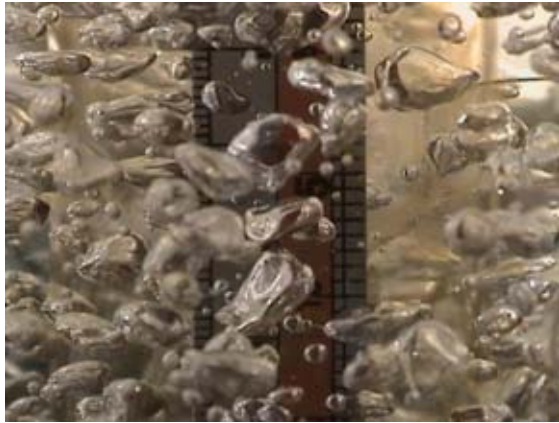
b) Superficial Gas Velocity = 0.012 m/s
Middle Section



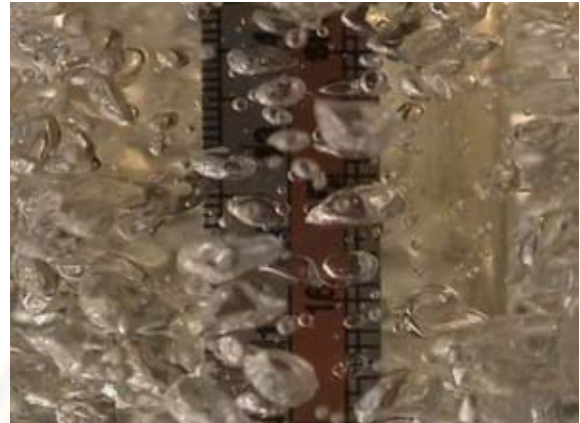
c) Superficial Gas Velocity = 0.008 m/s
Bottom Section



B -1 15 ppt with $A_d/A_r = 0.067$
c) Superficial Gas Velocity = 0.012 m/s
Bottom Section



a) Superficial Gas Velocity = 0.018 m/s
Top Section



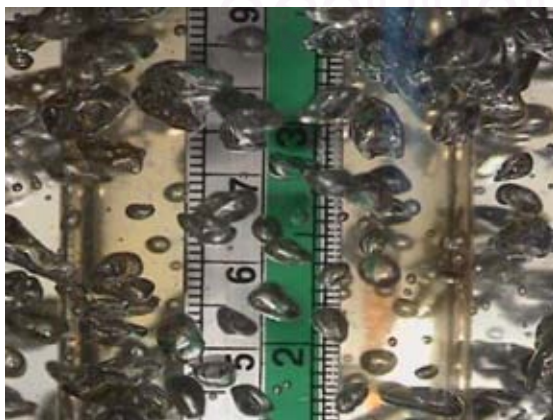
a) Superficial Gas Velocity = 0.022 m/s
Top Section



b) Superficial Gas Velocity = 0.018 m/s
Middle Section



b) Superficial Gas Velocity = 0.022 m/s
Middle Section



c) Superficial Gas Velocity = 0.018 m/s
Bottom Section



c) Superficial Gas Velocity = 0.022 m/s
Bottom Section
B-1 15 ppt with $A_d/A_r = 0.067$



a) Superficial Gas Velocity = 0.030 m/s
Top Section



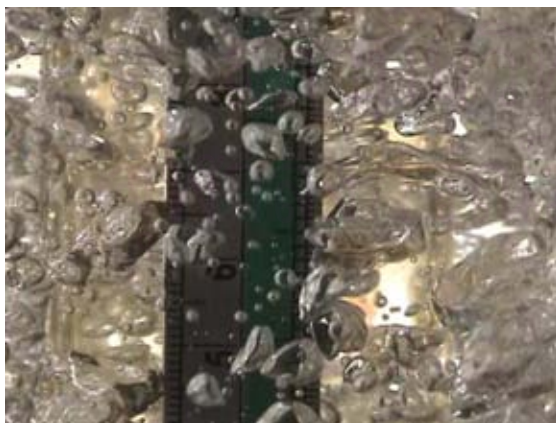
a) Superficial Gas Velocity = 0.035 m/s
Top Section



b) Superficial Gas Velocity = 0.030 m/s
Middle Section



b) Superficial Gas Velocity = 0.035 m/s
Middle Section

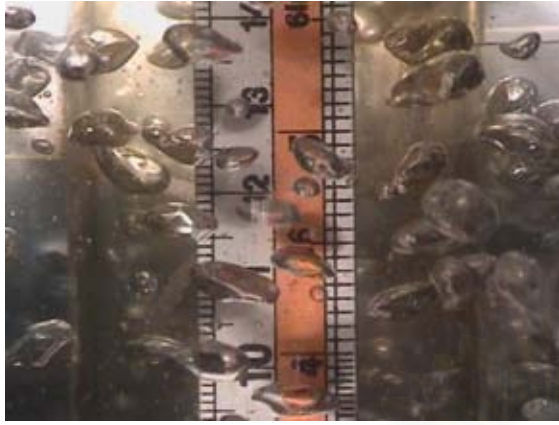


c) Superficial Gas Velocity = 0.030 m/s
Bottom Section

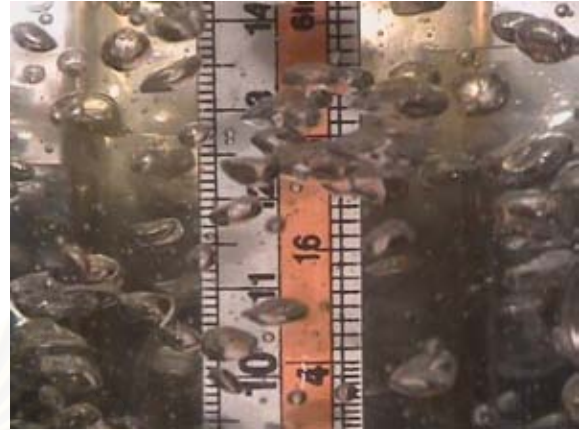


c) Superficial Gas Velocity = 0.035 m/s
Bottom Section

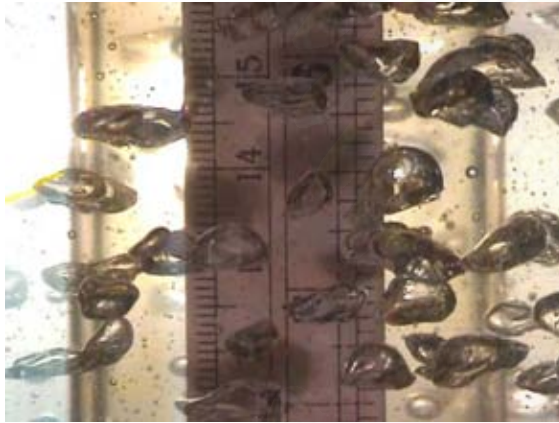
B-2 30 ppt with $A_d/A_r = 0.067$



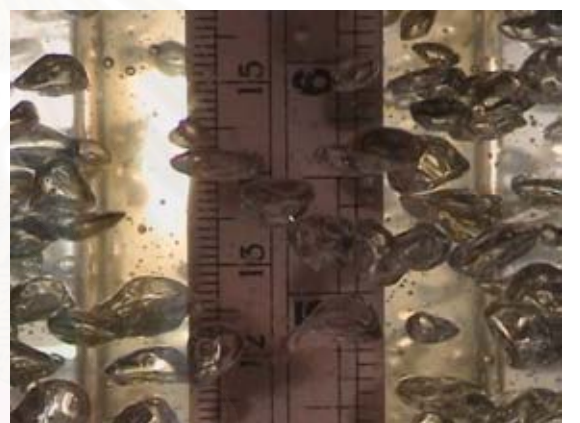
a) Superficial Gas Velocity = 0.008 m/s
Top Section



a) Superficial Gas Velocity = 0.012 m/s
Top Section



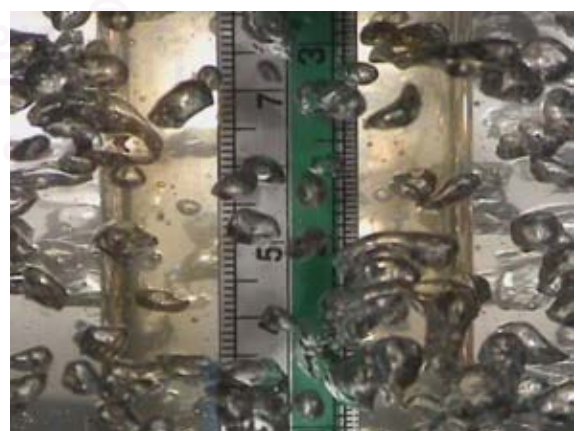
b) Superficial Gas Velocity = 0.008 m/s
Middle Section



b) Superficial Gas Velocity = 0.012 m/s
Middle Section



c) Superficial Gas Velocity = 0.008 m/s
Bottom Section



c) Superficial Gas Velocity = 0.012 m/s
Bottom Section

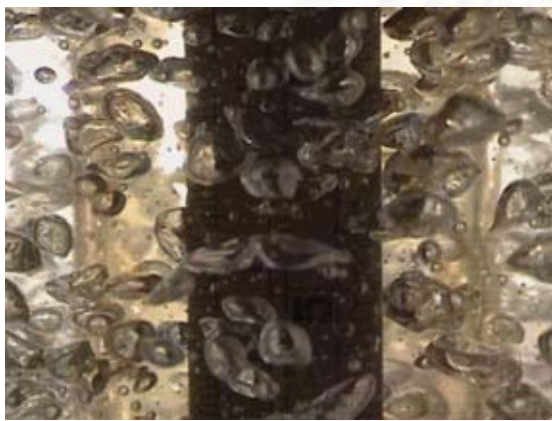
B-2 30 ppt with $A_d/A_r = 0.067$



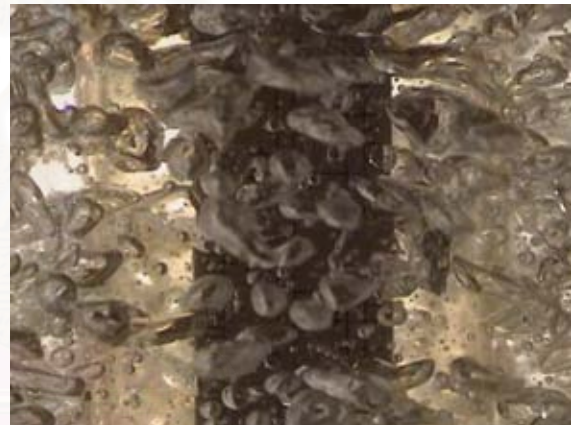
a) Superficial Gas Velocity = 0.018 m/s
Top Section



a) Superficial Gas Velocity = 0.022 m/s
Top Section



b) Superficial Gas Velocity = 0.018 m/s
Middle Section



b) Superficial Gas Velocity = 0.022 m/s
Middle Section

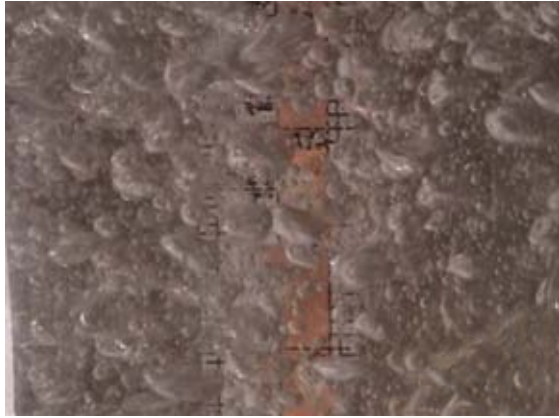


c) Superficial Gas Velocity = 0.018 m/s
Bottom Section



c) Superficial Gas Velocity = 0.022 m/s
Bottom Section

B-2 30 ppt with $A_d/A_r = 0.067$



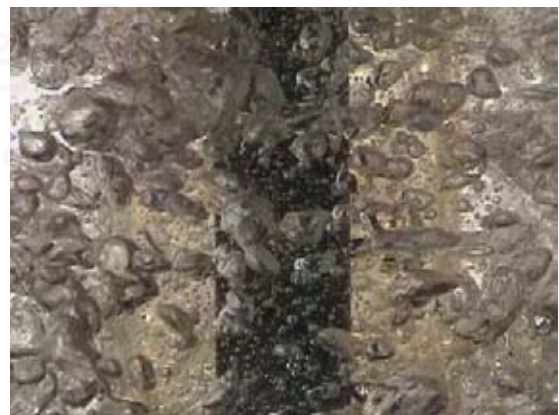
a) Superficial Gas Velocity = 0.030 m/s
Top Section

a) Superficial Gas Velocity = 0.035 m/s
Top Section



b) Superficial Gas Velocity = 0.030 m/s
Middle Section

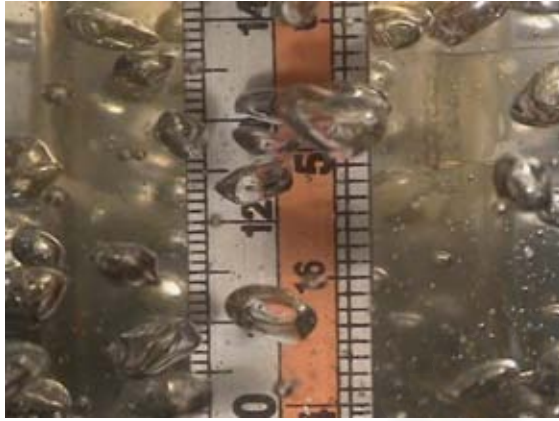
b) Superficial Gas Velocity = 0.035 m/s
Middle Section



c) Superficial Gas Velocity = 0.030 m/s
Bottom Section

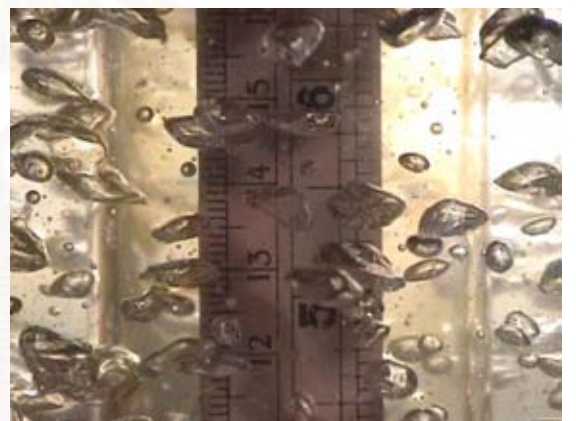
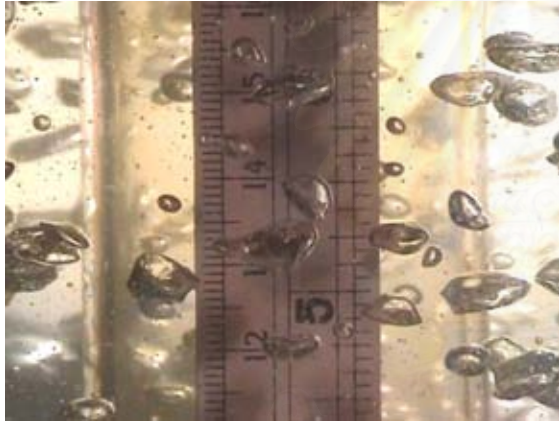
c) Superficial Gas Velocity = 0.035 m/s
Bottom Section

B-3 45 ppt with $A_d/A_r = 0.067$



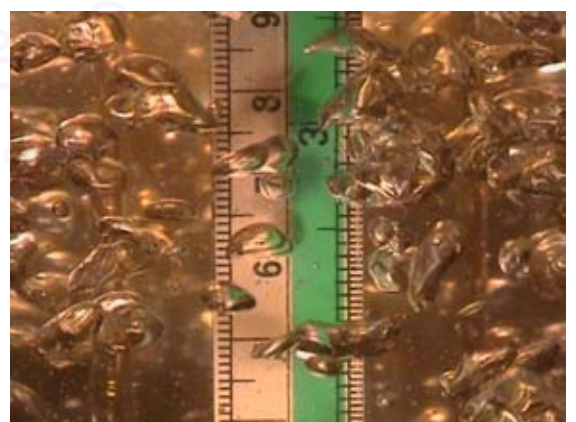
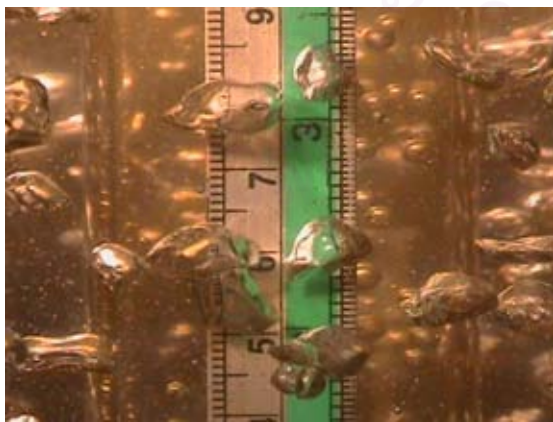
a) Superficial Gas Velocity = 0.008 m/s
Top Section

a) Superficial Gas Velocity = 0.012 m/s
Top Section



b) Superficial Gas Velocity = 0.008 m/s
Middle Section

b) Superficial Gas Velocity = 0.012 m/s
Middle Section



c) Superficial Gas Velocity = 0.008 m/s
Bottom Section

c) Superficial Gas Velocity = 0.012 m/s
Bottom Section

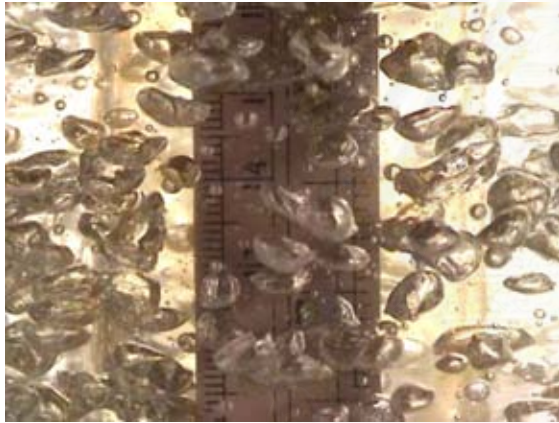
B-3 45 ppt with $A_d/A_r = 0.067$



a) Superficial Gas Velocity = 0.018 m/s
Top Section



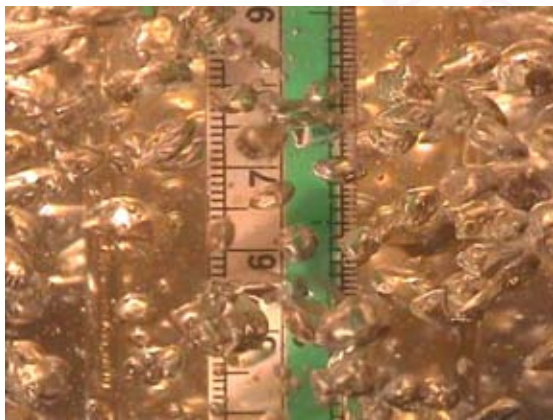
a) Superficial Gas Velocity = 0.022 m/s
Top Section



b) Superficial Gas Velocity = 0.018 m/s
Middle Section



b) Superficial Gas Velocity = 0.022 m/s
Middle Section



c) Superficial Gas Velocity = 0.018 m/s
Bottom Section



c) Superficial Gas Velocity = 0.022 m/s
Bottom Section

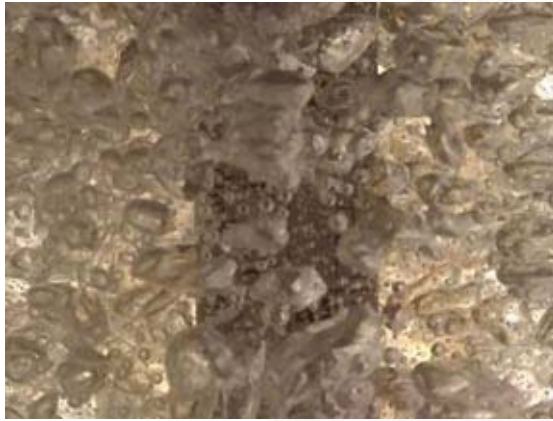
B-3 45 ppt with $A_d/A_r = 0.067$



a) Superficial Gas Velocity = 0.030 m/s
Top Section



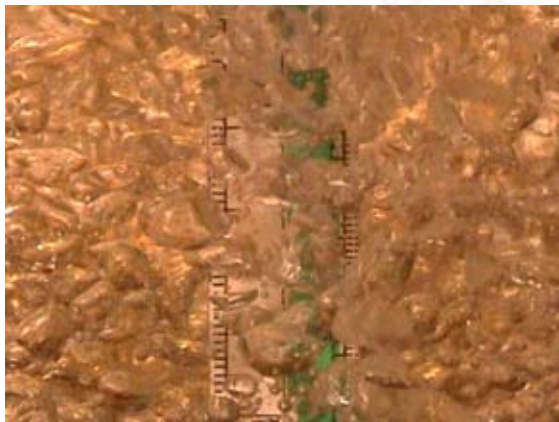
a) Superficial Gas Velocity = 0.035 m/s
Top Section



b) Superficial Gas Velocity = 0.030 m/s
Middle Section



b) Superficial Gas Velocity = 0.035 m/s
Middle Section



c) Superficial Gas Velocity = 0.030 m/s
Bottom Section



c) Superficial Gas Velocity = 0.035 m/s
Bottom Section

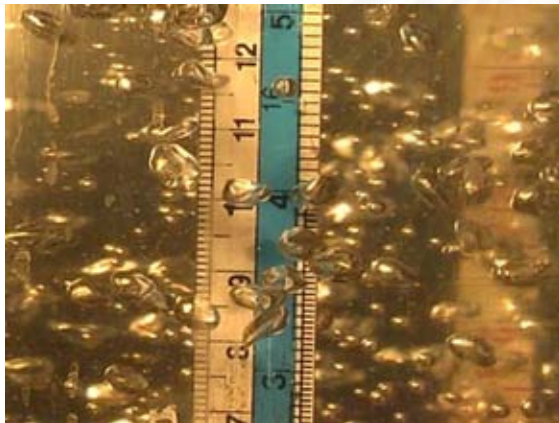
B-4 30 ppt with $A_d/A_r = 0.443$



a) Superficial Gas Velocity = 0.011 m/s
Top Section



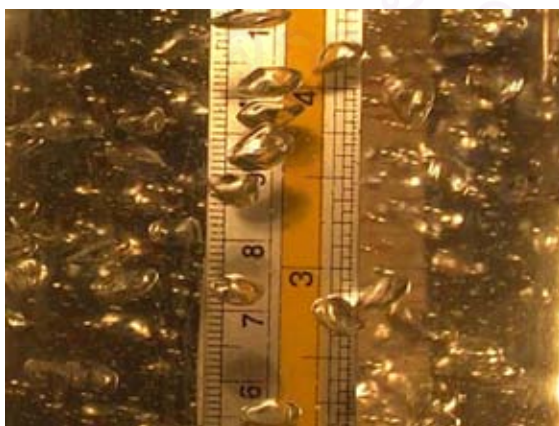
a) Superficial Gas Velocity = 0.016 m/s
Top Section



b) Superficial Gas Velocity = 0.011 m/s
Middle Section



b) Superficial Gas Velocity = 0.016 m/s
Middle Section

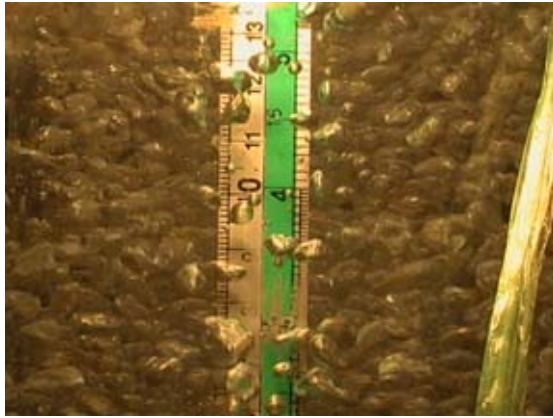


c) Superficial Gas Velocity = 0.011 m/s
Bottom Section



c) Superficial Gas Velocity = 0.016 m/s
Bottom Section

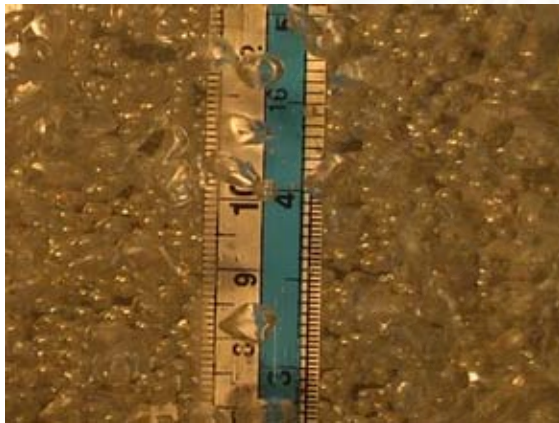
C-4 30 ppt with $A_d/A_r = 0.443$



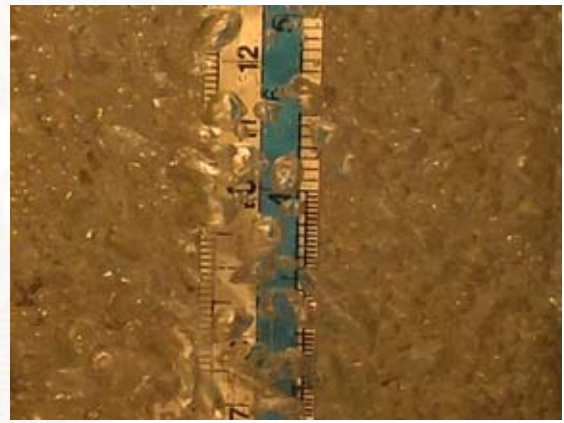
a) Superficial Gas Velocity = 0.025 m/s
Top Section



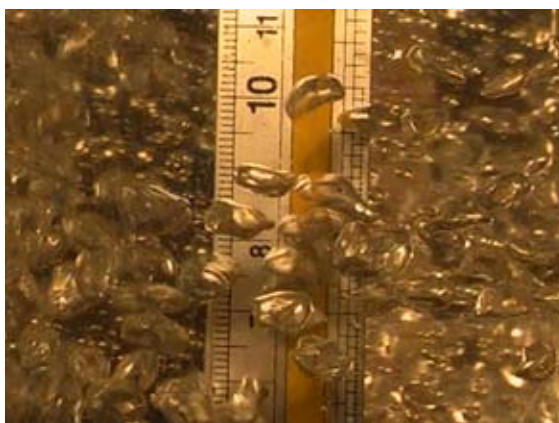
a) Superficial Gas Velocity = 0.031 m/s
Top Section



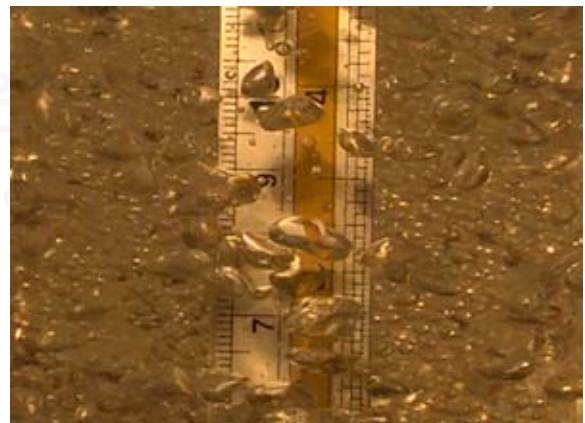
b) Superficial Gas Velocity = 0.025 m/s
Middle Section



b) Superficial Gas Velocity = 0.031 m/s
Middle Section

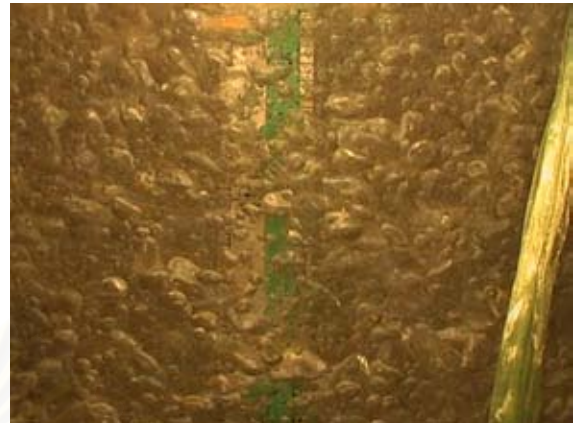
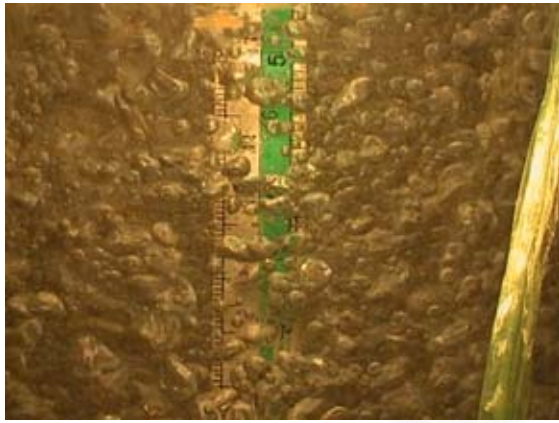


c) Superficial Gas Velocity = 0.025 m/s
Bottom Section



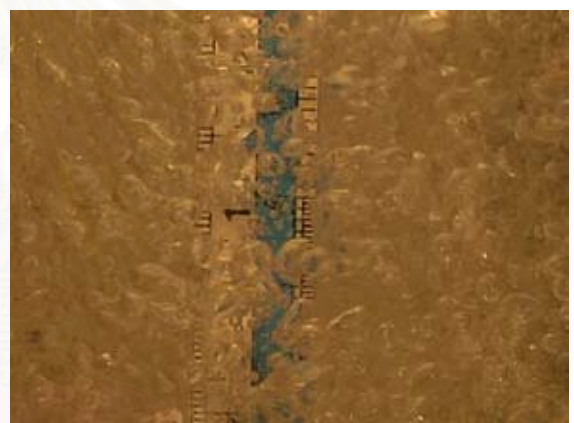
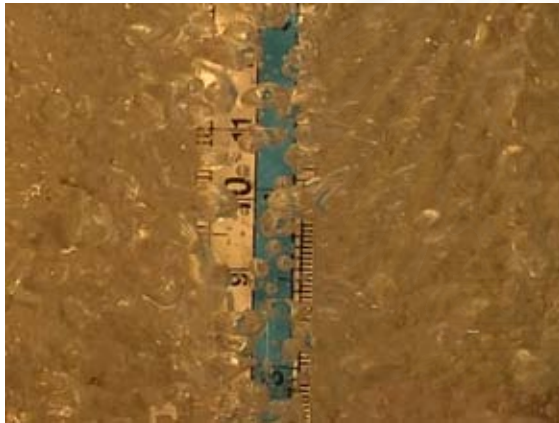
c) Superficial Gas Velocity = 0.031 m/s
Bottom Section

B-4 30 ppt with $A_d/A_r = 0.443$



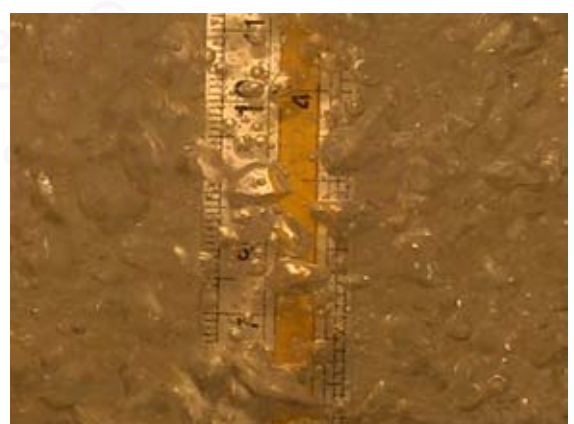
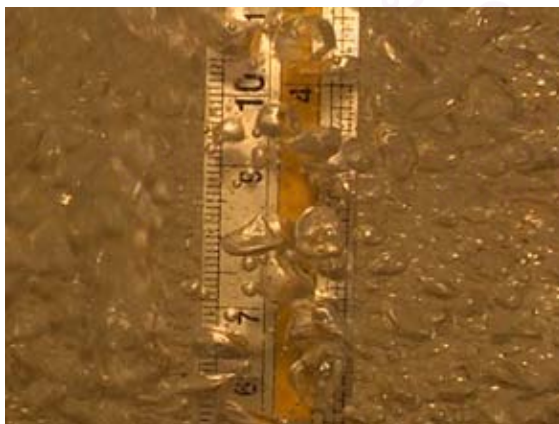
a) Superficial Gas Velocity = 0.041 m/s
Top Section

a) Superficial Gas Velocity = 0.048 m/s
Top Section



b) Superficial Gas Velocity = 0.041 m/s
Middle Section

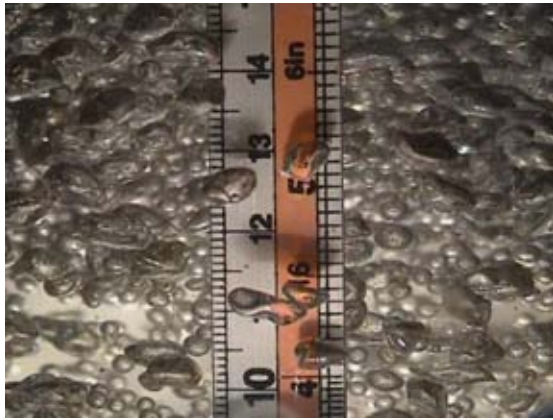
b) Superficial Gas Velocity = 0.048 m/s
Middle Section



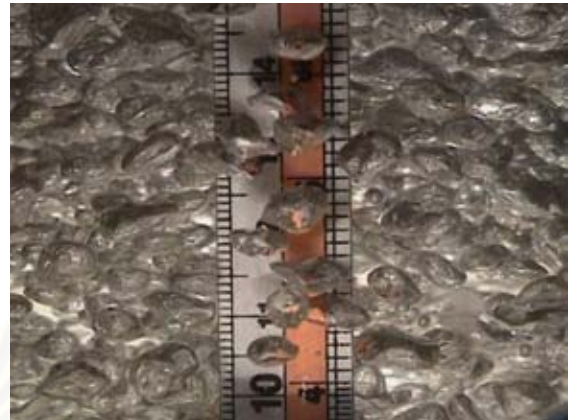
c) Superficial Gas Velocity = 0.041 m/s
Bottom Section

c) Superficial Gas Velocity = 0.048 m/s
Bottom Section

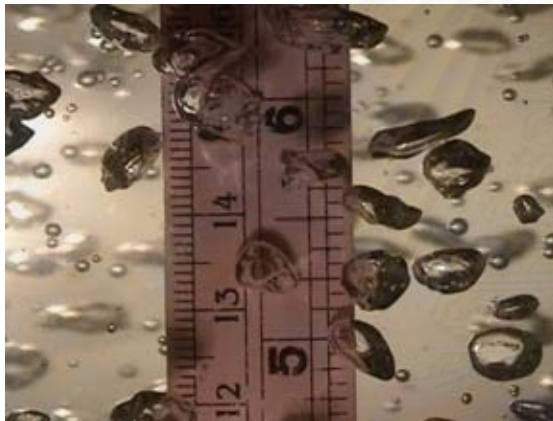
B-5 15 ppt with $A_d/A_r = 0.661$



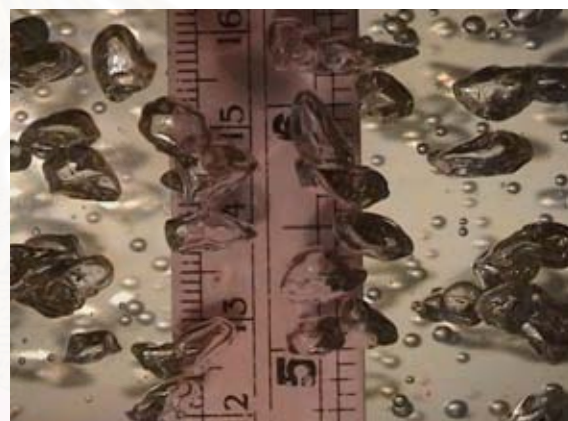
a) Superficial Gas Velocity = 0.013 m/s
Top Section



a) Superficial Gas Velocity = 0.019 m/s
Top Section



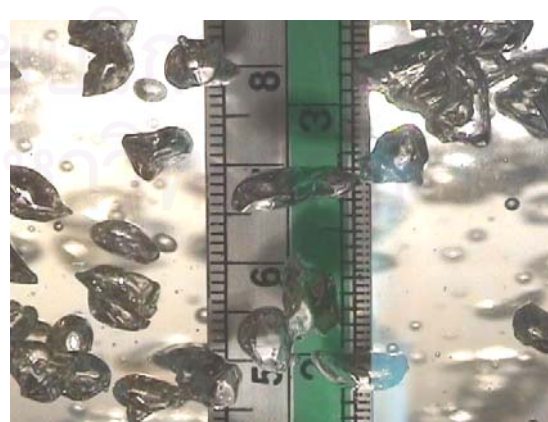
b) Superficial Gas Velocity = 0.013 m/s
Middle Section



b) Superficial Gas Velocity = 0.019 m/s
Middle Section



c) Superficial Gas Velocity = 0.013 m/s
Bottom Section



c) Superficial Gas Velocity = 0.019 m/s
Bottom Section

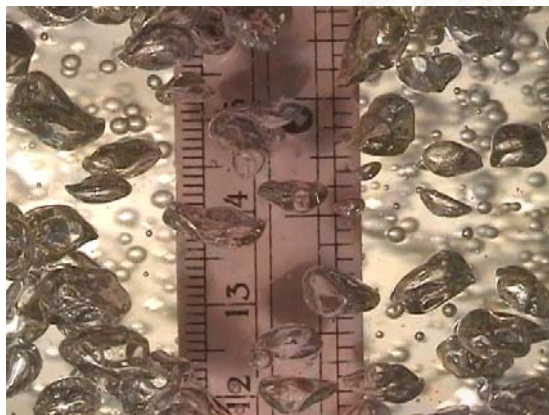
B-5 15 ppt with $A_d/A_r = 0.661$



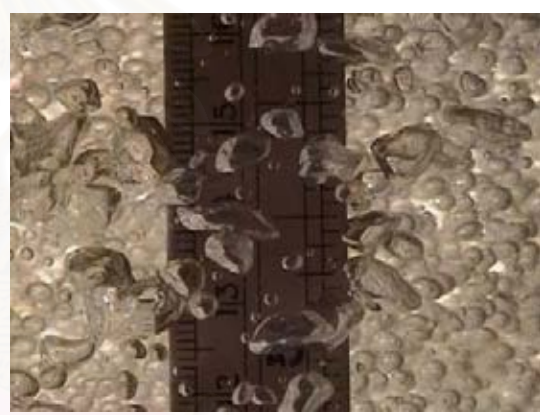
a) Superficial Gas Velocity = 0.029 m/s
Top Section



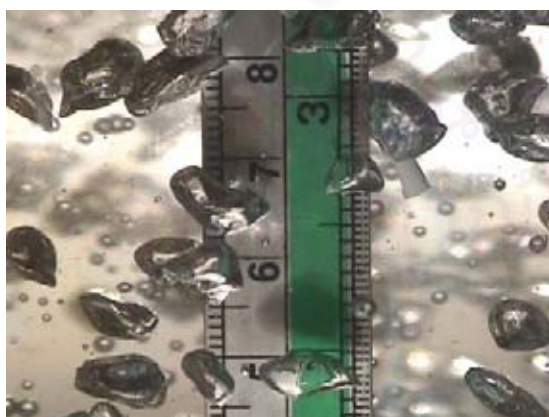
a) Superficial Gas Velocity = 0.036 m/s
Top Section



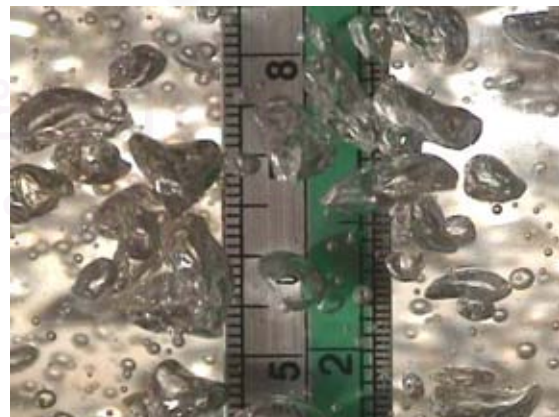
b) Superficial Gas Velocity = 0.029 m/s
Middle Section



b) Superficial Gas Velocity = 0.036 m/s
Middle Section

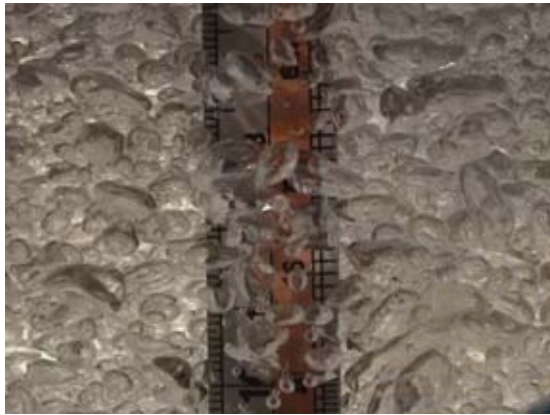


c) Superficial Gas Velocity = 0.029 m/s
Bottom Section



c) Superficial Gas Velocity = 0.036 m/s
Bottom Section

B-5 15 ppt with $A_d/A_r = 0.661$



a) Superficial Gas Velocity = 0.048 m/s
Top Section



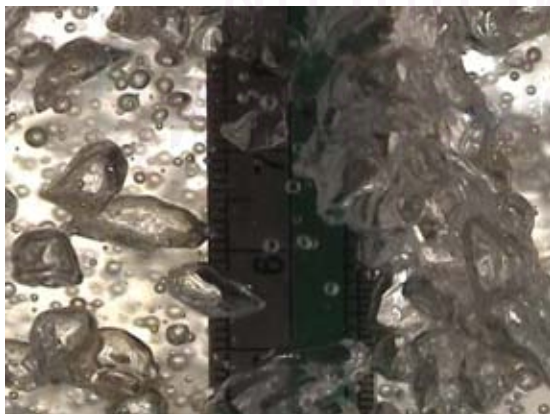
a) Superficial Gas Velocity = 0.056 m/s
Top Section



b) Superficial Gas Velocity = 0.048 m/s
Middle Section



b) Superficial Gas Velocity = 0.056 m/s
Middle Section

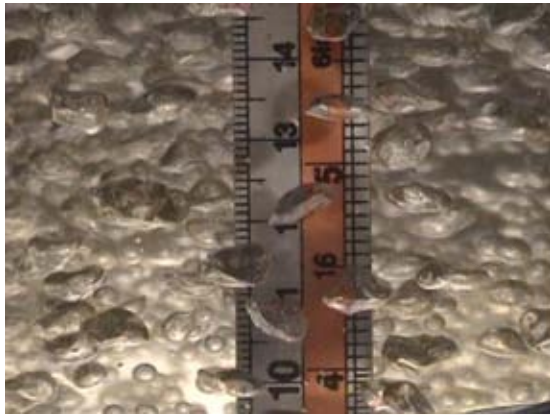


c) Superficial Gas Velocity = 0.048 m/s
Bottom Section

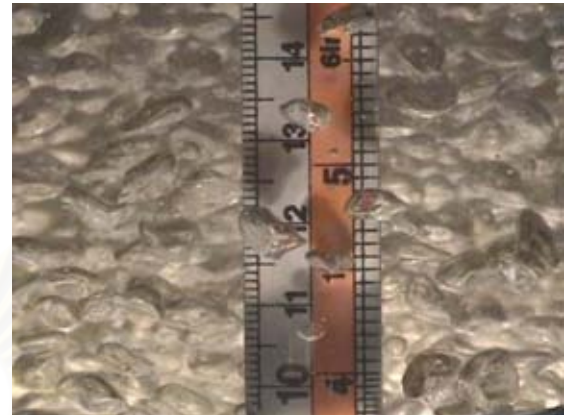


c) Superficial Gas Velocity = 0.056 m/s
Bottom Section

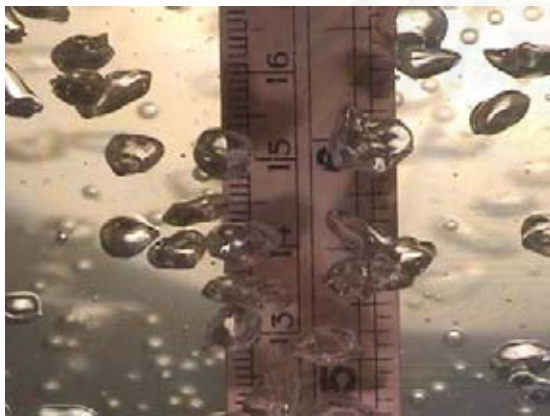
B-6 30 ppt with $A_d/A_r = 0.661$



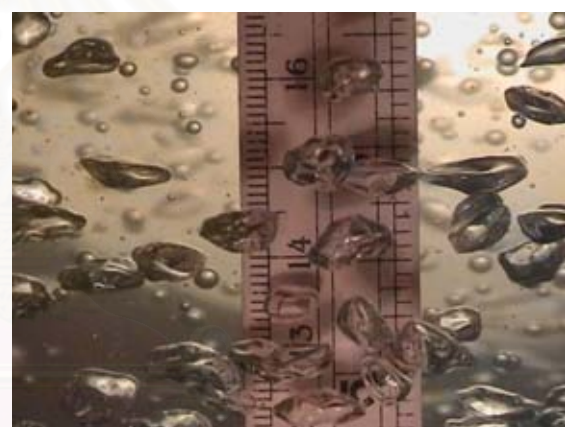
a) Superficial Gas Velocity = 0.013 m/s
Top Section



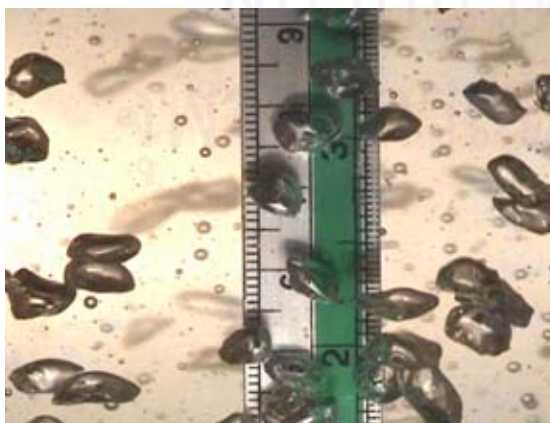
a) Superficial Gas Velocity = 0.019 m/s
Top Section



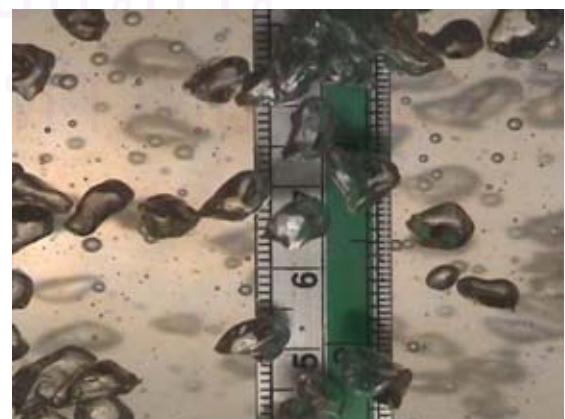
b) Superficial Gas Velocity = 0.013 m/s
Middle Section



b) Superficial Gas Velocity = 0.019 m/s
Middle Section



c) Superficial Gas Velocity = 0.013 m/s
Bottom Section



c) Superficial Gas Velocity = 0.019 m/s
Bottom Section

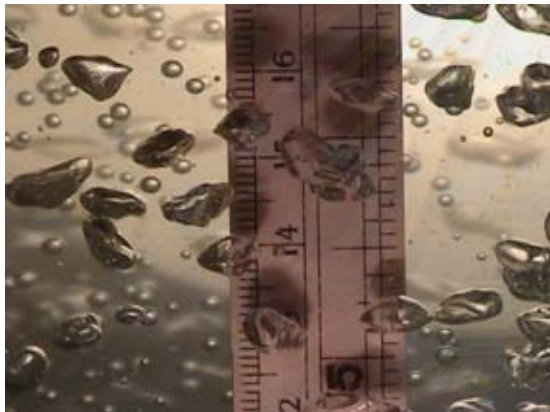
B-6 30 ppt with $A_d/A_r = 0.661$



a) Superficial Gas Velocity = 0.029 m/s
Top Section



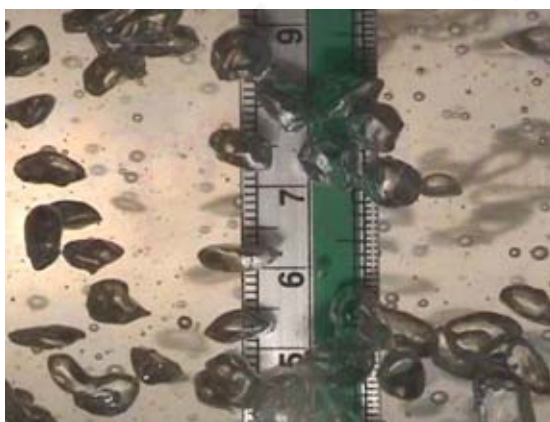
a) Superficial Gas Velocity = 0.036 m/s
Top Section



b) Superficial Gas Velocity = 0.029 m/s
Middle Section



b) Superficial Gas Velocity = 0.036 m/s
Middle Section



c) Superficial Gas Velocity = 0.029 m/s
Bottom Section



c) Superficial Gas Velocity = 0.036 m/s
Bottom Section

B-6 30 ppt with $A_d/A_r = 0.661$



a) Superficial Gas Velocity = 0.048 m/s
Top Section



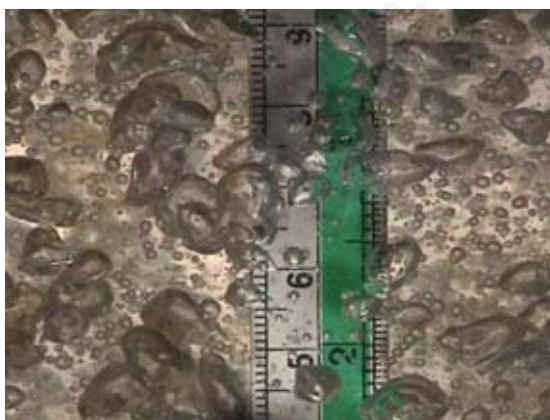
a) Superficial Gas Velocity = 0.056 m/s
Top Section



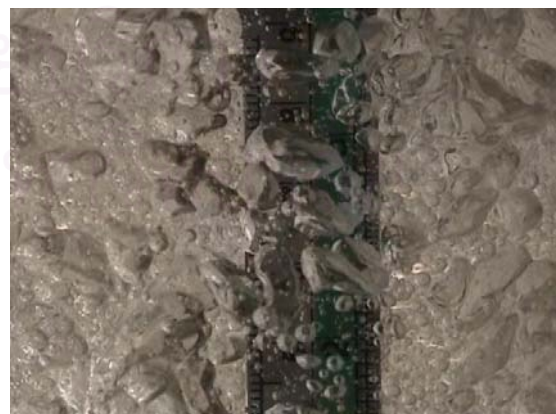
b) Superficial Gas Velocity = 0.048 m/s
Middle Section



b) Superficial Gas Velocity = 0.056 m/s
Middle Section



c) Superficial Gas Velocity = 0.048 m/s
Bottom Section



c) Superficial Gas Velocity = 0.056 m/s
Bottom Section

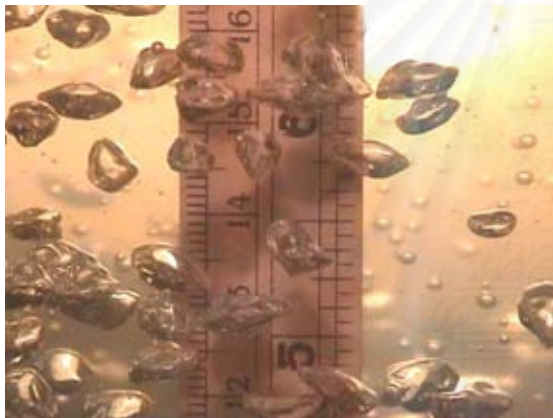
B-7 45 ppt with $A_d/A_r = 0.661$



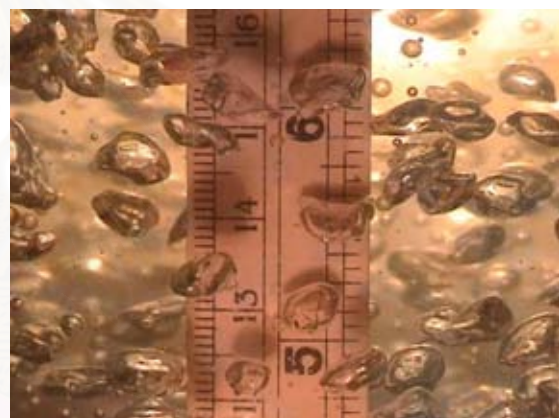
a) Superficial Gas Velocity = 0.013 m/s
Top Section



a) Superficial Gas Velocity = 0.019 m/s
Top Section



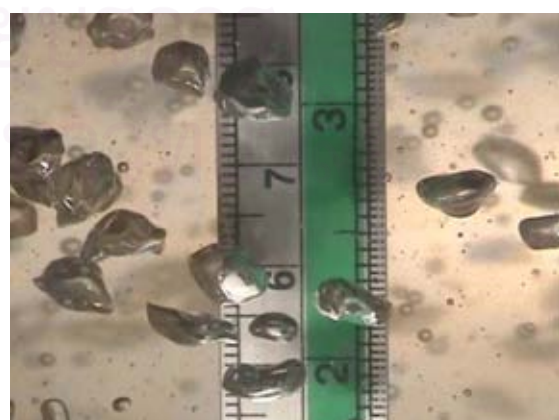
b) Superficial Gas Velocity = 0.013 m/s
Middle Section



b) Superficial Gas Velocity = 0.019 m/s
Middle Section



c) Superficial Gas Velocity = 0.013 m/s
Bottom Section



c) Superficial Gas Velocity = 0.019 m/s
Bottom Section

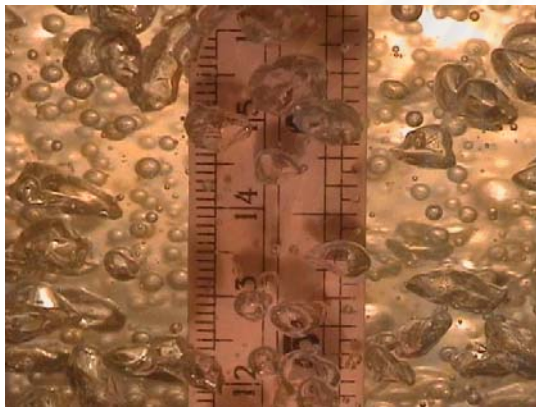
B-7 45 ppt with $A_d/A_r = 0.661$



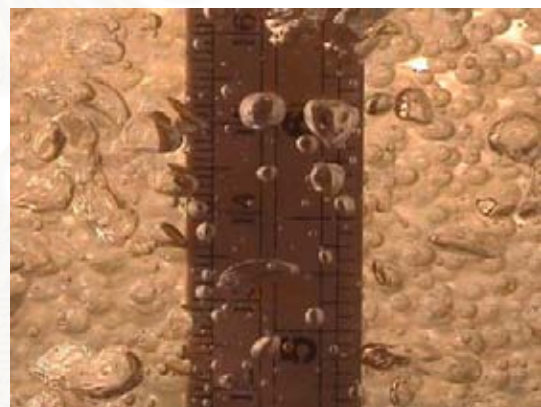
a) Superficial Gas Velocity = 0.029 m/s
Top Section



a) Superficial Gas Velocity = 0.036 m/s
Top Section



b) Superficial Gas Velocity = 0.029 m/s
Middle Section



b) Superficial Gas Velocity = 0.036 m/s
Middle Section



c) Superficial Gas Velocity = 0.029 m/s
Bottom Section



c) Superficial Gas Velocity = 0.036 m/s
Bottom Section

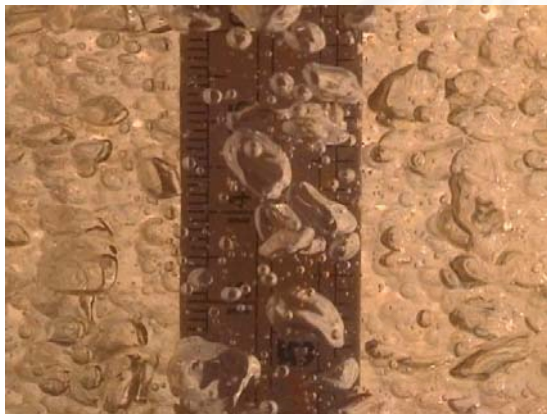
B-7 45 ppt with $A_d/A_r = 0.661$



a) Superficial Gas Velocity = 0.048 m/s
Top Section



a) Superficial Gas Velocity = 0.056 m/s
Top Section



b) Superficial Gas Velocity = 0.048 m/s
Middle Section



b) Superficial Gas Velocity = 0.056 m/s
Middle Section

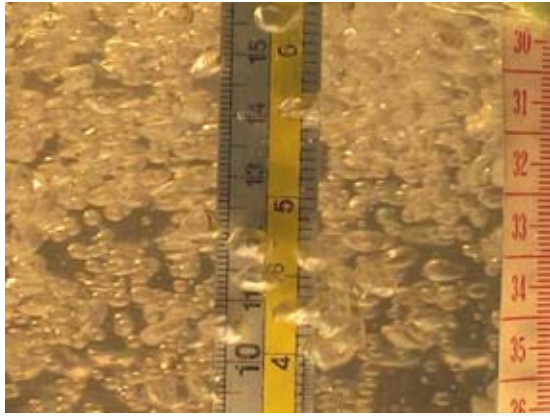


c) Superficial Gas Velocity = 0.048 m/s
Bottom Section



c) Superficial Gas Velocity = 0.056 m/s
Bottom Section

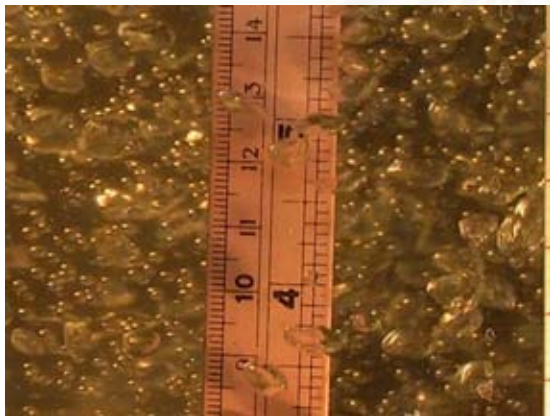
B-8 30 ppt with $A_d/A_r = 1.008$



a) Superficial Gas Velocity = 0.016 m/s
Top Section



a) Superficial Gas Velocity = 0.023 m/s
Top Section



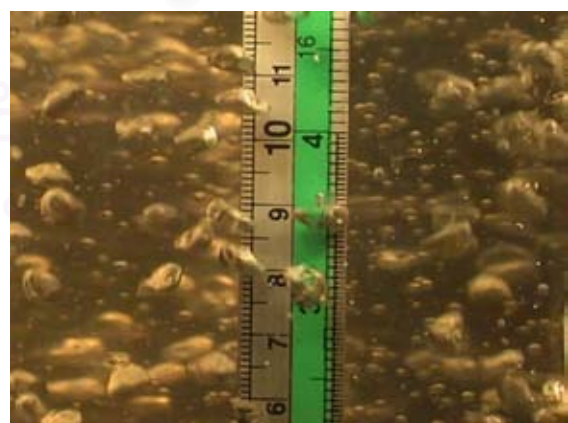
b) Superficial Gas Velocity = 0.016 m/s
Middle Section



b) Superficial Gas Velocity = 0.023 m/s
Middle Section

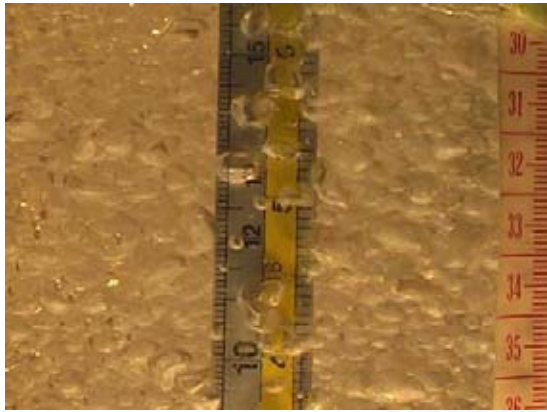


c) Superficial Gas Velocity = 0.016 m/s
Bottom Section

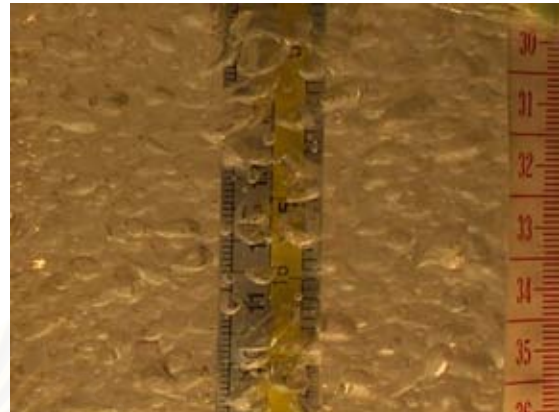


c) Superficial Gas Velocity = 0.023 m/s
Bottom Section

B-8 30 ppt with $A_d/A_r = 1.008$



a) Superficial Gas Velocity = 0.035 m/s
Top Section



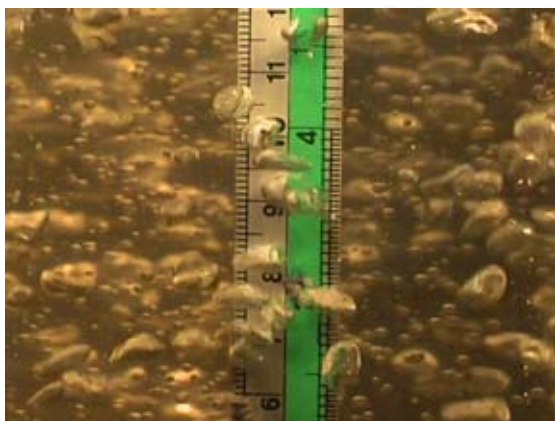
a) Superficial Gas Velocity = 0.044 m/s
Top Section



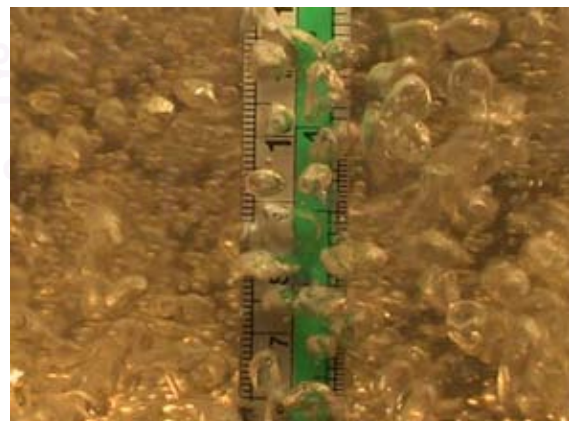
b) Superficial Gas Velocity = 0.035 m/s
Middle Section



b) Superficial Gas Velocity = 0.044 m/s
Middle Section

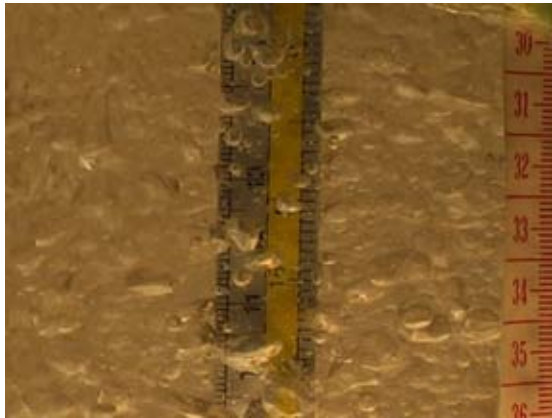


c) Superficial Gas Velocity = 0.035 m/s
Bottom Section

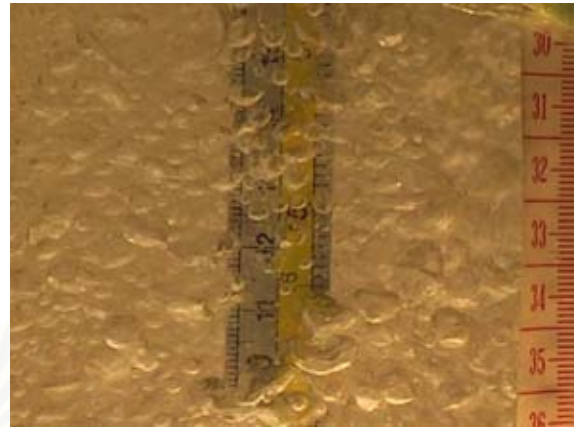


c) Superficial Gas Velocity = 0.044 m/s
Bottom Section

B-8 30 ppt with $A_d/A_r = 1.008$



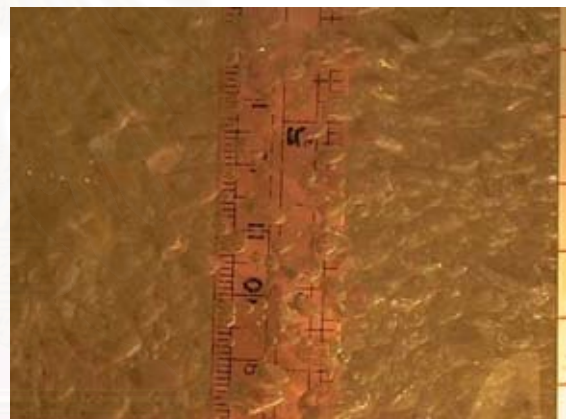
a) Superficial Gas Velocity = 0.058 m/s
Top Section



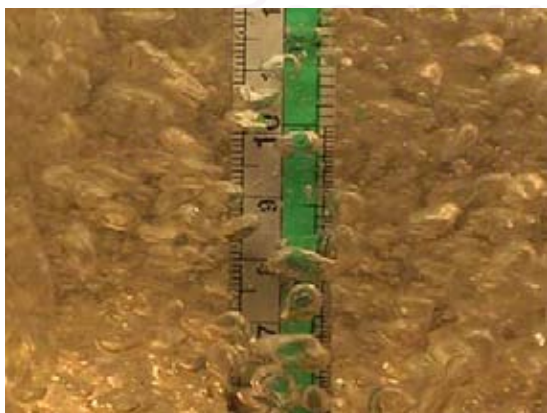
a) Superficial Gas Velocity = 0.068 m/s
Top Section



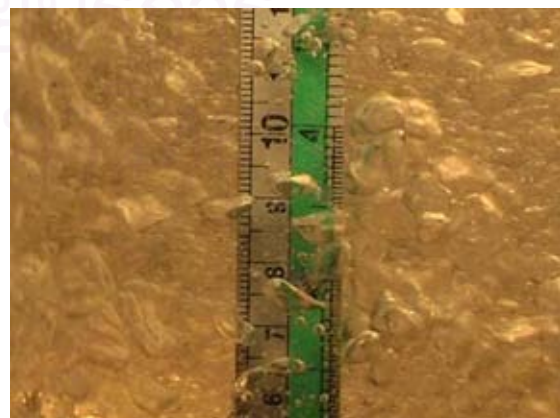
b) Superficial Gas Velocity = 0.058 m/s
Middle Section



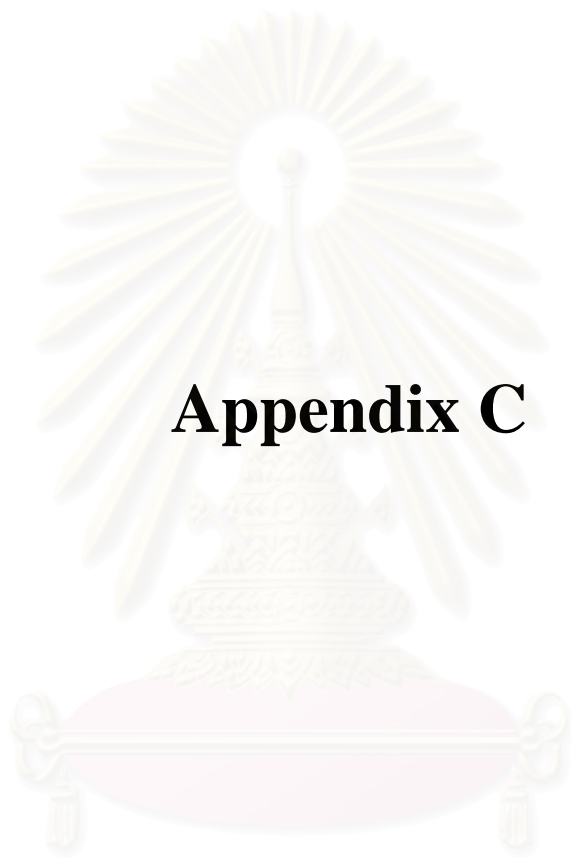
b) Superficial Gas Velocity = 0.068 m/s
Middle Section



c) Superficial Gas Velocity = 0.058 m/s
Bottom Section



c) Superficial Gas Velocity = 0.068 m/s
Bottom Section



Appendix C

สถาบันวิทยบริการ
จุฬาลงกรณ์มหาวิทยาลัย



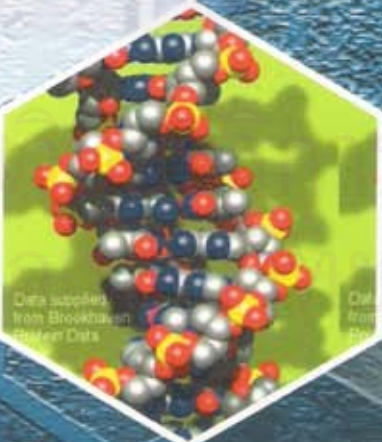
วิทยาศาสตร์กำแพงแสน Kamphaengsaen Academic Journal

วารสารวิชาการของมหาวิทยาลัยเกษตรศาสตร์ วิทยาเขตกำแพงแสน ปีที่ 2 ฉบับพิเศษ ธันวาคม 2547

Volume 2 Supplement
December 2004



การประชุมวิชาการ มหาวิทยาลัยเกษตรศาสตร์
วิทยาเขตกำแพงแสน ครั้งที่ 1
7-9 ธันวาคม 2547



The 1st KU-KPS Conferences
7-9 December 2004



วันพฤหัสบดีที่ 9 ธันวาคม 2547

ภาคบ่ายเวลา 13:00 – 14:40 น.

ประธาน รศ. ดร. ประภาศรี สิงห์รัตน์

เวลา	ชื่อผู้เสนอผลงาน	เรื่อง
13:00 – 13:20 น.	น.ส. อีสยา ดำรงเกียรติสกุล	การประเมินความปลอดภัยทั้งร่างกายของพนักงานขับรถจากการสัมผัสเทือนของยานยนต์
13:20 – 13:40 น.	น.ส. นลินี ดันติกุล	พฤติกรรมทางด้านอุทกพลศาสตร์และการถ่ายเทมวลสารภายในถึงสัมผัสแบบอากาศยกที่มีท่อภายในหลายท่อ
13:40 – 14:00 น.	น.ส. ดวงมล เรือนงาม	การกระจายขนาดฟองอากาศและการถ่ายโอนมวลสารในถังสัมผัสแบบอากาศยกที่ดำเนินการในสภาวะน้ำเค็ม
14:00 – 14:20 น.	น.ส. กมลพรรณ แก้วปิ่นทอง	การเลี้ยงสาหร่าย <i>Haematococcus pluvialis</i> ในถังปฏิกรณ์ชีวภาพแบบอากาศยก
14:20 – 14:40 น.	นายวรเนติ อธิสิสุนรัตน์	การตรวจวัดร่องรอยแฉะเพื่อสร้างดอกกุญแจต้นแบบสำหรับเครื่องทำกุญแจ

วันพฤหัสบดีที่ 9 ธันวาคม 2547

ภาคบ่ายเวลา 15:00 – 16:00 น.

ประธาน รศ. ดร. ประภาศรี สิงห์รัตน์

เวลา	ชื่อผู้เสนอผลงาน	เรื่อง
15:00 – 15:20 น.	นายณรงค์ สุทธิเวช	การศึกษาปัญหาและอุปสรรคในการจัดทำระบบคุณภาพ ISO 9000 ของมหาวิทยาลัยเอกชนในเขตกรุงเทพมหานคร
15:20 – 15:40 น.	นายสมนึก ตันประเสริฐ	การศึกษาปัญหาและอุปสรรคของการดำเนินการระบบ ISO 14001 ภายหลังจากได้รับรองมาตรฐานกรณีศึกษาอุตสาหกรรมยานยนต์
15:40 – 16:00 น.	นายสุภัทร์ ฟ้ารุ่งสาง	ระบบคอมพิวเตอร์แบบพกพาและยั่งยืนเพื่อแก้ปัญหาเครือข่ายในหน่วยงานมหาวิทยาลัยเกษตรศาสตร์

การกระจายขนาดฟองอากาศและการถ่ายโอนมวลสารในถังสัสม์แบบอากาศยกที่ดำเนินการในสภาวะน้ำเค็ม

ดวงกมล เรือนงาม อภิรดี ลิ้มปานภาพ พรทิพย์ วงศ์สุโขโต* และ ประเสริฐ ภาสันต์

ภาควิชาวิศวกรรมเคมี คณะวิศวกรรมศาสตร์ จุฬาลงกรณ์มหาวิทยาลัย

* สำหรับการติดต่อ: โทร 0 2218 6888, email: ppuud@yahoo.com

โดยทั่วไปแบบระบบถังปฏิกรณ์ทางชีวภาพที่นิยมใช้ในระดับอุตสาหกรรม เช่น การผลิตเบียร์ น้ำส้มสายชู ยีสต์ การผลิตแลคติกจากยีสต์ เป็นต้น มักจะมีรูปแบบเป็นถังกวน เนื่องจากเป็นถังปฏิกรณ์ที่มีข้อมูลการออกแบบค่อนข้างมาก ทำให้สามารถขยายขนาดได้ง่าย มีความเร็วในการถ่ายโอนมวลสูง สามารถควบคุมการแพร่ของก๊าซและการผสมโดยควบคุมความเร็วในเครื่องกวน อย่างไรก็ตามถังกวนยังมีข้อจำกัดในการใช้งาน เนื่องจากเป็นถังปฏิกรณ์ที่ใช้พลังงานค่อนข้างมาก และทำให้เกิดแรงเฉือนสูง ซึ่งอาจเป็นอันตรายสำหรับการเพาะเลี้ยงเซลล์ที่มีความอ่อนแอและไม่สามารถทนต่อแรงเฉือนได้ เช่น เซลล์สาหร่าย หรือ เซลล์ไดอะตอมบางประเภท ถังสัสม์อากาศยกจึงเป็นทางเลือกสำหรับใช้ในกระบวนการทางชีวภาพ เพราะเป็นระบบที่มีสภาวะการดำเนินงานไม่รุนแรง อีกทั้งยังใช้พลังงานน้อย เกิดแรงเฉือนต่ำและมีการกระจายตัวของแรงเฉือนค่อนข้างสม่ำเสมอ สามารถควบคุมความเร็วของเหลวได้ ต้นทุนต่ำ ใช้งานและบำรุงรักษาง่าย

งานวิจัยเกี่ยวกับการออกแบบถังสัสม์แบบอากาศยกส่วนใหญ่เน้นการศึกษาผลของลักษณะรูปร่างของถังสัสม์อากาศยก และคุณสมบัติของของเหลว แต่ในปัจจุบันมีการนำระบบถังสัสม์แบบอากาศยกไปใช้ในอุตสาหกรรมสัตว์น้ำหลายประเภท รวมถึงการเพาะเลี้ยงสิ่งมีชีวิตขนาดเล็กในน้ำเค็มซึ่งมีบทบาทสำคัญในแง่ของการให้อาหารแก่ตัวอ่อนของการเพาะเลี้ยงสัตว์น้ำ เช่น กุ้ง ปลา เป็นต้น ดังนั้นงานวิจัยนี้จึงมีวัตถุประสงค์หลักเพื่อศึกษาผลของความเข้มข้นของน้ำเค็มต่อพฤติกรรมของระบบอากาศยก โดยเน้นในเรื่องการกระจายขนาดฟองอากาศและการถ่ายโอนมวลสารในถังสัสม์แบบอากาศยกที่มีหัวพ่นอากาศแบบวงแหวน ถังสัสม์แบบอากาศยกที่ใช้ในงานวิจัยนี้มีสัดส่วนระหว่างพื้นที่หน้าตัดระหว่างส่วนของการไม่ให้อากาศและการให้อากาศเท่ากับ 0.066 และ 0.66 ความเข้มข้นของน้ำเกลือที่ใช้คือ 15 30 45 ส่วนในพันส่วน และแปรเปลี่ยนความเร็วของอากาศให้อยู่ในช่วง 0.01 ถึง 0.04 เมตรต่อวินาที โดยทำการวัดขนาดฟองอากาศในช่วงความสูง 3 ระดับโดยใช้กล้องวิดีโอแบบดิจิทัลเพื่อตรวจสอบการกระจายขนาดฟองที่เปลี่ยนแปลงตามแนวแกน จากการทดลองเรื่องการกระจายขนาดฟอง พบว่าระบบที่ใช้ความเร็วลมต่ำจะให้การกระจายตัวของขนาดฟองที่มีขนาดใหญ่กว่าระบบที่ดำเนินการที่ความเร็วลมที่สูง ในส่วนล่างของคอลัมน์จะพบฟองที่มีขนาดโดยเฉลี่ยใหญ่กว่าส่วนกลางและส่วนบน ความเค็มของน้ำมีผลทำให้ขนาดฟองเล็กลง ในการทดลองเรื่องการถ่ายโอนมวล น้ำเค็มเข้มข้น 30 ส่วนในพันส่วน ให้ค่าสัมประสิทธิ์การถ่ายโอนมวลสูงกว่าน้ำกลั่นโดยเฉพาะที่ความเร็วลมสูง ๆ และเมื่อเปรียบเทียบระบบที่มีสัดส่วนพื้นที่หน้าตัดระหว่างบริเวณการไม่ให้อากาศและการให้อากาศ (A_u/A_d) เท่ากับ 0.66 พบว่ามีค่าสัมประสิทธิ์การถ่ายโอนมวลน้อยกว่าระบบที่มี A_u/A_d เท่ากับ 0.066

Bubble size distribution and mass transfer in airlift contactors operated with saline water

Duangkamol Ruenggam, Apiradee Limpanuphap, Porntip Wongsuchoto* and Prasert Pavasant

Department of Chemical Engineering, Faculty of Engineering, Chulalongkorn University, Bangkok, Thailand

*Corresponding Author. Tel: 0 2218 6888. email: ppuud@yahoo.com

Design of gas-liquid contactors which have been generally used in several biochemical processes such as production of beer, vinegar, yeast, lactic acid (from yeast), etc. has long been restricted to stirred tank reactors because of its well defined performance and scale-up characteristics, high mass transfer, and the easy control of the gas dispersion and medium mixing by stirrer speed. However there are several limitations on the use of such reactors as they often require high power consumption, and the stirrer always causes high shear stress which is harmful to the cultivation of several shear sensitive microorganisms. Milder condition pneumatic reactors such as airlift contactors (ALCs) are therefore alternative designs of gas-liquid contacting devices for biochemical processes as they provide several advantages over the stirred tanks such as low power consumption, low and homogeneous shear stress region, controllable liquid circulation rate, low capital cost, easy maintenance and better defined flow pattern.

Previous research on airlift contactors with air-water systems have been extensively conducted which focused mainly on the effect of geometrical design of the system and liquid properties. Recent applications of airlift systems involve the cultivation of saline water microorganisms as they are significant as a feed supplement in most aqua cultural larvae, e.g. shrimp, fish, etc. Thus, this work concentrated on the effect of saline concentration on the performance of airlift systems. Bubble size distribution and mass transfer characteristics of annulus sparged airlift contactor were the main focus of this research. The airlift contactor employed in this work had the ratio between the cross sectional areas of downcomer and riser (A_d/A_r) of 0.066 and 0.66. The saline water concentration was proposed in three conditions, i.e. 15, 30 and 45 ppt where the air flow rate was varied in a range of superficial gas velocity from 0.01 to 0.04 m/s. The bubble sizes were measured at three different heights (top, middle and bottom sections) of the column by a digital video camera to investigate the axial variation in bubble size distribution. The results indicated that the ALC system operated with lower gas velocity possessed larger bubble size than the system at high gas velocity. The average bubble size at the bottom section was generally larger than those at the middle and top sections. The salinity was found to decrease the bubble size in the system. At the salinity of 30 ppt, the system exhibited higher mass transfer rate than the system with fresh water. Moreover, a lower mass transfer coefficient was obtained in the system with A_d/A_r of 0.66 than in the system with A_d/A_r of 0.066.



▶ DISCUSS SCIENCE



▶ EXCHANGE OF IDEAS



▶ NETWORKING

○ RSCE | ○ SINGAPORE | ○ 2006

International Symposium on Chemical Engineering **RSCE**

ADVANCES IN CHEMICAL AND BIOMOLECULAR ENGINEERING
3 – 5 DECEMBER 2006
NANYANG TECHNOLOGICAL UNIVERSITY

Book of Abstracts

- Nanotechnology
- Energy & Environmental Technology
- Petrochemicals
- Food, Polymer, Fine Chemicals and Pharmaceuticals
- Biochemical Engineering
- Novel Materials Chemical Analysis Techniques
- Molecular Modeling and Simulation
- Chemical Engineering Fundamentals
- Chemical and Biomolecular Engineering Education

Organized by



**NANYANG
TECHNOLOGICAL
UNIVERSITY**

School of Chemical & Biomedical Engineering



Sponsored By



Pfizer Asia Pacific Pte Ltd



Merck Sharp & Dohme (Singapore) Ltd.



Quantachrome Instruments



semiconductor pacific (singapore) pte limited

Teltec Semiconductor Pacific (S)
Pte Ltd



天美

Techcomp (Singapore) Pte Ltd



Bruker Singapore

Supported By



PEACE
STABILITY
COURAGE
DIVERSITY
PROSPERITY



School of Chemical and Biomedical Engineering

Reg. No. 200604393R

Dear Miss Duangkamol Ruen-ngam

Paper ID: **I-9-OR1**

Paper Title: **Influence of salinity on gas-liquid mass transfer in airlift contactors with annulus sparger**

The review process for the 13th Regional Symposium on Chemical Engineering 2006 - Advances in Chemical and Biomolecular Engineering has been completed. Based on the recommendations of the reviewers, we are pleased to inform you that your paper identified above has been accepted for presentation in RSCE 2006. You are cordially invited to present the paper at RSCE 2006 to be held on **3 – 5 December 2006*** in Singapore.

This notification email serves as our formal acceptance of your paper as well as an invitation to present your work at RSCE 2006.

Please kindly refer to RSCE 2006 website (<http://www.ntu.edu.sg/scbe/cbe/rsce2006/>) for further information on the registration, accommodation reservation, venue, program and preparation of extended abstract.

The acceptance of your paper is made with the understanding that at least one author will PRE-REGISTER (i.e. one registration per paper) and attend the Symposium to present the paper. In order for your extended abstract to be included in the book of abstracts, we require that:

1. your final extended abstract in PDF or plain text is received by 31 August 2006;
1. the Copyright Transfer Form for your extended abstract is received by 31 August 2006;
2. the Registration with payment is received by 31 August 2006.

If the above requirements are not met by the set deadlines, the extended abstract will not be published in the book of abstracts. It is our obligation to eliminate 'no shows' if at all possible since missing presentation cause a lot of disruptions in a session.

For the most updated information on the symposium, please check the website <http://www.ntu.edu.sg/scbe/cbe/rsce2006/>. The program will be available at the website soon.

We would like to take this opportunity to thank you for choosing RSCE 2006 to present your research results.

We look forward to seeing you in Singapore!

Yours sincerely

Xu Rong (Assistant Professor)
For RSCE Secretariat

** Please note that RSCE 2006 has been re-scheduled to 3 – 5 December 2006 instead of 4 – 5 December 2006. Apologies for any inconvenience caused.*

4 December 2006 (Monday)

Venue: Seminar Room 2

Session: Chemical Engineering Science-1

- 10:15 Influence of salinity on gas-liquid mass transfer in airlift contactors with annulus sparger
Duangkamol Ruen-ngam, Apiradee Limpanuphap, Porntip Wongsuchoto, Prasert Pavasant, Chulalongkorn University/TH 2
- 10:35 A reaction rate expression for partial oxidation of methane to synthesis gas over Ni-MgO/ γ -Al₂O₃ catalysts using spinning basket reactor
Izza Aliyatul Muna, Luis F. Razon, Hiroo Niyama, Takashi Aida, De La Salle University/PH 2
- 10:55 The influence of mesh refinement on the accuracy of twin-screw extrusion modelling
Edi Soetaredjo F., Nicholson T., Torley P., Widya Maridala Catholic University/ID 2
- 11:15 Application of the Van der Waals equation of state to the separation of paraffin wax from lube based oil refinery plant
Praphon Preeyaratanchote, Aus Klubnuam, Pitiphat Thaipitak, Surat Areerat, King Mongkut Institute of Technology/TH 2
- 11:35 Effect of sodium dodecyl sulphate on the transfer rate of volatile organic compounds from agitated water
Juntima Chungsiripom, Charun Bunyakan, Prince of Songkla University/TH 2
- 11:55 Alteration of Light Illumination in a Serial Photobioreactors, an Enhancement Effort of Biomass Production by *Chlorella vulgaris* Buitenzorg
Anondho Wijanarko, Dianursanti, Heidi, Misri Gozan, Roekmijati Widaningroem Soemantojo, Kazuhisa Ohtaguchi, University of Indonesia/ID 2
- 12:15 Physico-chemical and anti-microbial properties characterisation of essential oils extracted from lemongrass and patchouli using supercritical carbon dioxide
Mith Hasika, Pag-asa Gaspillo, Julius Maridable, Roberto Malaluan, Marvelisa Marve, Junjiro Kawasaki, Huynh Ky Phuong Ha, De La Salle University/PH 2
- 12:45 Lunch @ Function Room
- 14:05 Experimental observations on hydrodynamically and chemically induced insitu colloidal particles release and transport in subsurface flow
Tushar Kanti Sen, Universiti Teknologi Petronas/MY 2
- 14:25 Design of a One-Dimensional, Horizontal flow HFCVD reactor for fluorocarbon film deposition
Chutima Jarusiripot, David S. Dandy, Burapha University/TH 2
- 14:45 Influence of Configuration of Draft Tubes on Hydrodynamic and Mass Transfer Behavior in Multiple Draft Tube Airlift Contactors
Chenwit Linthong, Prasert Pavasant, Chulalongkorn University/TH 2
- 15:05 Adsorption and Kinetics of Methylene blue uptake by magnetic montmorillonite
Ratanawan (Wibulswas) Kiatlikomol, Papis Chanaroke, Suriya Sripathong, Suranaree University of Technology/TH 2
- 15:25 Solvent evaporation from drops of natural dye extract in spray drier
E. Rahayuningsih, S.S. Rahayu, Gadjah Mada University/ID 2
- 15:45 Water vapour adsorption on activated carbon with surface oxygen functional groups
Yuvarat Ngernyen, Chaiyot Tangsathitkulchai, Malee Tangsathitkulchai, Suranaree University of Technology/TH 2
- 16:05 Study of physical and chemical-physical phase equilibria for biomolecules-supercritical CO₂ system
J.P. Sitompul, H. Wahyudi, Institute of Technology, Bandung/ID 2
- 16:25 Coffee Break
- 16:40 Temperature Control tuning in CSTR for transesterification (methyl ester) process
Kulchanant Prasertsit, Anuwat Prasertsit, Prince of Songkla University/TH 2
- 17:00 Removal of arsenic from groundwater by adsorption using activated carbon and laterite
Dang Son Van, Leonila Abella, Joseph Auresenia, Pag-asa Gaspillo, Junjiro Kawasaki, De La Salle University/PH 2
- 17:20 Production of Fine Granular Ices and Its Application to Energy Storage System
Chika Ohno, Megumu Yamagishi, Masakazu Matsumoto, Kaoru Onoe, Chiba Institute of Technology/JP 2
- 17:40 Kinetic modeling of soda delignification of maranta arundinaceae used in pulping process
Natalia Suseno, Lia Hwa, Akbarningrum Fatmawati, University of Surabaya/ID 2
- 18:00 Influence of epoxidation reaction period and temperature on the quality of polyol synthesized from soybean oil
Purwanto, E., Fatmawati, A., Swtyoprato, P., Junedi, Rosmiati M., University of Surabaya/ID 2

Influence of salinity on gas-liquid mass transfer in airlift contactors with annulus sparger

Duangkamol Ruen-ngam, Pomtip Wongsuchoto and Prasert Pavasant*

Department of Chemical Engineering, Faculty of Engineering
Chulalongkorn University, Bangkok, 10330, Thailand

* Corresponding author, Tel: 0 2218 6870, email: prasert.p@chula.ac.th

ABSTRACT

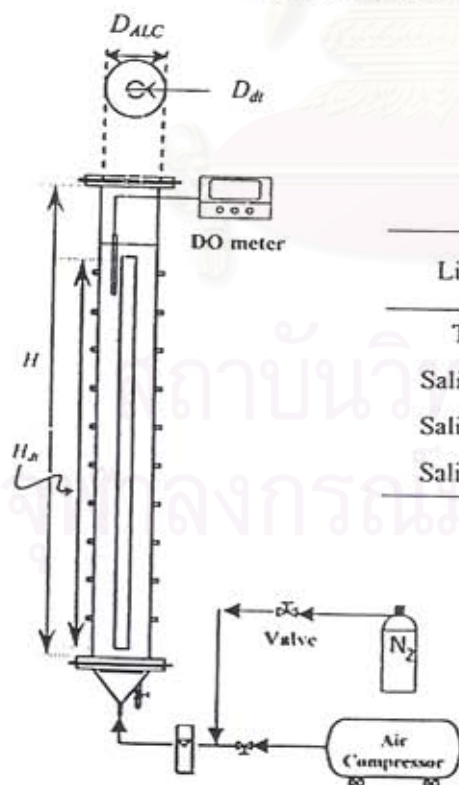
An airlift contactor was operated in the water-air system where the salinity of the water was altered in the range of 0-45 ppt and the aeration rate as measured in terms of superficial gas velocity varied from 0-7 cm/s. For all systems, the overall volumetric mass transfer coefficient (k_La) increased steadily with an increase in the aeration rate. Salinity decreased the equilibrium dissolved oxygen level in the liquid phase but clearly increased the mass transfer rate when compared with the pure water. The effect of salinity was more complicated where the highest mass transfer rate occurred in the system with the salinity of 30 ppt.

1. INTRODUCTION

Airlift contactors were often proposed as an alternative culture system for the microorganisms. This was due to its several advantages over other types of culture systems such as low shear rate, sufficient gas liquid mass transfer rate, low power consumption, and relatively controllable liquid circulation rate [1]. Recently, airlift contactors are proposed for aqua-culture larvae such as shrimp and fish [2], and there are certain cases where these have to be operated with saline water system. However, thus far, information on the effect of salinity on the performance of the airlift systems was scarce. This research, hence, focused on the effects of salinity on overall volumetric mass transfer coefficient (k_La) obtained in the airlift contactor.

2. APPARATUS AND CALCULATION

Experiments were carried out in a transparent cylindrical column with dimension as provided in Fig.1. Experimental procedure and calculation details were demonstrated in Wongsuchoto et al. [3]. The medium salinities were measured by refractometer.



Liquid phase	Surface tension $\times 10^3$ [N/m]	Viscosities $\times 10^3$ [Pa.s]	Density [kg/m ³]
Tap water	56.5	1.28	996
Saline at 30 ppt	58.0	1.44	1005
Saline at 30 ppt	66.2	1.47	1016
Saline at 45 ppt	68.7	1.49	1027

Symbols	[cm]
H	120
H_a	100
D_{ALC}	13.7
D_d	3.4

Figure 1 A schematic diagram of experimental setup and liquid properties employed in this work.

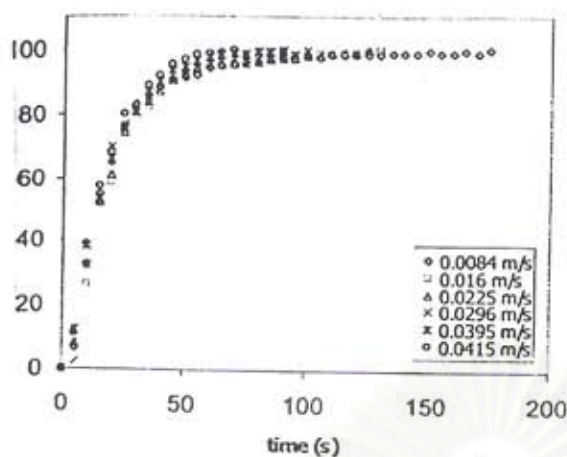


Figure 2 Relation between superficial gas velocity and %DO in 30 ppt

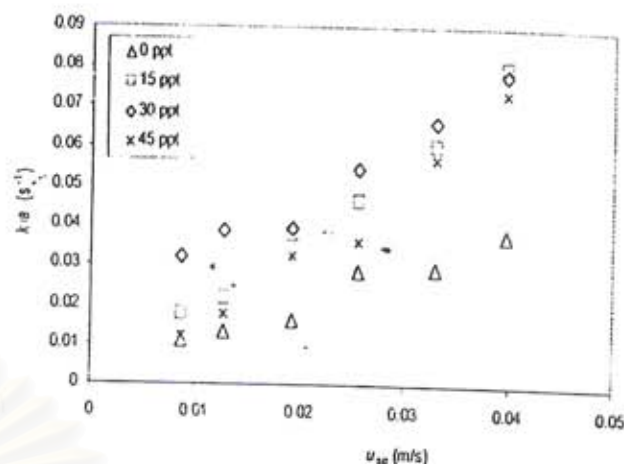


Figure 3 Relation between superficial gas velocity and overall volumetric mass transfer coefficient

3. RESULTS AND DISCUSSION

3.1 Superficial gas velocity

Fig. 2 shows the dissolved oxygen time profile at various superficial gas velocity (u_{sg}) at the system with 30 ppt salinity. This can be converted to the relationship between k_La and u_{sg} as shown in Fig. 3 which also includes the relationships at other salinity levels. It is clear that k_La increased steadily with u_{sg} for all systems investigated here. This is due to two main reasons. Firstly, a high turbulence generated from the aeration increased with the aeration rate or u_{sg} which resulted in a higher level of k_L in the system. Also an increase in the aeration also led to a higher gas holdup and therefore increased the mass transfer area or specific surface area (a). Wongsuchoto et al. [3] demonstrated that the quantity a increased with the aeration rate because when more gas was supplied to the system, the size of bubbles distributed in the system was smaller due to the bubble breakup mechanism. This also led to an increase in the mass transfer rate.

3.2 Salinity

Fig. 3 illustrates that salinity significantly increased the mass transfer rate in the system. This was due to the breakup of the bubbles in the saline water system and the bubble size in the saline water was significantly smaller than that in the pure water system. This resulted in a high mass transfer area as observed from this figure. Although mass transfer rates at various salinity levels were not significantly different from each other, the system with 30 ppt salinity seemed to provide the highest k_La . From visual observation, a system with higher salinity level contained a marginally smaller bubble size which should increase the mass transfer area and also k_La , an opposite expected results from the experimental inspection. This could be due to the fact that salinity affected the interface between gas and liquid, and it was reported that a more viscous interface was obtained with a higher level of salinity [4], and this retarded the mass transfer rate. Therefore the level of k_La depended on the compromise between the two factors, i.e. larger mass transfer area due to bubble breakup and higher mass transfer resistance due to viscous interface. In this case, the salinity at 30 ppt was found to be most favorable from the mass transfer point of view. Note that the rate of mass transfer does not reflect the amount of oxygen dissolved in the water as the solubility of oxygen is typically lower when the salinity increases.

4. ACKNOWLEDGMENTS

The study was financially supported by Thailand Research Fund (TRF).

5. REFERENCES

- [1] Chisti M.Y., 1989. *Airlift bioreactors*. NY: Elsevier Science Publishing.
- [2] Krichnavaruk S., Loataweesup W., Powtongsook S., and Pavasant P., 2005. Optimal Growth Conditions and the Cultivation of *Chaetoceros calcitrans* in Airlift Photobioreactor. *Chemical Engineering Journal* 105: 91-98.
- [3] Wongsuchoto P., Charinpanikul T., and Pavasant P., 2003. Bubble Size Distribution and Gas-Liquid Mass Transfer in Airlift Contactors. *Chemical Engineering Journal* 92: 81-90.
- [4] Prince Michael J. and Blanch Harvey W., 1990. Transition Electrolyte Concentrations for Bubble Coalescence. *AIChE Journal* 36: 1425-1429.

**Influence of Salinity on Bubble Size Distribution and Gas-liquid Mass Transfer in
Airlift Contactors**

Duangkamol Ruen-ngam, Porntip Wongsuchoto, Apiradee Limpanuphap,
Tawatchai Charinpanitkul, Prasert Pavasant*

*Department of Chemical Engineering, Faculty of Engineering, Chulalongkorn University
Bangkok, 10330, Thailand*

สถาบันวิทยบริการ
จุฬาลงกรณ์มหาวิทยาลัย

* Corresponding author. Tel.: +66-2-218-6870; Fax: +66-2-218-6877

Email: prasert.p@chula.ac.th (P. Pavasant)

Abstract

Alternative pneumatic reactor design, airlift contactor was advantages for shear sensitive microorganisms and provided adequate oxygen concentration. This induced to further develop configuration of reactor for aqua-culture industries. In this research using column with 1.2 m height and 0.137 m diameter installs central with 1 m draft tube height. Gas applied through a PVC perforated ring sparger with 30 holes (1 mm in diameter) at the bottom base of the annulus section. This investigation concentrated on the effect of salinity in different configurations such as draft tube sizes ($A_d/A_r = 0.061-1.01$), gas supply flow rate ($u_{sg} = 0.01- 0.07$ m/s) and salinity levels (0, 15, 30, and 45ppt) on bubble size distribution and hydrodynamic characteristics. Nevertheless gas-liquid mass transfer used for investigate the efficiency of airlift contactor in various configuration designs. Saline water proposed smaller bubble size than fresh water due to saline water properties and ions effects that inhibited coalescence and pronounced bubble stable. Double electric layer at the gas-liquid film interface enhanced disjoining pressure and balanced the Laplace's pressure that inhibited bubble coalescence. Moreover this film at interface retarded gas-water structure moving pass through the interface that resulted to lower overall mass transfer coefficient in saline water. However overall volumetric mass transfer and hydrodynamics properties as gas holdup and liquid characteristics also affected to overall mass transfer coefficient. Further established equation for finding overall mass transfer coefficient in the form of dimensionless Sherwood number referred that mass transfer in saline water in this work depended solely on the natural convection.

Key words: Disjoining pressure, Laplace pressure, Bubble coalescence, Film thinning

สถาบันวิทยบริการ
จุฬาลงกรณ์มหาวิทยาลัย

Introduction

An airlift system is an example of gas-liquid contacting device for which its application in biotechnology area has grown significantly in recent years (Chisti, 1989, Colella et al., 1999, Polli et al., 2002 and Wongsuchoto et al., 2003). One of the significant parameters controlling the rate of gas-liquid mass transfer in such system is the bubble size distribution as it determines the level of interfacial mass transfer and other hydrodynamic behavior of the systems. Bubble breakage was often reported to be a predominant factor in the gas-liquid contacting devices particularly at high gas throughputs. (Bo and Lant, 2004, Kantarci et al., 2005, Bouaifi et al., 2001 and Merchuk et al., 1998) Hence, the systems at high aeration rate are typically operated with smaller bubble size range which enhances gas holdup and consequently gas-liquid mass transfer. Bubble breakage was also found to take place along the height of the column due to an increasing interaction between bubbles as they traveled up the top of the column (Colella et al., 1999). The information on bubble size distribution in airlift systems has been investigated by several researchers. (Bo and Lant, 2004, Kantarci et al., 2005, Bouaifi et al., 2001 and Merchuk et al., 1998) Similar results were reported for this system where small bubbles were often found at elevated height and with high gas throughput. In particular, Wongsuchoto et al. (2003) reported that bubble breakage caused the bubble size at the top part to be smaller than that at the lower part of the ALC.

The overall volumetric mass transfer coefficient was commonly employed to demonstrate the efficiency of oxygen transfer from gas to liquid. This quantity depends on the system geometry and liquid properties which are related to several other parameters. Principally, this parameter is constituted of the mass transfer coefficient (k_L) and the specific interfacial area (a_L) which then depends on the flow regimes, hydrodynamics and bubble characteristics in the system. In addition, electrolyte solutions such as sea water were reported to provide a better $k_L a$ than in fresh water as the bubble size in such systems was relatively small. Moreover Contreras et al., 1999 believed that in sea water overall mass transfer coefficient depended on gas holdup and liquid velocity in the system. On the other hand, systems with higher viscosity such as CMC (carboxymethyl cellulose) exhibited a lower $k_L a$ than those running with lower viscosity mediums (Guo-Qing et al., 1995 and Vasconcelos et al., 2003). The presence of antifoam promoted bubble coalescence and therefore reduced $k_L a$ (Al-Masry, 1999 and Vasconcelos et al., 2003). Apart from the liquid properties, the reactor design parameters such as the height of the column and the ratio between riser and downcomer cross-sectional area (A_d/A_r) are important parameters which

affect the flow pattern in the system. For ALCs, it was reported that a larger A_d/A_r ALC usually encountered lower k_La than the systems running with smaller A_d/A_r (Wongsuchoto et al., 2003).

The gas-liquid mass transfer is commonly considered as a function of bubble sizes, and this was explicitly described in several empirical correlations such as Frossling's equation and Higbie's theory for bubble column (Painmanakul et al., 2005). Most investigations on bubble size distribution were often confined to the system operated with water – air as liquid and gas phases, respectively. Salinity is known to alter the properties of water, for instance, it decreases the surface tension of the solution, and this could significantly affect the bubble size distribution. This, in turn, will have notable influence on the gas-liquid mass transfer. This work therefore focuses on the quantitative analysis of the influence of salinity on the hydrodynamics and mass transfer behavior of the annulus sparged internal loop airlift contactor.

Experimental

Apparatus

Experiments were carried out in an acrylic transparent airlift contactor as detailed in Figure 1. The column was 1.2 m in height with an inside diameter of 0.137 m. The column was equipped with pressure taps along the contactor height for the measurement of pressure drop, ΔP , which was used to determine the riser gas holdup, $\varepsilon_{g,r}$. A 1 m draft tube height was installed centrally in the column with a bottom clearance of 5 cm for liquid circulation. The anaerated liquid height was controlled at 3 cm above the draft tube. The ratio between cross sectional area was altered by changing the draft tube diameter as provided in Table 1. In this work was operated in a semi-batch operation where a continuous air was supplied through this perforated ring sparger and saline water was filled in to the column which was always controlled at 3 cm above draft tube. Air flow rate was controlled by a calibrated rotameter to give a range of superficial gas velocities, u_{sg} , from 0.01-0.07 m/s. The aeration was accomplished through a perforated ring sparger with 30 holes (1 mm in diameter) provided at the bottom base of the annulus section. The sparger was made from PVC tubing with of 0.8 cm diameter.

Bubble size distribution measurement

The bubble size measurement was performed in riser section using a photographic technique. More than 200 bubbles were photographed using a digital camcorder (Panasonic® NV-GS75) at three different heights (h_i): 10 cm (bottom section), 50 cm (middle section) and 90 cm (top section) from the base of the draft tube as illustrated in Fig 1 and Table 3. The correction to real size was based on the scale attached to the draft tube with the same focal distance as the measured bubbles. The focus was adjusted on the scale and only the well-focalized bubbles were measured (Wongsuchoto et al., 2003). For ellipsoidal bubbles, the major and minor axes of bubble images were measured. The equivalent size of the bubble (d_B), representing the diameter of a sphere whose volume was equal to that of the bubble, was calculated using Eq. (6) (Hebrard et al., 1996, Couvert et al., 1999).

Aeration was supplied at the bottom of the column through the annulus riser section in ALCs with various draft tube sizes. Table 1 provides detail of the operation of this system. The salinity was measured by OPTIK Handheld Refractometer and was controlled at 15, 30, and 45 ppt. The density of the solution was measured by pycnometer (UL/Y ADAPTER, MIDDLE BORO, MA 02346 U.S.A., Brook field ENGINEERING LABS INC) at 100 rpm, 26.5°C, and the surface tension was measured with KRUSS K10T (Du Noüy Ring). These properties were summarized in Table 2.

Determination of hydrodynamic and mass transfer behavior of ALCs

The overall gas holdup, $\varepsilon_{g,o}$, was determined by the volume expansion method. The unaerated and aerated liquid heights were measured and $\varepsilon_{g,o}$ was then calculated from:

$$\varepsilon_{g,o} = \frac{H_D - H_L}{H_D} \quad (1)$$

The riser gas holdup, $\varepsilon_{g,r}$, was estimated by measuring the pressure difference (ΔP) between two pressure taps located along the height of the column (Δh) where:

$$\varepsilon_{g,r} = 1 - \frac{\Delta P}{\rho_l g \Delta h} \quad (2)$$

It was assumed that gas holdup in the top section was approximately equal to that in the riser and therefore the downcomer gas holdup, $\varepsilon_{g,d}$, can be computed from:

$$\varepsilon_{g,d} = \frac{\varepsilon_{g,o} H_D (A_d + A_r) + (H_{dt} A_d - H_D (A_d + A_r)) \varepsilon_{g,r}}{H_{dt} A_d} \quad (3)$$

Liquid velocities both in riser and downcomer were measured using the color tracer technique. The pressure taps were employed as injection points of the color tracer and the recorded time of color tracer between the two points in the contactor was measured for the calculation of liquid velocity.

The overall volumetric mass transfer coefficient ($k_L a$) was determined by the dynamic method (Chisti and Moo-Young, 1988, Koide et al., 1983, Lessard and Zieminski, 1971, Bouaifi et al., 2001, Vasconcelos et al., 2003 and Wongsuchoto et al., 2003). A dissolved oxygen meter (Jenway 9300) was used to record the changes in oxygen concentration with time in the ALC. The system was initially freed of O_2 by bubbling N_2 through the liquid for approx. 10 min. The calculation of $k_L a$ follows Equation (4):

$$\ln \frac{(c^* - c_o)}{(c^* - c_L)} = k_L a_L t \quad (4)$$

Results and Discussion

Effect of salinity on average bubble size

Figure 2 illustrates that, at low range of u_{sg} (<0.02 m/s), the effect of salinity on bubble size was not obvious and bubble sizes were in the range of 6.0 to 7.5 mm in all ALC systems. At higher u_{sg} , the effect of salinity on bubble size became more apparent where the bubble size appeared to be smaller in the saline solution than that in fresh water. This was in contrast with the fact that saline solution possesses a stronger surface tension and viscosity than water and the bubble size in such solution should be larger than in water. However, the effect of electrolyte on viscosity (Marangoni effect) was reported not to be adequate to regulate the bubble size (Li 2007, Marrucci, 1969, Prince and Blanch, 1990(a)), and therefore the effects of salinity on bubble size were mainly due to its ionic properties. This finding was in good agreement with several past reports which stated that electrolyte solutions inhibited bubble coalescence and retarded bubble riser velocity which then caused the bubble size to be smaller than that in water (Marrucci and Nicodemo, 1967, Lessard and Zieminski, 1971, Prince and Blanch, 1990(a), Prince and Blanch, 1990(b), Weissenborn and Pugh, 1996 and Malysa et. al., 2005). Types and concentration of electrolyte can impose different effects on bubble coalescence, for instance, Lessard and Zieminski, 1971 ordered efficiency of coalescence in various electrolytes as follows: $MgSO_4 < MgCl_2 < CaCl_2 < Na_2SO_4 < LiCl < NaCl < NaBr < KCl$.

There are two types of forces or pressures dealing with the coalescence or breakup of the bubbles. The first one is the Laplace pressure which promotes bubble coalescence from

the drainage of the liquid film located in between the two adjacent bubbles. This pressure depends on the reciprocal of the bubble diameter. However, if the Laplace pressure is too strong, bubbles coalesce very rapidly and this caused instability of the bubbles. Therefore, at this condition, bubble breakage dominates in the system. The other type of force is repulsive force. Electrolytes such as salt increased the repulsive **hydration force** by enhancing water structure due to hydrogen bond at the interface leading to a more stable bubble than that in the fresh water system. This formation of repulsive force balances the Laplace pressure, inhibiting bubble coalescence (Tsang et al, 2004). The two forces can be written in a mathematical form as follows:

$$\Delta P = \frac{\sigma}{r_p} - \Pi \quad (5)$$

when σ is surface tension, r_p is radius of intersection of three films called the Plateau border channel and the ratio between the surface tension and radius of intersection or $\left(\frac{\sigma}{r_p}\right)$ is equal to Laplace pressure. Π is the **disjoining pressure** which is the summation of various forces between ions interaction at the gas and liquid interface according to Equation (6).

$$\Pi = \Pi_{vdw} + \Pi_{DL} + \Pi_{hyd} \quad (6)$$

where Π_{vdw} is attractive Van der Waals force, Π_{DL} is the dielectric double layer force or repulsive force and Π_{hyd} is short-range repulsive or hydration force. An attractive van der Waals force (Π_{vdw}) was weak force attraction and caused from the polarization of molecules into dipoles, and can be expressed mathematically as in Equation (7). A dielectric double layer (Π_{DL}) was the repulsive force caused from confinement of the ion charge at gas-liquid interface. A hydration forces was short-range repulsive force (Π_{SR}) resulting from the formation of the water molecules near charged surfaces as in Equation (8),

$$\Pi_{vdw} = \frac{-A}{6\pi h^3} \quad (7)$$

$$\Pi_{hyd} = \left(\frac{W}{\lambda}\right) \exp(-h/\lambda) \quad (8)$$

where A is the Hamaker constant which is equal to 10^{-20} J, h the film rapture thickness, λ the decay length of the hydration interaction, mostly takes the value of about 8.5 nm, and W the pre-exponential constant ≈ 6 mN/m² (Tsang et. al., 2004). The film rapture thickness or h was reported to be a function of salinity by Cain and Lee (1985) which were equal to 114.7, 106.8

98.8, and 90.9 for the water with salinity levels of 0, 15, 30, and 45 ppt, respectively. In the same work (Cain and Lee, 1985), it was reported that the dielectric double layer force (Π_{DL}) was negligible compared with the hydration force and should be disregarded from the calculation. Moreover, Van der Waals attraction was generally reported to be relatively small and was also negligible compared with the hydration force (Marrucci, 1969, Prince and Blanch, 1990(a)). Therefore Equation (5) is reduced to

$$\Delta P = \frac{\sigma}{r_p} - \Pi_{hyd} \quad (9)$$

The pressure difference, ΔP , in Equation (...9) was important in controlling the level of bubble coalescence or bubble breakage in the system. ΔP is low for the condition with inhibiting bubble coalescence, and high for the bubble coalescence promoting conditions. Nevertheless, as mentioned above, a much higher ΔP would result in a breakup of bubbles (Stanley 2004). A summary of these forces acting on the bubbles in the airlift systems is given in Table 5.

Let's define the parameter ΔP_C which is the range of ΔP that results in the bubble coalescence. The conditions with smaller ΔP lead to the inhibition of bubble coalescence, whilst higher ΔP than this would cause bubble breakage, and in both cases, this results in smaller bubble sizes. From the results obtained in this work (Table 6), it was clear that the bubble size in the water system was the largest (ΔP in water = approx. 20 N/m² for the whole range of u_{sg} employed in this work). This was due to the absence of repulsive force to balance the Laplace pressure. With the presence of salinity, the repulsive force became stronger. However, it was illustrated that this repulsive force was not strong enough to bring ΔP down. In contrast, the Laplace pressure in the presence of salinity seemed to be quite large which could be the result from the increasing surface tension. This resulted in ΔP having a much value than 20 N/m². Therefore bubbles tended to break in such condition.

In the airlift with A_d/A_r of 0.067 running with 45 ppt salinity, ΔP was about 43-75 N/m² at $u_{sg} > 0.02$ m/s and therefore bubble breakup was expected. The bubble size in this case was quite small, at 0.001-0.002 m (see Figure 2). Figure 3 illustrates that when the A_d/A_r was altered (from 0.067 to 0.661), the condition in the system changed, and despite using the same level of u_{sg} , the system running with 45 ppt salinity had ΔP of 12-25 N/m² and larger bubbles (0.005-0.006 m) than that at lower A_d/A_r were observed.

Figure 4 illustrates the relationship between pressure driving forces and the average bubble size in all airlift systems employed in this work. It seemed that ΔP that gave the

largest bubble size was in the range from 15 – 20 N/m². A lower ΔP would inhibit bubble coalescence and therefore the bubble size was slightly lower than that at ΔP of 15 - 20 N/m². At high ΔP , the bubble size became quite small which suggested that bubble breakup was quite significant in controlling the bubble size distribution inside the system. Hence, for this work, ΔP_C lies at the range of 15-20 N/m².

Effect of superficial velocity

Figure 2-3 demonstrates that Sauter mean diameter of the bubbles decreased with superficial gas velocity at all salinity levels. This finding agreed well with the reported data in the airlift systems operated with various types of liquid (Colella et al., 1999, Contreras et al., 1999, Polli et al., 2002 and Wongsuchoto et al., 2003). The bubble sizes were regulated by the level of pressure difference in the airlift system as described above. At low range of gas flow rate (<0.02 m/s) as shown in Figure 2, the pressure difference was in the range of 15-20 N/m². Therefore this range of ΔP enhanced bubble size. At a higher range of superficial gas velocity (>0.02 m/s), the ΔP was higher than 20 N/m² which promoted the breakup of the bubbles. In addition, at this high gas throughput conditions, the airlift contained a relatively high gas hold-up which also enhanced the chance of bubbles collision and breaking up.

Local bubble size distribution in airlift systems

Figure 5 illustrates examples of the bubble size distribution curves obtained from the various sections of the ALC system operated with saline water at 30 ppt and with draft tube # DT3. As a general trend, bubble size was quit large, in the range of 6.0-8.2 mm at low superficial velocity. When the system was operated with higher gas throughput, bubbles became smaller in size and the variation in bubble size became bimodal distribution where there were two main bubble sizes present at the same time (2 and 6.5 mm). At high gas throughput, bubble size became small and the distribution illustrated that there was only one main bubble size in the system at this condition (2 mm). Bubble size did not seem to be smaller when the superficial velocity became higher than 0.036 m/s. This finding was for the system operated with water at salinity of 30 ppt, and it agreed well with the report by Wongsuchoto et al., 2003 who carried out the experiment in fresh water systems that bubble no longer changed its size distribution $u_{sg} > 0.05$ m/s. The difference was that the airlift operated with saline solution had smaller bubble sizes than those with fresh water.

Axial bubble size distribution in airlift contactors

The axial bubble size distribution was obtained by taking photographs of bubbles in the airlift at different heights. Bubble distribution frequency was then formulated for each sampling point, and the results were shown in Figure 5. In the top and middle sections, the distribution changed from uni-modal to multi-modal curve at $u_{sg} \approx 0.019$ m/s whereas the bottom section saw this change at $u_{sg} \approx 0.029$ m/s. The breakage of the bubbles at high gas throughput was caused by higher amount of energy dissipation and turbulent which promoted more interaction between bubbles. The results suggested, therefore, that there was a higher level of turbulence in the top and middle sections than that in the bottom. The Sauter mean diameters of bubbles in the three sections in the airlift system with A_d/A_r of 0.661 are illustrated in Figure 6. This revealed that bubble size in the bottom section was slightly larger than in those in the other sections, particularly at a lower range of u_{sg} (< 0.04 m/s) examined in this work. At a higher u_{sg} range, the effect of column height on the bubble size was not obvious and the sizes of bubbles were approximately the same throughout the length of the airlift. The same finding was found for the system running with tap water as described in Wongsuchoto et al. (2003).

Effect of the ratio between downcomer and riser cross-sectional areas on bubble size

To investigate the effect of the ratio between the downcomer and riser cross-sectional areas (A_d/A_r), the experiment was conducted in the airlift contactors running with sea water at 30 ppt with four different draft tube sizes as detailed in Table 1 and the average bubble sizes are shown in Figure 7. At a low range of u_{sg} (< 0.015 m/s), no significant differences in bubble size were observed in all systems. At u_{sg} greater than 0.015 m/s, the differentiation of the bubble sizes in the systems with different draft tube sizes became more obvious, i.e. the bubble size was larger with increasing draft tube size (d_{Bs} , $DT4 > DT3 > DT2 > DT1$). In other words, the bubble size was larger in the system with smaller riser cross sectional area. It was possible that turbulence in the system with smaller riser area was stronger than those with larger riser areas, and the chance of bubbles being coalesced at this high turbulent regime was relatively high. Figure 6 also illustrates that the effect of A_d/A_r on bubble size was more obvious at the bottom section, and not as much in the middle and top sections. As stated earlier, the level of turbulence in the middle and top sections of the airlift with the size used in this work was stronger than that in the bottom section. With similar level of turbulent intensity in the top part of the various airlift systems, bubble sizes in this section were not

significantly regulated by A_d/A_r . Unlikely, the bottom section was operated at lower turbulent intensity where the airlift with different A_d/A_r might exert noticeable levels of turbulence intensities. This resulted in a distinguishable bubble sizes as observed in Figure 7. This finding was also similar to the performance of airlift contactor operated with fresh water as reported in Wongsuchoto et al. (2003).

Overall volumetric mass transfer coefficient (k_La) in the airlift systems operating with sea water

The overall volumetric mass transfer coefficient (k_La) was calculated from Equation (4). The change in the overall volumetric mass transfer coefficient (k_La) with superficial gas velocity and salinity level was shown in Figure 8. This illustrated that k_La increased with superficial gas velocity but decreased with an increase in salinity. As an overall observation, salinity seemed to have adverse effects on k_La and the system with fresh water always imposed a higher k_La than those running with sea water. The effect of salinity on k_La was quite complicated. At low range of u_{sg} (<0.03 m/s), the effect of salinity did not seem to be significant, however, the effect became more pronounced at high aeration rate ($u_{sg} > 0.03$ m/s) and k_La was the highest at 30 ppt followed by those at 15 and 45 ppt, respectively.

This k_La quantity composed two main parameters, i.e. “ k_L ” or overall mass transfer coefficient, and “ a ” or specific interfacial area. Generally k_L was reported to be a function of turbulence, liquid properties and bubble size. As the salinity did not have notable effect on liquid properties, k_L should be controlled only by turbulence and bubble size. The two film theory suggested that k_L was more regulated by the shear rate at the gas-liquid interface which was controlled by the slip velocity or the difference in the bubble and liquid velocity. However, the estimate of k_L required the use of certain empirical correlation whereby the coefficients needed to be obtained from experimental data. These parameter fittings would be described shortly after the calculation of specific area.

The specific interfacial area (a) was estimated using Equation (9):

$$a = \frac{6\varepsilon_g}{d_{Bs}(1 - \varepsilon_g)} \quad (9)$$

where $\varepsilon_{g,r}$ is the riser gas holdup and d_{Bs} Sauter mean diameter which is defined as:

$$d_{Bs} = \frac{\sum n_i d_{B,i}^3}{\sum n_i d_{B,i}^2} \quad (10)$$

where n_i is the occurrence frequency number of the sphere bubbles diameter, $d_{B,i}$. The two parameters significant for the determination of the specific mass transfer area were average bubble size (Figure 3) and gas holdup. Figure 9 illustrates that the effect of salinity on gas holdups in the system was only marginal and the specific area should only vary with bubble size. As discussed earlier in this article, the bubble size in sea water was smaller than that in fresh water and became smaller with an increase in superficial gas velocity. Therefore the specific interfacial areas obtained in the systems at all salinity levels were higher than that in the fresh water system.

It was primarily assumed that the gas holdup was uniform throughout, both in axial and radial directions. The estimates of specific interfacial area (a) in the airlift system with $A_d/A_r = 0.661$ at various salinities is displayed in Figure 10. This finding revealed that effect of salinity on specific area was only marginal at low range of superficial gas velocity ($u_{sg} < 0.028$ m/s), and became more significant at higher u_{sg} . The largest gas-liquid surface area was obtained from the airlift operating with saline water at 15 ppt, followed by those at 30 and 45 ppt. This corresponded well with the information on the effect of salinity on bubble size in Figure 3.

Now that once the information on $k_L a$ and a became known, the overall mass transfer coefficient or k_L could simply be calculated by dividing $k_L a$ with a and the results are given in Figure 11

Estimate of $k_L a$

The mass transfer rate for entire contactor was proposed in the terms of the overall volumetric mass transfer coefficient $(k_L a)_T$ and could be calculated from sum of the mass transfer rates in riser and downcomer section as follows:

$$(k_L a)_T = \frac{(k_L a)_r V_{L,r} + (k_L a)_d V_{L,d}}{V_{L,T}} \quad (11)$$

where $V_{L,r}$ is the volume of liquid in riser, $V_{L,d}$ the volume of liquid in downcomer and $V_{L,T}$ the volume of total liquid. $(k_L a)_r$ and $(k_L a)_d$ were obtained from $k_{L,r}$ multiplied by $a_{L,r}$ and $k_{L,d}$ multiplied by $a_{L,d}$.

As a was obtained from the measurement, the estimate of $k_L a$ requires only the estimation of k_L . As mentioned above, the mass transfer coefficient, k_L was reported as a function of liquid properties and bubble size. It was assumed that Schmidt number remained constant as salinity did not significantly alter the properties of the liquid (Higbie et. al., 1935,

Calderbank, 1967., Bailey et. al., 1977, Painmanakul et. al., 2005), and hence, the dimensionless relationship between Sherwood number (Sh), Reynold number (Re) and Grashof number (Gr) could be formulated as follows:

$$Sh = a + bGr^c Sc^d + eRe^f Sc^h \quad (12)$$

forced convection
 ↓
 ↑
 free convection

Generally, Grashof number, Gr represents the mass transfer by natural convection or free rise velocity whilst Reynolds number, Re , is the mass transfer form forced convection:

$$Gr = \frac{d_{Bs}^3 \rho_l \Delta \rho g}{\mu_l^2} \quad (13)$$

$$Re = \frac{d_{Bs} v_s \rho_l}{\mu_l} \quad (14)$$

The velocity and bubble diameter used in the calculation of Reynolds number were the slip velocity, v_s , and Sauter mean diameter, d_{Bs} . The slip velocity in riser, $v_{s,r}$ was calculated as a function of the terminal rise velocity of a single bubble, u_∞ , which were related to hindering effects from neighboring bubbles in the riser section. Information on bubble sizes was then employed to estimate the slip velocity of the gas bubbles in the system using the following equation (Marrucci, 1965; Wallis, 1969):

$$v_{s,r} = \frac{u_\infty}{(1 - \epsilon_{g,r})} \quad (15)$$

where u_∞ is the terminal bubble riser velocity which can be calculated using the correlation proposed by Jamialahmadi et al., 1994.

$$u_\infty = \frac{(1/8)((\rho_l - \rho_g) / \mu_l) g d_{Bs}^2 ((3\mu_l + 3\mu_g) / (2\mu_l + 3\mu_g)) \sqrt{2\sigma / d_{Bs} (\rho_l + \rho_g) + g d_{Bs} / 2}}{\sqrt{[(1/8)((\rho_l - \rho_g) / \mu_l) g d_{Bs}^2 ((3\mu_l + 3\mu_g) / (2\mu_l + 3\mu_g))]^2 + 2\sigma / d_{Bs} (\rho_l + \rho_g) + g d_{Bs} / 2}} \quad (16)$$

The parameters $a - h$ in Equation (12) was then determined from experiments.

Equation 14 must be used to predict $k_{L,r}$ and $k_{L,d}$, and in doing so, the slip velocities or terminal rise velocities in both riser and downcomer must be known (from Equations 7 and 8) for the calculation of Reynolds number. As the photographic technique could only be used to measure the bubble size in riser, bubble size in downcomer was not known and the determination of slip velocity in downcomer was not possible. However, the average bubble size in downcomer ($d_{B,d}$) could be estimated from the downcomer liquid velocity, $u_{L,d}$, by assuming that the liquid must have velocity equaled to the terminal velocity to be able to drag the bubble down into the downcomer, or

$$v_{s,d} = u_{L,d} \quad (17)$$

Once the terminal velocity was known, the Levich equation (Levich, 1962) as shown in Equation (16) was proposed for the calculation of bubble size:

$$d_{B,d} = \frac{1.8}{g} \left(\frac{u_{L,d}}{2} \right)^2 \quad (18)$$

Assume that there was no variation of bubble size along the radial and axial directions in downcomer:

$$d_{Bs,d} = d_{B,d} \quad (19)$$

The $a_{L,d}$ was calculated from substitution of $d_{Bs,d}$ from Equation (19) and $\varepsilon_{g,d}$ from the experiment to Equation (3).

The parameters $a-h$ in Equation 12 were evaluated using non-linear parameter fittings using all the results available in this work, and the results are given in Table 7 (noted that these parameters were obtained from the solver function in the MS Excel 97 where the objective was a minimal error between experimental and simulation data). For the case of tap water, the results from parameter fitting were reasonably close to those proposed from Wongsuchoto et al. (2003) (as shown in the last row of Table 7). The fittings for the saline water gave somewhat different results from that for pure water in that the terms Reynolds number was not involved in the pure water system, but it was, to certain extent, for the saline water systems. This meant that the mechanism controlling the mass transfer coefficient in pure water was only the natural convection whereas the force convection as represented by the Reynolds term also was significant in the system operated with saline water. Figure 12 illustrates the comparison between the calculated and experimental k_{La} of the airlift contactor operated with various saline solutions.

Conclusion

This work concentrated on bubble distribution and related with oxygen transfer from gas to liquid phase in internal loop airlift contactor. Apart researches about effect of salinity was very sparse. This research found that the bubble size was smaller than operating with fresh water due to hydrodynamics properties and liquid properties. Bubble break-up/coalescence depended on two bubble came to contact then breakage or coalescence. The bubble pronounced coalescence to large bubble size when there appeared driving pressure different in the range of pressure different from 15 – 20 N/m². After enhancing pressure different would promote bubble break-up due to external force that accelerated film thinning at the gas-liquid interface. This lower range of pressure different appeared smaller bubble size due to hydrophilic repulsive forces inhibited bubble coalescence. This smaller bubble size in saline water caused to higher amount of specific interfacial area that enhanced the overall volumetric mass transfer coefficient whereas decreased overall mass transfer coefficient due to bubble size effect. Moreover this research also calculated overall mass transfer from Sherwood number by using empirical data. From this correlation insisted that gas transferred to liquid phase by means of natural convection that related to bubble size.

Acknowledgements

The authors wish to acknowledge the Thailand Research Fund, Graduated Research Fund at Chulalongkorn University, THAILAND for their financial supports.

สถาบันวิทยบริการ
จุฬาลงกรณ์มหาวิทยาลัย

BIOGRAPHY

Miss Duangkamol Ruen-ngam was born on 4th January, 1982 in Bangkok. Her native home was Ayutthaya province. She finished her secondary school from Triam Udom Suksa School. She got bachelor degree from Food Technology in Faculty of Science at Chulalongkorn University. She continued her further study for master's degree in Chemical Engineering at Chulalongkorn University. She participated in the Biochemical Engineering Research Group and achieved her Master's degree in April, 2007.



สถาบันวิทยบริการ
จุฬาลงกรณ์มหาวิทยาลัย